# Remote sensing methods for lake management

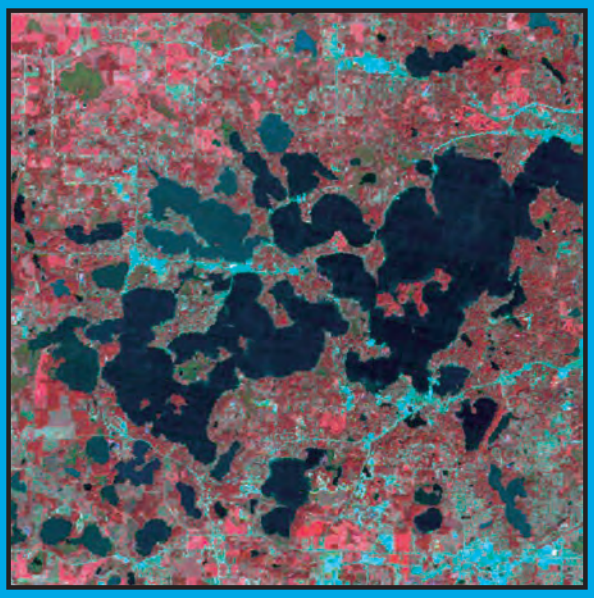
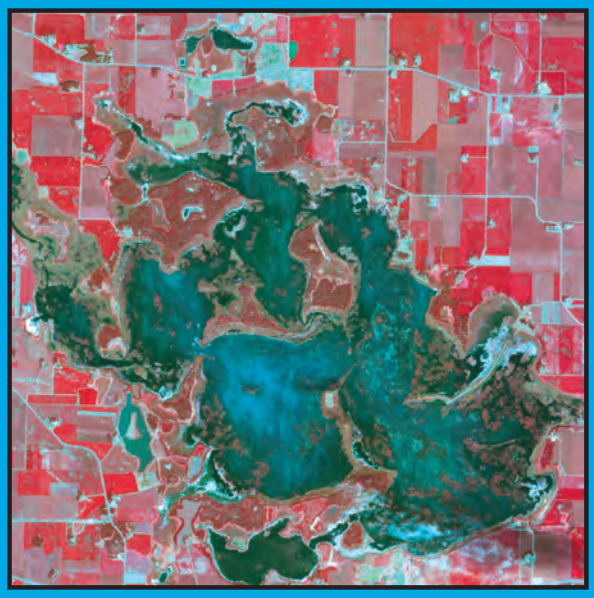

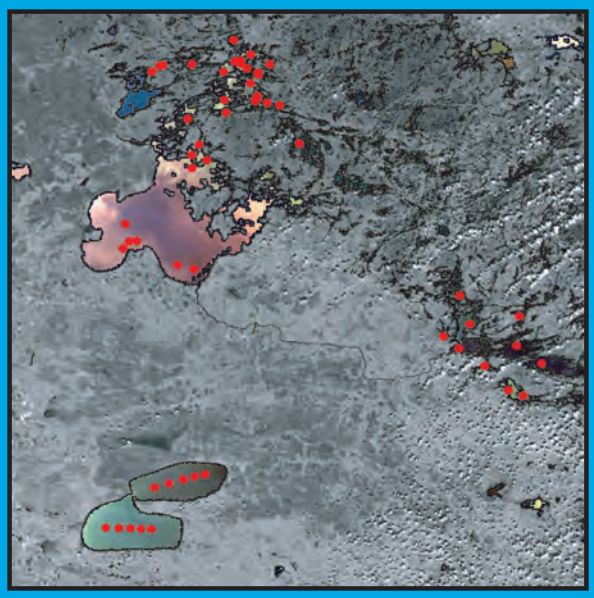

## A guide for resource managers and decision-makers

# *Remote sensing methods for lake management: A guide for resource managers and decision-makers*

Developed by

**The North American Lake Management Society**
***Madison, Wisconsin***

In collaboration with:

**University of Minnesota**
**University of Nebraska**
**University of Wisconsin**

**For the United States Environmental Protection Agency**

2009

## Remote sensing methods for lake management: A guide for resource managers and decision-makers.

This manual is the product of a collaborative effort that included researchers from three universities, assistance from several states and monitoring programs that provided field data, and overall coordination by the North American Lake Management Society. The individual contributions to the manual are listed below. Affiliations and further acknowledgements are noted on the following page. The manual should be cited as follows:

> Chipman, J.W., L.G.Olmanson and A.A.Gitelson. 2009. Remote Sensing Methods for Lake Management: A guide for resource managers and decision-makers. Developed by the North American Lake Management Society in collaboration with Dartmouth College, University of Minnesota, and University of Nebraska for the United States Environmental Protection Agency.

## Contents

**Chapter 1. Overview.** Steven A. Heiskary

**Chapter 2. Real-time proximal sensing of water quality.** Anatoly A. Gitelson, Donald C. Rundquist, Giorgio Dall'Olmo, Wesley Moses, and Bryan C. Leavitt

**Chapter 3. Airborne hyperspectral remote sensing.** Richard L. Perk, Donald C. Rundquist, Giorgio Dall'Olmo, and Anatoly A.Gitelson

**Chapter 4. Satellite remote sensing I: Landsat and other moderate-resolution systems.** Leif G. Olmanson, Marvin E. Bauer, and Patrick L. Brezonik

**Chapter 5. Satellite remote sensing II: High-resolution systems.** Leif G. Olmanson, Marvin E. Bauer, and Patrick L. Brezonik

**Chapter 6. Satellite remote sensing III: Regional-to global-scale systems.** Jonathan W. Chipman

**Chapter 7. Future developments in remote sensing for lake management.** Jonathan W. Chipman and Annette Schloss

**Chapter 8. Conclusions.** Jonathan W. Chipman, Leif G. Olmanson, Anatoly A. Gitelson, and Steven A. Heiskary

**Glossary**

**Appendix A. Remotely sensed spectra and bio-optical properties of lakes.** Anatoly A. Gitelson, Giorgio Dall'Olmo, and Wesley Moses

**Appendix B. The CDAP software package for field spectroradiometry.** Bryan Leavitt and Arthur I. Zygielbaum

**Appendix C. Processing AISA Eagle airborne hyperspectral imagery.** Richard L. Perk

**Appendix D. Recommended AISA Eagle band centers for aquatic targets (97 Bands).** Richard L. Perk and Anatoly A. Gitelson

**Appendix E. Example of CALMIT AISA Eagle mission planning form.** Richard L. Perk

**Principal authors:** Dr. Jonathan W. Chipman, Dartmouth College; Leif G. Olmanson, University of Minnesota; Dr. Anatoly A. Gitelson, University of Nebraska

**Technical review:** Dr. Marvin E. Bauer, University of Minnesota; Dr. Donald C. Rundquist, University of Nebraska; Dr. Annette Schloss, University of New Hampshire

**Redactory editing:** Janice Faaberg, Faaberg Editing Services, LLC

**Project management:** Steven A. Heiskary, Minnesota Pollution Control Agency

**Grant management and manual graphic design:** Philip S. Forsberg, North American Lake Management Society

This project and development of this manual was funded by the U.S. Environmental Protection Agency through a grant from the Office of Wetlands, Oceans and Watersheds.

## Contents

**Chapter 1. Introduction ..... 10**

1.1. Remote sensing methods for lake management: A guide for resource managers and decision-makers ..... 10

1.2. Remote sensing ..... 10

1.3. Summary ..... 11

**Chapter 2. Real-time proximal sensing of water quality ..... 12**

2.1. Terminology and physical principles ..... 12

2.2. Dual-spectroradiometer instrument configuration ..... 12

2.3. Data collection and calibration process ..... 13

2.4. Calculation of chlorophyll *a* and suspended matter concentrations ..... 16

2.5. Case studies ..... 17

2.6. Costs and resource requirements ..... 24

2.7. Conclusions ..... 25

2.8. References ..... 26

**Chapter 3. Airborne hyperspectral remote sensing ..... 27**

3.1. The AISA Eagle Hyperspectral Imager ..... 27

3.2. Case Study 1 – Fremont Lakes, Fremont, NE ..... 28

3.3. Case Study 2 – Pawnee Lake, NE ..... 33

3.4. Case Study 3 – Lake Minnetonka, MN ..... 34

3.5. Planning a successful mission ..... 36

3.6. Cost estimation ..... 39

**Chapter 4. Satellite remote sensing I: Landsat and other moderate-resolution systems ..... 41**

4.1. Introduction ..... 41

4.2. Acquiring Landsat imagery ..... 44

4.3. Case Study 1 – Statewide water clarity assessments for Minnesota, Wisconsin and Michigan ..... 45

4.4. Case Study 2 – Pilot water clarity assessments for Illinois, Indiana and Ohio ..... 47

4.5. Costs and resource requirements ..... 55

4.6. References ..... 56

**Chapter 5. Satellite remote sensing II: High-resolution systems ..... 58**

5.1. Introduction ..... 58

5.2. Acquiring high resolution imagery ..... 61
5.3. Case Studies – Overview ..... 62
5.4 Case Study 1 – Lake water clarity classification with IKONOS ..... 63
5.5 Case Study 2 – Aquatic vegetation surveys ..... 70
5.6. References ..... 75

**Chapter 6. Satellite remote sensing III: Regional- to global-scale systems ..... 77**

6.1. Introduction ..... 77
6.2. Acquiring MODIS and MERIS imagery ..... 82
6.3. Case study 1 – Estimating chlorophyll *a* concentration in Minnesota lakes ..... 83
6.4. Case study 2 – Estimating Secchi depth, chlorophyll *a* concentration, suspended solids, and turbidity in Green Bay and Lake Michigan ..... 87
6.5. Determining the number of lakes suitable for monitoring with MODIS at 500 m ..... 90
6.6. Costs and resource requirements ..... 91
6.7. References ..... 92
6.8. Acknowledgments ..... 92

**Chapter 7. Future developments in remote sensing for lake management ..... 93**

7.1. Access to new sensors ..... 93
7.2. Improvements in cyberinfrastructure ..... 94
7.3. Improvements in data analysis algorithms ..... 94

**Chapter 8. Conclusion ..... 95**

**Remote Sensing Glossary ..... 96**

**Appendix A. Remotely sensed spectra and bio-optical properties of lakes ..... 111**

A.1. Chlorophyll concentration retrieval ..... 111
A.2. Suspended matter concentration retrieval ..... 114
A.3. References ..... 114

**Appendix B. The CDAP software package for field spectroradiometry ..... 115**

B.1. CDAP features ..... 115
B.2. Examples of CDAP screens ..... 116

**Appendix C. Processing AISA Eagle airborne hyperspectral imagery ..... 121**

C.1. Level 1 data processing ..... 121
C.2. Level 2 processing ..... 124

**Appendix D. Recommended AISA Eagle band centers for aquatic targets (97 Bands) ..... 125**

**Appendix E. Example of CALMIT AISA Eagle mission planning form..... 126**

## List of Figures

**Figure 2.1.** Typical spectral reflectance curve from a eutrophic lake in midsummer.....13

**Figure 2.2.** Position of upwelling sensor.....14

**Figure 2.3.** Reflectance spectra of Nebraska and Iowa lakes and reservoirs taken in 2001 and 2002. .....20

**Figure 2.4.** Chlorophyll *a* concentrations measured in Nebraska and Iowa lakes and reservoirs. .....21

**Figure 2.5.** Comparison between predicted chlorophyll *a* concentration and lab-measured chlorophyll *a* in water samples.....23

**Figure 3.1.** Example of a spectral cube. .....27

**Figure 3.2.** The AISA Eagle airborne hyperspectral sensor. .....28

**Figure 3.3.** False-color composite image using three spectral bands of AISA Eagle data. .....29

**Figure 3.4.** Spectral reflectance for one pixel in the hyperspectral image. .....30

**Figure 3.5.** Pixels containing only water areas in the Fremont Lakes, NE imagery. .....30

**Figure 3.6.** Thematic map highlighting distribution of chlorophyll *a* .....31

**Figure 3.7.** Thematic map highlighting distribution of total suspended solids.....31

**Figure 3.8.** Chlorophyll *a* concentration and phycocyanin for the Fremont Lakes, NE 2005: (a) 3 May; (b) 6 June; (c) 7 July; (d) 5 August; (e) 9 September.....32

**Figure 3.9.** Multi-temporal series of chlorophyll, phycocyanin and total suspended solids concentration for Pawnee Lake, NE, April–July 2006.....33

**Figure 3.10.** Lake Minnetonka, MN, August 2005. .....34

**Figure 3.11.** Chlorophyll, Lake Minnetonka, MN, August 2005.....35

**Figure 3.12.** Phycocyanin, Lake Minnetonka, MN, August 2005. .....35

**Figure 3.13.** AISA estimates of chlorophyll *a* plotted vs. laboratory measurements of chlorophyll *a* concentrations.....36

**Figure 3.14.** Directional affects related to solar azimuth: (a) flying perpendicular to the solar azimuth; (b) flying parallel to the solar azimuth. .....37

**Figure 3.15.** AISA Eagle image illustrating problems with sun-glint and cloud shadows. .....38

**Figure 4.1.** Landsat TM imagery of east-central Minnesota, including the 7-county Twin Cities Metropolitan Area. .....43

**Figure 4.2.** Landsat TM imagery of the Lake Minnetonka area near Minneapolis, MN. .....44

**Figure 4.3.** Land-use/land-cover distribution and water clarity in three Minnesota ecoregions (Fig. 3 in Brezonik et al. 2007). .....46

**Figure 4.4.** Three-state Landsat-based 2000 water clarity map for Minnesota, Wisconsin and Michigan. .....47

**Figure 4.5.** 31 July 2006, path 23/rows 31– 5, Landsat TM image used for Illinois; 21 September 2004, path 21/rows 31–33, ETM+ SLC off image used for Indiana; and 12 August 2006, path 19/rows 31–33, ETM+ SLC off image used for Ohio water clarity assessments. .....49

**Figure 4.6.** 31 July 2006 Landsat lake clarity map of Illinois lakes with Landsat TM band 2 as the background. .....51

**Figure 4.7.** 21 September 2004 Landsat lake clarity map of Indiana lakes with Landsat ETM+ band 2 as the background. .....52

**Figure 4.8.** 12 August 2006 Landsat lake clarity map of Ohio lakes with Landsat ETM+ band 2 as the background. .....53

**Figure 4.9.** Example of variable water clarity in Lake Monroe near Bloomington, IN. The black lines across the lake are missing data due to the scan line corrector problem with Landsat 7 ETM+ data.....54

**Figure 4.10.** Water clarity distribution of Illinois, Indiana and Ohio lakes >6 ha. .....55

**Figure 5.1.** Comparison of spatial resolution of 30 m Landsat TM, 4 m IKONOS multispectral, 1 m IKONOS panchromatic and 0.6 m pan-sharpened mulitspectral QuickBird imagery.....59

**Figure 5.2.** Comparison of spatial coverage of Landsat TM and IKONOS images. .....60

**Figure 5.3.** Comparison of spatial coverage of IKONOS, QuickBird and SPOT 5 imagery with portion of Landsat TM image in background (a full Landsat TM image is 170 × 183 km). .....61

**Figure 5.4.** 1 September 2001 IKONOS imagery of the Lake Minnetonka area near Minneapolis, MN. Note haze and thin clouds on image with "less than" 10% cloud cover. .....63

**Figure 5.5.** 4 September 2001 IKONOS image of the City of Eagan, MN. .....64

**Figure 5.6.** 1 September 2001 IKONOS image of Swan Lake in Nicollet County, MN. .....65

**Figure 5.7.** 28 July 2002 QuickBird image of the Lake Minnetonka Area and three lakes used for aquatic vegetation surveys near Minneapolis, MN. .....66

**Figure 5.8.** Comparison of IKONOS and field measurements of lake water clarity, TSI(SD). .....68

**Figure 5.9.** Comparison of Landsat and IKONOS estimates based on Landsat modeling of lake water clarity, TSI(SD). .....69

**Figure 5.10.** Lake level lake water clarity classification of IKONOS multispectral data overlaid on panchromatic land image. (Imagery © Space Imaging L.P.).....70

**Fig. 5.11.** IKONOS image classification of aquatic vegetation of Swan Lake in Nicollet County, MN. .....72

**Fig. 5.12.** QuickBird image classification of aquatic vegetation of Christmas Lake near Minneapolis, MN (note Eurasian water milfoil associated with submerged plants dense class). .....74

**Fig. 5.13.** QuickBird image classification of aquatic vegetation of Christmas Lake near Minneapolis, MN. .....74

**Figure 6.1.** Terra MODIS true color image, 15 October 2005, bands 1, 4 and 3 displayed as red, green and blue. (a) Raw HKM image of entire scene. (b) Enlargement of southeast Wisconsin area. (c) Further enlargement of Madison Lakes region, showing 500-m resolution pixels. (d) For comparison, Landsat-7 ETM+ image of area shown in (c), 2 September 2001. .....79

**Figure 6.2.** Lake surface temperature map of the entire Great Lakes region, derived from the Aqua MODIS thermal-infrared bands, 18 April 2006. .....80

**Figure 6.3.** Estimated chlorophyll *a* concentration in Green Bay from Aqua MODIS imagery, 5 October 2004. (a) From standard MODIS Level-2 chlorophyll product, based on oceanographic chlorophyll algorithm using 1000 m MODIS bands. (b) From lake-specific algorithm using 500 m MODIS bands, resampled to 250 m. (c) Comparison of MODIS estimates from (b) with field-measured chlorophyll *a* concentrations. ....81

**Figure 6.4.** Re-projected true color MODIS image of Minnesota and western Ontario. ....84

**Figure 6.5.** Enlargement of the 1 August 2005 MODIS image of the Minnesota–Ontario border region. Bands 1, 4 and 3 displayed as RGB. ....85

**Figure 6.6.** Relationship between the MODIS blue/red spectral radiance ratio (bands 3/1) and the natural logarithm of chlorophyll *a* concentration for field-sampled lakes. ....85

**Figure 6.7.** Estimated chlorophyll *a* concentration for lakes along the Minnesota–Ontario border region, based on MODIS imagery, 1 August 2005. ....86

**Figure 6.8.** Error analysis of MODIS chlorophyll *a* predictions. ....86

**Figure 6.9.** Locations of GBMSD sampling stations in southern Green Bay, Lake Michigan. ....87

**Figure 6.10.** Analytical process for MODIS water quality mapping in Green Bay, Lake Michigan, WI. ....88

**Figure 6.11.** Example of MODIS water quality mapping in Green Bay, WI. ....89

**Figure 6.12.** Examples of MODIS-based turbidity maps for Green Bay, WI for dates in 2004: (a) June 4; (b) July 26; (c) August 6; and (d) September 10. White areas represent cloud cover on each date. ....89

**Figure 6.13.** Examples of lakes with buffers. Lakes that include any dark blue polygons are suitable for MODIS monitoring when viewing geometry is adequate. ....91

**Figure A.1.** Typical reciprocal reflectance (upper panel) and reflectance (lower panel) spectra of inland waters. Chl, CDOM, Tripton = maximal absorption by all chlorophyll (isoforms) present as well as absorption by colored dissolved organic matter and tripton; Car = maximal absorption by carotenoids; PC = maximal absorption by phycocyanin; A = the position of minimum absorption by chlorophyll *a*, inorganic suspended matter and water; B = minimal absorption by phytoplankton pigments; chl-*a* = maximal absorption by chlorophyll *a*. ....112

**Figure A.2.** Reflectance spectra of inland waters. ....113

**Figure B.1.** CDAP start-up screen. ....115

**Figure B.2.** Equipment configuration screen. Establishes which instruments are available and how they are connected to the computer. ....117

**Figure B.3.** Calibration screen. Provides data showing instrument response to measurement of white reference panel during instrument calibration (left panel) and its reflectance (right panel). ....117

**Figure B.4.** Data collection screen. Fields provided show Ocean Optics operating conditions, data from a GPS, datalogger, and other information. Graphs provide real-time measured upwelling radiance of reflectance panel, raw reflectance and calibrated reflectance (left panel); calibrated reflectances (central panel); and reciprocal of reflectance (right panel). ....118

**Figure B.5.** Current scan graph. Shows response from white reference panel (magenta), raw reflectance (green) and calibrated reflectance (white). Note: all graphs can be magnified to full screen. ....118

**Figure B.6.** Calculated reflectance graph. Traces are color-coded by age of scan; most recent scan is white. ....119

**Figure B.7.** Calculated inverse reflectance graph. Trace colors correspond to those in Fig. B.6. ....119

**Figure B.8.** Post-processing set-up screen. Indicates the source directory for data and required parameters. CDAP will automatically process all raw data in the directory. During processing reflectance, upwelling radiance and downwelling irradiance are retrieved and are written to tab-delimited text files that can be imported into an Excel spreadsheet.... 120

**Figure B.9.** Post-processed reflectance for waters studied. Data were exported from CDAP as text files and imported into an Excel spreadsheet for analysis.... 120

**Figure C.1.** Raw AISA image.... 121

**Figure C.2.** C-Midgets III Inertial Motion Unit.... 122

**Figure C.3.** Labsphere URS-600, NIST traceable power supply, light source and integrating sphere.... 122

**Figure C.4.** Level 1 AISA Processing Stream.... 123

**Figure C.5.** Rectified reflectance image.... 124

**Figure C.6.** Spectral reflectance graph.... 124

**Figure C.7.** Atmospherically corrected spectral reflectance profile.... 124

## List of Tables

**Table 1.1.** Remote sensing sensor characteristics.... 11

**Table 2.1.** Descriptive statistics of the measured optical water quality parameters. (a) Calibration dataset. Nebraska and Iowa lakes and reservoirs measured in 2001–2002; 145 stations. (b) First validation dataset. Nebraska lakes and reservoirs measured in 2003; 155 stations. (c) Second validation dataset. Nebraska lakes and reservoirs measured in 2005; 85 stations. (d) Third validation dataset. Lake Minnetonka, MN, August 2005; 17 stations. (e) Fourth validation dataset. Choptank River, MD, April 2006; 18 stations.... 19

**Table 2.2.** (a) Results of the three-band algorithm (Eq. 2.2) validation with wavebands (center/width) $\lambda_1$ = 670/10 nm, $\lambda_2$ = 720/30 nm, $\lambda_3$ =740/20 nm. (b) Results of three-band algorithm (Eq. 2.2) validation after removing outliers.... 22

**Table 4.1.** Specifications of satellite systems suitable for lake monitoring.... 42

**Table 4.2.** Lake clarity classifications statistics for Illinois, Indiana and Ohio.... 50

**Table 5.1.** Specifications of satellite systems suitable for lake monitoring.... 62

**Table 5.2.** Comparison of IKONOS and field survey estimates of the distribution of aquatic vegetation diversity in Swan Lake, MN.... 73

**Table 5.3.** Accuracy of IKONOS image classification of aquatic vegetation for Swan Lake, MN.... 73

**Table 6.1.** Spectral bands on MODIS. Bands 1–5 and 8–16 are the most useful bands for lake water quality monitoring. Bands 17–36 are primarily used for atmospheric applications.... 78

**Table 6.2.** Lakes that should be routinely suitable for MODIS monitoring.... 90

**Table 6.3.** Routine MODIS lakes in Wisconsin, as a function of lake size.... 90

# Chapter 1. Introduction

## 1.1. Remote sensing methods for lake management: A guide for resource managers and decision-makers

The U.S. Environmental Protection Agency (EPA) and the states have a responsibility to assess the water quality of the nation's lakes. According to EPA's 2000 Water Quality Report, the overall percentage of assessed lakes has not increased in recent years, and comparisons in that same report suggest that the percentage may have decreased relative to previous assessments. Financial resources at the federal, state and local level are insufficient to assess lakes in a timely fashion using conventional methods.

The EPA has stated the need to survey the nation's lakes to answer key questions about their quality. Drawing from their 2005 fact sheet:

- What percent of the nation's lakes are in good, fair and poor condition for key indicators of ecological health and human activities?
- What is the relative importance of stressors such as nutrients and pathogens?

The EPA collaborated with the states, tribes and USGS to develop a statistically-based survey that allows national and regional estimates of the condition of lakes and reservoirs. The 2007 survey employed random sample sites and consistent procedures at all sites to ensure the results can be compared across the country. Given the goals of the national survey, remote sensing may serve to complement the on-the-ground assessment of lakes and has the potential to allow cost effective assessment of all lakes.

Recent improvements in sensor design and advances in data analysis have made the prospect of the remote sensing of lake-water quality an emerging technology. The results from various projects using remote sensing for assessment of lake water quality are quite promising and are now being used routinely in some states (*e.g.*, Michigan, Minnesota, and Wisconsin) as part of their overall lake assessment efforts.

Several questions remain, however, concerning the most appropriate platforms (sensors) for different applications; true costs associated with the various platforms; availability of remote-sensed images and appropriateness of the various models for translating the images into usable estimates of water quality; and various related details. The North American Lake Management Society (NALMS) has recognized the role remote sensing can play in the assessment of water quality and has drawn on the expertise of several universities and states with experience in remote sensing to answer these questions and make the techniques more widely available for states interested in using these technologies.

## 1.2. Remote sensing

NALMS, EPA and the Universities of Minnesota, University of Nebraska, Lincoln and University of Wisconsin, Madison collaborated on this retrospective assessment of several available remote sensing platforms (*e.g.*, AISA, IKONOS, Landsat, MODIS and MERIS). In addition, Landsat assessment of lakes was applied to paths of Landsat imagery in Illinois, Indiana and Ohio. Each participating state received a prototype water clarity assessment for their state.

The platforms represent remote sensing at a broad range of spatial, spectral and radiometric resolutions (Table 1.1) to allow direct comparison and assessment of the limitations and strengths of each platform and help determine

the resolutions best suited for specified water quality monitoring goals, with an emphasis on developing remote sensing methods that can be used effectively for routine regional monitoring of lakes.

**Table 1.1.** Remote sensing sensor characteristics.

| Sensor | | Spatial Resolution | Spectral Resolution | Spatial Coverage | Notes |
|---|---|---|---|---|---|
| Proximal sensing | *In situ* | Very high | High | Low | Selected water bodies |
| Aircraft-based Hyperspectral / Multispectral | 0.5 - 3 m | High | High | Low | Selected water bodies |
| Commercial High Resolution. Satellite: IKONOS & Quick Bird | 0.6 - 4 m | High | Low | Low | Small water bodies |
| Landsat | 30 m | Moderate | Moderate | Moderate | Archive: 1972-present lakes ≥10 acres |
| MERIS | 300 m | Relatively Low | High | High | Large water bodies |
| MODIS | 500 – 1000 m | Low | High | High | Large; daily coverage |

An overview of each platform and sampling methodology follows in subsequent chapters. Case studies are used to demonstrate applications of the platform and specific considerations for its use; cost and resource requirements are addressed. The discussion proceeds from high resolution, low spatial coverage sensors (*e.g.,* boat-based, real time) to low resolution, high spatial coverage satellite-based applications (*e.g.*, MODIS). References are provided at the end of each chapter to provide ready access to pertinent literature associated with each platform. A glossary of terms and sources of additional information, including web site links for further information, are also provided.

## 1.3. Summary

Remote sensing holds great promise for lake assessment. Numerous platforms are available for application that can address a variety of questions routinely encountered in the course of lake and watershed studies. Selection of the appropriate platform will be dependent on several factors, including the size and number of lakes to be assessed, degree of resolution and cost of the various applications. NALMS, along with the Universities of Nebraska, University of Wisconsin, University of Minnesota and the U.S. EPA, provide detailed explanations of the various platforms currently in use, preferred applications, limitations, costs and other factors that should help users select the best platform for their data needs. While remote sensing cannot replace all on-the-ground (or on-the-lake, as the case may be) sampling, it can serve to complement existing sampling programs and often allows a broader extrapolation of information.

# Chapter 2. Real-time proximal sensing of water quality

This chapter describes methods for using data collected *in situ* (on or in the water) to assess various components of the water column in real time. The technique, which is based on specific spectral features associated with reflected light, allows identification of pigments (*e.g.*, chlorophyll *a*) and total suspended matter in water bodies. Thus, Chapter 2 objectives are to: (1) explain the terminology and physical principles of real-time proximal sensing of chlorophyll *a* and total suspended solids in the water column; (2) describe the hardware and software necessary to implement such a system; (3) provide an overview of the calculations and procedures used in data analysis; and (4) summarize some of the research findings from case studies.

## 2.1. Terminology and physical principles

The term "proximal sensing" refers to data collection using an instrument in close proximity to the target (*i.e.*, the water body being studied), as opposed to "remote sensing" or data collection by means of aircraft or satellites. For the system described in this chapter, the light-collecting mechanism associated with the instrument is positioned slightly below the surface of the water.

The water-quality inferences drawn from the data will be the result of spectroscopic analyses conducted in a field setting, known as "field spectroscopy." This technology can be defined as the production and analysis of spectra and the physics related to the theory and interpretation of interactions between matter and electromagnetic radiation (Bauer *et al*. 1986). In simple terms, our interest is determining how light of many different wavelengths is reflected or absorbed by various components of the water column.

The specialized field instrument used to collect *in situ* spectral data is a spectroradiometer. In contrast to the systems described in subsequent chapters of this report, the principal output product from a spectroradiometer is not an image, but rather numerical data summarizing reflectance values acquired in different spectral channels at a single location. These measurements can be used to compile a graph (or spectral profile). The most detailed spectral-response profiles are constructed with data collected by "hyperspectral" instruments. Such instruments have higher than multispectral resolution (*i.e.*, hundreds or even thousands of spectral channels or "bands"), each covering a very small part of the total electromagnetic spectrum (as little as one nanometer). The sensor may include bands in different spectral regions, such as visible and/or near-infrared. The resulting spectral curves are often considered diagnostic because distinct reflectance and/or absorbance features provide useful information to the skilled analyst.

The reflectance spectrum produced by a spectroradiometer is generally displayed as a simple graph with wavelength on the x-axis and reflectance, or the reciprocal (inverse) of reflectance, on the *y*-axis (Fig. 2.1). These spectral profiles or curves are viewed and interpreted by the analyst to identify specific spectral features associated with each constituent, and the characteristics of the spectral features help determine the concentrations of components comprising the water column (see Appendix A for a detailed discussion).

## 2.2. Dual-spectroradiometer instrument configuration

The hardware configuration used for all studies described in this chapter was developed at the Center for Advanced Land Management Information Technologies (CALMIT), University of Nebraska-Lincoln. It consists of two Ocean Optics USB-2000 spectroradiometers, along with the fiber-optic cables, calibration panel, portable computer and software needed to collect and record data. This system is operated from a boat and is designed to

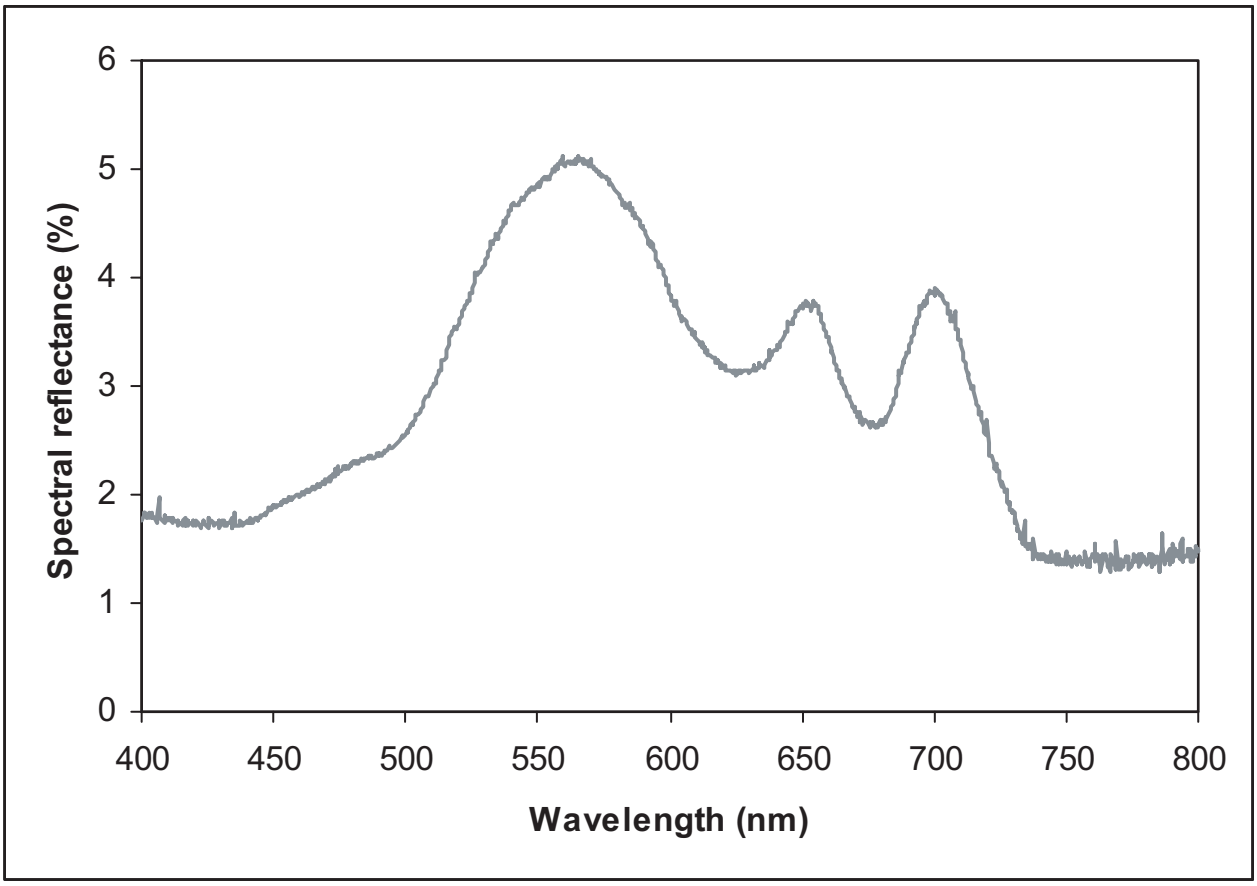


**Figure 2.1.** Typical spectral reflectance curve from a eutrophic lake in midsummer.

produce simultaneous measurements of the downwelling sunlight, or incident solar irradiance, and the upwelling reflected light (radiance) from the water. Using this dual-spectroradiometer system, data can be collected in the range of 400–900 nm with a sampling interval of 0.3 nm and a spectral resolution of ~1.5 nm.

A fiber-optic cable used to capture the light upwelling in the water column is attached to one Ocean Optics spectroradiometer and the other end of the cable is placed slightly below the surface of the water. Simultaneously, a second fiber-optic cable pointed at the sky delivers the downwelling sunlight to the second spectroradiometer. Each spectroradiometer divides the incoming signal (downwelling solar irradiance or upwelling reflected radiance) into many channels or bands, each covering a narrow range of wavelengths. Software installed on a laptop computer then calculates spectral reflectance, dividing the amount of upwelling light by the amount of downwelling light, in each narrow spectral band. This ability to simultaneously measure incoming and reflected radiation makes the calculated reflectance values much less dependent on weather and illumination conditions than upwelling irradiance alone.

The software used to process the data collected by the spectroradiometer, referred to as the CALMIT Data Acquisition Program (CDAP; see Appendix B), is available to users for a license fee from CALMIT at the University of Nebraska-Lincoln.

## 2.3. Data collection and calibration process

This system includes two fiber-optic probes, one pointed downward (at nadir) to measure the light upwelling from a water column within a field of view (FOV) of 25°, and another pointed upward to measure incident

light within a FOV of 180° (*i.e.*, measuring incoming light from the entire hemisphere of the sky). The sensor measuring the upwelling energy (connected to spectroradiometer 1) is pointed downward to measure the below-surface upward radiance on the sunny side of the boat. The tip of the fiber-optic cable should be positioned slightly below (5–10 cm) the surface (Fig. 2.2). If the tip is above the surface of the water, data may be affected by sun glint and water surface conditions (Han and Rundquist 1998). Maintaining the tip at a uniform depth should be the goal but may be difficult due to wave motions. Likewise, the end of the fiber-optic cable should be kept in a fixed vertical position if possible. If the cable is to be hand-held (*e.g.*, at the end of a pole), the same sensor orientation (and depth) should be maintained during the entire data-collection campaign. It may be helpful to have the same person position the sensor during data collection to facilitate consistency. Further, the fiber-optics cable should be held as far away from the boat as possible to minimize any extraneous reflections from the surface of the hull itself. If data are to be taken over a white reference panel for calibration purposes following immersion, watch for and remove any water droplets adhering to the fiber tip. Above all, use the exact same procedures each time data are collected.

To simultaneously measure incident irradiance, the second fiber-optic cable (connected to radiometer 2) should be fitted with a cosine collector, mounted on a mast at least 2–2.5 m in length, pointed upward, and positioned so the 180° field of view does not include people and/or parts of the boat platform itself. The integration time of this radiometer is up to 10 times shorter than that of radiometer 1; however, the variations in illumination conditions can be considered negligible during the short time required to collect one measurement (~30 sec). The data recorded by radiometer 2 are considered representative of the overall downward irradiance. (Note that solar zenith angles should be higher than 25° during data collection.)

Fiber-optic cables must be handled with care. Cable kinks can lead to broken fibers and thus significant expense to replace it. Coil the fibers in large loops for storage and house them in a hard-plastic case to prevent crushing during transport (and use caution when closing the lid of such cases). Similarly, organize and tie all cables out of the way on the boat so they will not be crushed by the feet of researchers during data collection.

Using the proper equipment configuration (Fig. 2.2), water quality can be inferred in real time by travelling at a relatively rapid rate across a water body while characterizing the water column. In doing so, locations that are anomalous or in need of physical sampling can be quickly and easily discerned. Alternatively, the sensor could be attached to a fixed platform (*e.g.*, a bridge or a buoy) and used to document changing water-quality conditions over time.

**Figure 2.2.** Position of upwelling sensor.

Finally, note that all measurements should be taken over optically deep water (*i.e.*, where the bottom of the water body cannot be seen).

### Calibration procedures

Calibration of the spectroradiometers is a necessary prerequisite for the collection of high-quality data. This includes an initial intercalibration of the two spectroradiometers by a trained technician at CALMIT and a series of calibrations during each field campaign using a white reference panel. The latter process involves simultaneously measuring the upwelling radiance $L_{cal}(\lambda)$ from the white reference panel and the corresponding incident irradiance $E_{cal}(\lambda)$. This calibration should be performed before and just after measurement at each water body.

Reference panels are made of a bright, white, highly reflective hard plastic material called "Spectralon." Panels provide a link to national standards. The principal assumptions related to white reference (calibration) panels are: (a) they are "Lambertian," thus reflecting incoming solar energy in all directions; and (b) they reflect incoming solar energy equally at all wavelengths.

To help ensure a reliable calibration process:

- Use a boom or mast to position the fiber-optic above the panel
- Hold the boom or mast in a horizontal position, but orient it in the direction of the sun (ideally in the principal plane of the sun)
- Maintain the fiber in the same position (preferably vertical) above the panel during each calibration sequence
- Maintain the same distance above the panel from one calibration to the next
- Avoid shadowing the surface of the panel
- Do not stand near the panel when calibrating (or, if this is impossible, stand in the same position during each calibration)
- Maintain consistent clothing color from one calibration sequence to the next
- Do not scan the panel when sky conditions are fluctuating rapidly (*e.g.*, cirrus clouds)
- The best situation is a clear, steady sky
- Take at least three calibration scans

For proper maintenance of calibration panels:

- Do not touch the surface of a reference panel
- Protect panel during transport so the surface is not damaged
- Keep the calibration panel clean, but do not attempt to clean the surface without proper instruction

### Calculation of reflectance

The remote-sensing reflectance at nadir is computed as:

$$R_{rs}(\lambda) = 100\left(\frac{L_{up}(\lambda)}{E_{inc}(\lambda)}\right)\left(\frac{E_{cal}(\lambda)}{L_{cal}(\lambda)}\right)R_{cal}(\lambda)\left(\frac{t}{n^2}\right)\left(\frac{F(\lambda)}{\pi}\right) \qquad \text{[Eq. 2.1]}$$

where $L_{up}(\lambda)$ is the below-surface upwelling radiance at nadir; $E_{inc}(\lambda)$ is the downwelling irradiance measured by the cosine corrector simultaneously with the upwelling measurement; $L_{cal}(\lambda)$ is the upwelling radiance from the white Spectralon reflectance standard; $E_{cal}(\lambda)$ is the irradiance incident on the calibration panel; $R_{cal}(\lambda)$ is the reflectance of the Spectralon panel linearly interpolated to match the band centers of each radiometer; $t$ is the water-to-air transmittance taken equal to 0.98; $n$ is the refractive index of water relative to air taken equal to 1.33; $F = 0.303$ is the spectral immersion factor computed following Ohde and Siegel (2003); and $\pi$ is used to transform the irradiance reflectance $R_{cal}$ into a remote sensing reflectance.

The field data should be checked to be sure that useful, high-quality information is being obtained by the instruments and properly stored. If a problem is encountered, the measurements must be repeated immediately. Finally, it is imperative that field teams back up their data in the field. Do not leave the field without both the original dataset and one copy.

## 2.4. Calculation of chlorophyll *a* and suspended matter concentrations

A detailed discussion of the relationship between spectral features and water column constituents is provided in Appendix A. Those relationships can be used to calculate the concentration of chlorophyll *a* and suspended matter.

To calculate chlorophyll *a* (chl-*a*) concentration:

- Calculate the average of reflectance (R) in three spectral bands: band 1 = 665–675 nm; band 2 = 705–725 nm; band 3 = 730–755 nm
- Calculate reciprocal of reflectance ($R^{-1}$) in spectral band 1 = 665–675 nm and in band 2 = 705–725 nm
- Calculate chl-*a* using the equation (Gitelson *et al*. 2008, 2009):

$$chla = (23.09 \pm 0.98) + (117.42 \pm 2.49) \times \left(R^{-1}_{665-675} - R^{-1}_{705-725}\right) \times \left(R_{730-755}\right) \quad \text{[Eq. 2.2]}$$

To calculate total suspended matter (TSS) concentration (*e.g.*, Curran and Novo 1988; Doxaran *et al*. 2002, 2005):

- Calculate the average of reflectance (R) in spectral band 540–560 nm
- Calculate the average of reflectance (R) in spectral band at 730–740 nm
- Calculate non-calibrated TSS using the following equation:

$$TSS = \frac{R_{730-740}}{R_{540-560}} \quad \text{[Eq. 2.3]}$$

These TSS values are in arbitrary units that can be used to compare the relative levels of TSS at different locations in the water body under study; however, they do not represent the actual concentration of TSS. To calculate concentrations of TSS, calibrate equation 2.3 using a few analytical (derived in the lab) measurements of TSS. The coefficients for the relationship between TSS and R(730–740)/R(540–560) depends significantly on the origin and particle-size distribution of suspended matter, and may vary widely between water bodies with different compositions of suspended matter and origins of nonorganic particles.

## 2.5. Case studies

The methods described in this chapter have been used to retrieve "optically active" constituent concentrations and have yielded excellent results (Dall'Olmo *et al*. 2003; Dall'Olmo and Gitelson 2005, 2006; Gitelson *et al*. 2007, 2008). These studies establish that the spectral-reflectance information (*i.e.*, the signal upwelling from the water column) can provide accurate estimates of the concentration of chlorophyll *a*.

### Study sites

To assess the accuracy of this technique for predicting chl-*a* concentrations we used five independent datasets containing the spectral and optical water column properties. The first was used for model calibration while the second through fifth were used for model validation. The calibration dataset, containing 145 samples, was acquired in 2001–2002 in lakes and reservoirs in Nebraska and Iowa. Two complementary types of eastern Nebraska water bodies were sampled: (1) sandpit lakes with particulates dominated by algae, and (2) reservoirs with a gradient of suspended sediments elevated near the inlet and gradually declining near the dam. Data were collected in 19 campaigns, from June to October 2001 and from May to October 2002. The calibration dataset also included 16 stations collected at Lake Okoboji, Iowa (for details see Dall'Olmo and Gitelson 2005). The second and third datasets were collected from April to October 2003 and 2005 in sandpit lakes and reservoirs in eastern Nebraska and contained 155 and 85 stations, respectively. The fourth dataset containing 17 stations was collected in Lake Minnetonka (MN) on 17 August 2005, and the fifth one containing 18 stations was collected in the Choptank River (Chesapeake Bay, MD) on 5–6 April 2006.

### Accuracy assessment

To find the optimal positions and the width of each band to be used in the conceptual model, linear best-fit functions between chl-*a* and the three-band model (Eq. 2.2) were calculated using an iterative approach. The accuracy of chl-*a* prediction was then assessed for the four validation datasets by comparing the predicted chl-*a* values with those measured analytically in the laboratory. This comparison was quantified by means of the percent difference between predicted chl-*a* (chl$a_{pred}$) and analytically measured chl-*a* (chl$a_{meas}$):

$$\varepsilon_i = 100\left(\frac{chla_{\,pred,i} - chla_{\,meas,i}}{chla_{\,meas,i}}\right) \qquad \text{[Eq. 2.4]}$$

Systematic and random errors were characterized by the mean normalized bias (MNB) and by the normalized root mean square error (NRMS), respectively:

$$\text{MNB} = \text{mean}\,(\varepsilon_i)\ \% \qquad \text{[Eq. 2.5]}$$

$$\text{NRMS} = \text{stdev}\,(\varepsilon_i)\ \% \qquad \text{[Eq. 2.6]}$$

We also characterized the accuracy of chl-*a* prediction for all data acquired, with some outliers excluded. Stations for which $\varepsilon_i > 2\text{stdev}(\varepsilon)$ were considered outliers and removed (Zibordi *et al*. 2004), and MNB, NRMS, slopes and intercepts of the chl$a_{pred,i}$ – chl$a_{meas,i}$ relationships were recalculated.

### Field measurements

A standard set of water quality parameters was measured at each station, including Secchi disk depth (measured using a standard white disk) and turbidity (measured using a portable Hach 2100 turbidimeter). In addition, surface water samples were collected at a depth of 0.5 m below the surface and stored in the dark in a cooler with ice. Surface samples were filtered on the day of collection on Gellman type A/E glass-fiber filters and frozen for laboratory analyses of chl-*a*, CDOM and TSS.

Hyperspectral reflectance measurements were taken from a boat using the previously described dual-spectroradiometer system. The tip of the optical fiber was kept just below the water surface on the sunny side of the boat by means of a 2-m long, hand-held black pole. Interferences in the light field by the boat and the equipment were considered negligible owing to the small diameter (~0.5 cm) of the tip of the optical fiber and the high turbidity of these waters. Most of the waters sampled had rather short fetches (on the order of tens of meters) and were protected by trees; thus, even under windy conditions, waves were almost absent, except for the Choptank River, where waves of 1 m occurred on the first day of a two-day field campaign.

As described previously, downwelling irradiance measurements were taken simultaneously with the upwelling data. Solar zenith angles ranged from approximately 20° to a maximum of 55°. All measurements were taken over optically deep water.

The critical issue with regard to the dual-fiber approach is that the transfer functions, which describe the relationship of the incident flux impinging on the sensor to the data numbers produced by both radiometers, should be identical. We analyzed the identity of the two radiometers used in this study and confirmed that the difference between their transfer functions did not exceed 0.4% (Dall'Olmo and Gitelson 2005).

### Constituent concentrations and compositions

The datasets encompassed varying optical conditions and included a wide range of phytoplankton taxonomic groups including Chrysophyta, Chlorophyta, Cyanophyta, Cryptophyta and Pyrrophyta. In each of the datasets taken in Nebraska and Iowa from 2001 through 2005, the concentrations of chl-*a*, TSS, OSS and ISS, as well as the Secchi disk depth and turbidity, varied over two orders of magnitude (*e.g.*, 1–240 mg chl-*a* $m^{-3}$, 0.2 – 210 g TSS $m^{-3}$). In Lake Minnetonka, chl-*a* varied more than 10-fold while Secchi depth and TSS spanned 7-fold and 6-fold, respectively. In the Choptank River, chl-*a* varied 14-fold and turbidity changed more than 2-fold (Table 2.1).

As in the case of the first dataset taken in Nebraska in 2001–2002 (Dall'Olmo and Gitelson 2005), chl-*a* and TSS in the subsequent datasets were not significantly correlated. For all datasets the coefficient of determination ($r^2$) for a linear relationship between chl-*a* and TSS was lower than 0.1 ($p > 0.8$). The lack of a significant relationship between chl-*a* and TSS indicated that each parameter was independently controlling the optical properties of these waters.

### Reflectance spectra

Remote sensing reflectance was highly variable over the visible and near-infrared spectral regions. Spectra recorded in all five datasets (Fig. 2.3 for the Nebraska calibration dataset) were quite similar in magnitude and shape to typical reflectance spectra collected in turbid productive waters. Reflectance in the blue range (400–500 nm) was very low. In the lakes and reservoirs of Nebraska and Iowa, the reflectance was below 0.005 $sr^{-1}$, with more than a 10-fold variation between stations. In Lake Minnetonka the blue reflectance was even lower (below 0.003 $sr^{-1}$). Reflectance in this spectral region did not have pronounced spectral features for the broad range of turbidity and chl-*a* concentrations at all sites; a reflectance minimum near 440 nm, corresponding to the chl-*a* absorption peak, was distinct only when chl-*a* was >150 $mg/m^3$.

Reflectance in the green range (500–600 nm) was much higher than in the blue range (Fig. 2.3). Green reflectance (around 550 nm) varied from 0.002 to 0.02 $sr^{-1}$ for the lakes and reservoirs in Nebraska, manifesting high variability in scattering and also in $a_{CDOM}$ and $a_{tript}$ between samples. In Lake Minnetonka and the Choptank River, the variability of green reflectance was lower (3-fold and 4-fold, respectively), and minimal reflectance values were not as low as for the lakes and reservoirs in Nebraska and Iowa (about 0.005 $sr_{-1}$ as opposed to 0.002 $sr^{-1}$).

**Table 2.1.** Descriptive statistics of the optical water quality parameters measured: TSS, total suspended solids; ISS, inorganic suspended solids; OSS, organic suspended solids; $a_{cdom}$(440 nm), absorption coefficient of CDOM at 440 nm; $a_{tripton}$(440), absorption coefficient of tripton at 440 nm; SD, standard deviation and CV = (SD/average of parameter), coefficient of variation in %. (a) Calibration dataset. Nebraska & Iowa lakes and reservoirs measured in 2001–2002; 145 stations. (b) First validation dataset. Nebraska lakes and reservoirs measured in 2003; 155 stations. (c) Second validation dataset. Nebraska lakes and reservoirs measured in 2005; 85 stations. (d) Third validation dataset. Lake Minnetonka, Minnesota, August 2005; 17 stations. (e) Fourth validation dataset. Choptank River, Maryland, April 2006; 18 stations.

| a. | min | max | median | average | SD | CV |
|---|---|---|---|---|---|---|
| Chlorophyll *a*, mg/m$^3$ | 4.4 | 217.3 | 36.1 | 46.3 | 41.2 | 89 |
| Secchi disk depth, cm | 18 | 299 | 63 | 81 | 56.8 | 70 |
| Turbidity, NTU | 1.7 | 78.0 | 16.9 | 20.1 | 15.7 | 78 |
| TSS, mg/L | 0.2 | 213.5 | 14.0 | 20.4 | 25.9 | 127 |
| OSS, mg/L | 0.5 | 213.5 | 10.0 | 13.7 | 25.8 | 188 |
| ISS, mg/L | 0.0 | 139.8 | 2.5 | 7.6 | 15.3 | 201 |
| $a_{cdom}$(440), 1/m | 0.5 | 4.4 | 1.0 | 1.2 | 0.66 | 55 |
| $a_{trip}$(440), 1/m | 0.4 | 6.7 | 2.0 | 2.2 | 1.34 | 60 |

| b. | min | max | median | average | SD | CV |
|---|---|---|---|---|---|---|
| Chlorophyll *a*, mg/m$^3$ | 1.7 | 236.5 | 18.4 | 26.6 | 32.99 | 124 |
| Secchi disk depth (cm) | 27 | 409 | 83 | 111 | 79.66 | 72 |
| Turbidity, NTU | 1.3 | 67.5 | 8.5 | 11.6 | 10.08 | 87 |
| TSS, mg/L | 2.0 | 45.5 | 11.5 | 14.6 | 9.97 | 68 |
| OSS, mg/L | 2.0 | 34.5 | 8.0 | 9.3 | 5.76 | 62 |
| ISS, mg/L | 0 | 32.0 | 1.8 | 5.2 | 6.85 | 131 |
| $a_{cdom}$(440) , 1/m | 0 | 4.4 | 0.9 | 1.3 | 1.01 | 78 |
| $a_{trip}$(440) , 1/m | 0.3 | 6.5 | 1.3 | 1.5 | 0.98 | 64 |

| c. | min | max | median | average | SD | CV |
|---|---|---|---|---|---|---|
| Chlorophyll *a*, mg/m$^3$ | 1.2 | 202.8 | 15.0 | 41.2 | 50.1 | 122 |
| Secchi disk depth (cm) | 21 | 371 | 93 | 104 | 73.9 | 71 |
| Turbidity, NTU | 1.6 | 57.0 | 7.2 | 14.0 | 13.3 | 95 |
| TSS, mg/L | 2.0 | 32.5 | 7.8 | 12.0 | 9.0 | 75 |
| ISS, mg/L | 1.8 | 28.6 | 6.7 | 10.03 | 8.3 | 82 |
| $a_{cdom}$(440) , 1/m | 0.3 | 1.77 | 0.62 | 0.68 | 0.30 | 44 |
| $a_{trip}$(440) , 1/m | 0.13 | 4.34 | 0.78 | 0.94 | 0.75 | 80 |

| d. | min | max | median | average | SD | CV |
|---|---|---|---|---|---|---|
| Chlorophyll *a*, mg/m$^3$ | 7.03 | 97.1 | 16.39 | 32.2 | 26.4 | 0.99 |
| Secchi disk depth (cm) | 40 | 310 | 120 | 141 | 90 | 0.68 |
| TSS, mg/L | 2.8 | 19 | 5.2 | 8.6 | 5.9 | 0.69 |

| e. | min | max | median | average | SD | CV |
|---|---|---|---|---|---|---|
| Chlorophyll *a*, mg/m$^3$ | 4.26 | 60.9 | 8.7 | 15.6 | 14.2 | 0.91 |
| Turbidity, NTU | 8.9 | 25.3 | 13.9 | 15.1 | 25.3 | 1.68 |

Multiple factors contribute to the reflectance patterns in the blue and green spectral regions, including absorption by dissolved organic matter and tripton as well as backscattering by particulate matter. As a result, the blue to green ratio R(440)/R(550) (Gordon and Morel 1983) was poorly related to chl-*a*. For all datasets, the $r^2$ of the chl-*a* versus R(440)/R(550) relationship was below 0.3 ($p < 0.007$); thus, this algorithm was inadequate for estimating chl-*a* in these Case-2 waters.

In the red region (600–700 nm), reflectance had several spectral features. Waters containing blue-green algae exhibited a reflectance trough around 625 nm (Fig. 2.3). A second minimum around 675 nm corresponds to the red chl-*a* absorption maximum and was pronounced for chl-*a* >10 mg/m$^3$. However, as in Dall'Olmo and Gitelson (2005) and Gitelson *et al.* (2007), the reflectance around 675 nm was poorly correlated with chl-*a* concentrations, which was responsible for only 3–5% variation in $R_{rs}(675)$. As described above, in addition to chl-*a*, the reflectance near 675 nm was also affected by absorption and scattering by other constituents.

A distinct peak located between 690 nm and 715 nm (with the peak toward 690 nm for low chl-*a* and 715 nm for high chl-*a*), appeared in almost all spectra for chl-*a* exceeding 5 mg/m$^3$. This peak is the result of both high backscattering and a minimum in absorption by all optically active constituents (Vasilkov and Kopelevich 1982, Gitelson 1992). The magnitude of the peak varied widely, being comparable with the magnitude of the green peak for moderate-to-high chl-*a* (Fig. 2.3). As in other turbid productive waters, chl-*a* was poorly related to the magnitude of the peak; for all datasets the $r^2$ of the peak magnitude versus chl-*a* relationship was between 0.02 and 0.07 ($p < 0.7$), which illustrates that backscattering by inorganic and nonliving organic suspended matter played a critical role and largely controlled reflectance in this spectral region.

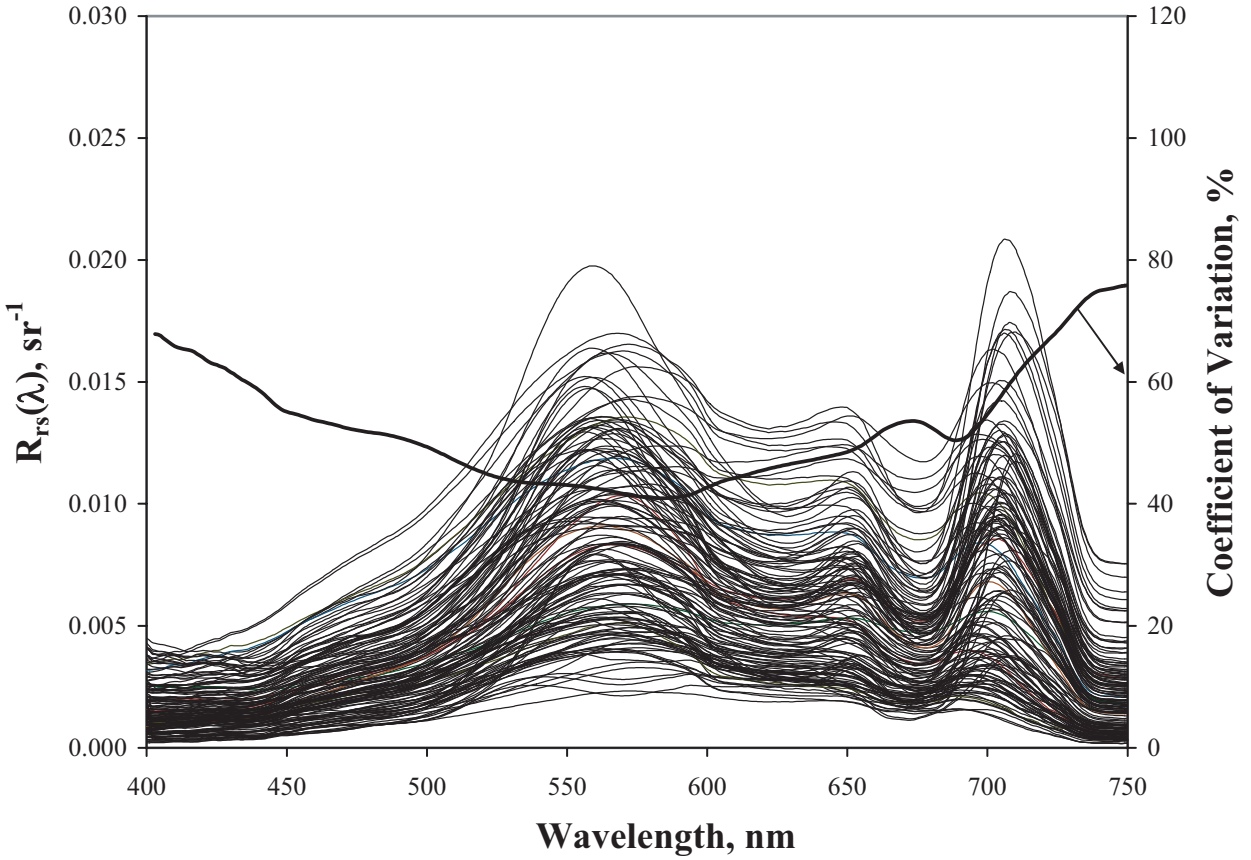


**Figure 2.3.** Reflectance spectra of Nebraska and Iowa lakes and reservoirs taken in 2001 and 2002. Coefficient of variation is calculated as std/average (R), where std is standard deviation of reflectance, R.

Finally, reflectance in the near-infrared range (700–750 nm) varied widely, reaching 0.008 $sr^{-1}$ and being consistently higher than the reflectance in the blue range (Fig. 2.3). The coefficient of variation of reflectance in this spectral region was greater than in the blue, green or red portions of the spectrum, varying between 75 and 110% for the lakes and reservoirs in Nebraska and Iowa as well as for Lake Minnetonka, and >30% for the Choptank River (Fig. 2.3). In this region of the spectrum, the reflectance is mostly controlled by the scattering by all particulate matter. Wide variations of near-infrared reflectance suggest large variations in inorganic and organic suspended matters in the waters studied, as confirmed by the ancillary data (Table 2.1).

### Model calibration

To find the optimal positions and widths of each band in the model shown in Eq. 2.2, we tuned the model according to the optical properties of the water bodies studied and found optimal spectral bands with minimal error of chl-*a* estimation. The calibration dataset contained 145 samples taken over water bodies with various optical properties (Table 2.1). The relationship between chl-*a* concentration in the calibration dataset (Table 2.1a), and the three-band model with optimal spectral bands was highly significant with $r^2 > 0.939$, $p < 0.0001$ (Fig. 2.4).

### Model validation

Comparison of the measured and predicted estimates of chl-*a* by the three-band algorithm (Eq. 2.2; Table 2.2a and 2.2b; Fig. 2.5a and 2.5b) show that for chl-*a* ranging from 1.2 to 236 $mg/m^3$, the root mean squared error (RMSE) of chl-*a* prediction did not exceed 7.8 $mg/m^3$. The slopes of linear relationships between $chla_{pred}$ and

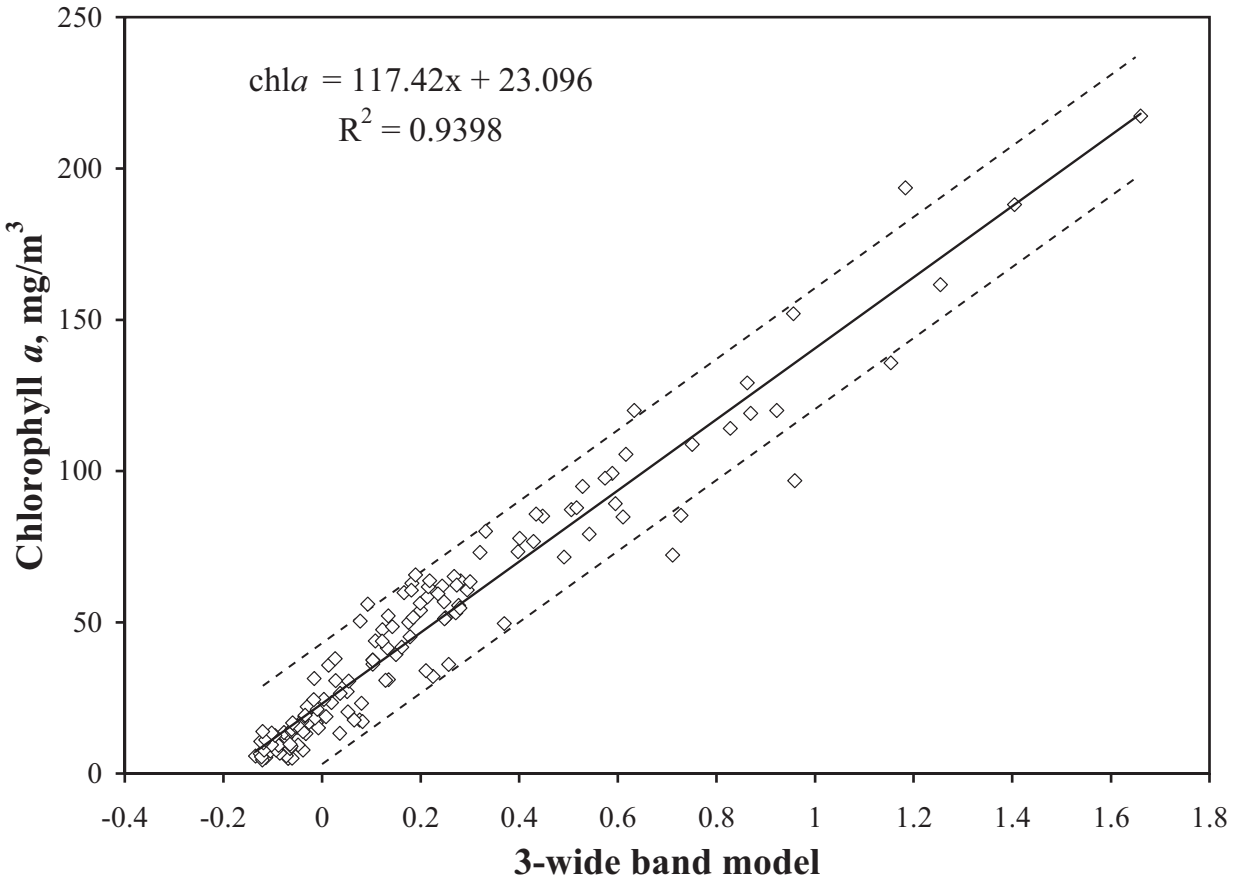


**Figure 2.4.** Chlorophyll *a* concentrations (chl-*a*) measured in Nebraska and Iowa lakes and reservoirs in 2001 through 2002, plotted vs. the three-band model from Eq. 2.2.

chl$a_{meas}$ varied among the datasets from 0.89 to 1.07 (Table 2.2a). The algorithm overestimated chl-*a* by 3–30% in three validation datasets, while it underestimated chl-*a* by about 12% in one dataset (Lake Minnetonka). When applied to all data, the algorithm overestimated chl-*a* concentration by MNB = 31.5%. Chl-*a* <5 mg/m$^3$ contributed greatly to NRMS and MNB (Table 2.2a).

When we ignored outliers with ε > 2stdev(ε), both the systematic and random errors decreased significantly (Table 2.2b). While the magnitudes of ε were still highest for chl-*a* <5 mg/m$^3$, NRMS ranged from 14.8 to 36.8% and MNB from –4.9 to 11.1%. Note that the removal of outliers did not significantly change the slope or the RMSE of chl-*a* estimation; however, the removal of outliers did move the intercept closer to the origin for each dataset. For all datasets combined, the coefficient of determination for the relationship between chl$a_{pred}$ and chl$a_{meas}$ was 0.96 ($p < 0.0001$) with a slope of 0.95 ± 0.02 and an RMSE of chl-*a* prediction of 7.8 mg/m$^3$.

**Table 2.2.** (a) Results of the three-band algorithm (Eq. 2.2) validation with wavebands (center/width) $\lambda_1$ = 670/10 nm, $\lambda_2$ = 720/30 nm and $\lambda_3$ =740/20 nm. N is the number of samples; m and n are the slope and intercept, respectively, of the chl$a_{pred}$ vs. chl$a_{meas}$ linear relationship with their standard errors (se) and the coefficient of determination ($r^2$); NRMS = stdev ($\varepsilon_i$) % is the normalized root mean square error; MNB = mean ($\varepsilon_i$) % is the mean normalized bias; RMSE is the root mean squared error of chl-*a* prediction; and CV = RMSE/mean chl-*a* is the coefficient of variation. (b) Results of three-band algorithm (Eq. 2.2) validation after removing of outliers with ε > 2stdev(ε).

a.

| Datasets | N | n (se) mg/m$^3$ | m (se) | $r^2$ | NRMS, % | MNB,% | RMSE mg/m$^3$ | CV % |
|---|---|---|---|---|---|---|---|---|
| NE&IA-2003 | 155 | 2.84 (0.86) | 0.89 (0.02) | 0.91 | 52.6 | 2.73 | 8.7 | 32.6 |
| NE-2005 | 85 | 4.57 (1.1) | 0.95 (0.02) | 0.97 | 46.0 | 14.9 | 11.2 | 27.3 |
| Lake Minnetonka | 17 | –2.39 (0.7) | 1.07 (0.03) | 0.98 | 20.7 | –12.2 | 4.2 | 13.7 |
| Choptank River | 18 | 3.33 (1.2) | 0.96 (0.02) | 0.93 | 47.9 | 29.7 | 6.0 | 38.1 |
| All together | 275 | 4.32 (0.90) | 0.94 (0.02) | 0.96 | 51.9 | 18.3 | 7.8 | |

b.

| Datasets | N | n (se) mg/m$^3$ | m (se) | $r^2$ | NRMS, % | MNB,% | RMSE mg/m$^3$ | CV % |
|---|---|---|---|---|---|---|---|---|
| NE&IA-2003 | 146 | 2.46 (0.95) | 0.89 (0.02) | 0.93 | 26.2 | 5.4 | 8.3 | 31.2 |
| NE-2005 | 78 | 3.78 (1.05) | 0.95 (0.02) | 0.97 | 36.8 | 4.9 | 8.6 | 20.9 |
| Lake Minnetonka | 14 | 1.31 (0.71)) | 1.05 (0.03) | 0.98 | 14.8 | –4.9 | 4.6 | 14.8 |
| Choptank River | 15 | 1.45 (0.64) | 1.01 (0.02) | 0.96 | 21.1 | 11.1 | 3.5 | 22.0 |
| All together | 253 | 2.17 (0.55) | 0.95 (0.02) | 0.96 | 32.1 | 7.25 | 7.8 | |

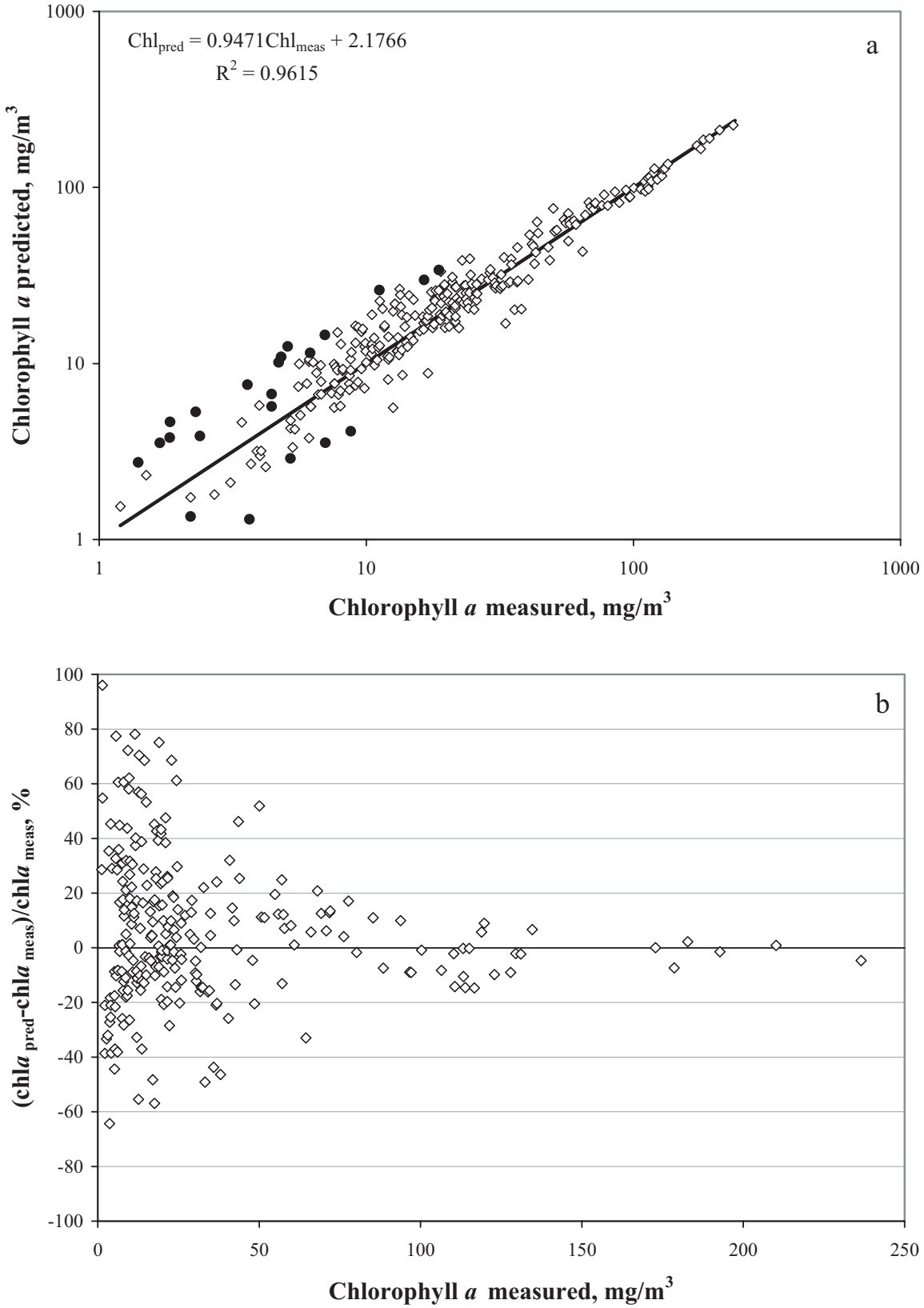


**Figure 2.5.** Comparison between the chlorophyll *a* concentration predicted and lab measured chlorophyll *a* in water samples. (a) Chlorophyll predicted vs. measured for four validation datasets; filled circles are outliers with $\varepsilon_i$>2stdev($\varepsilon$). (b) Relative error of chl-*a* prediction plotted vs. measured chl-*a* concentration.

In conclusion, these studies show that a model developed in one location can be applied to water bodies in other locations with good results.

## 2.6. Costs and resource requirements

### Ocean Optics spectroradiometers and reference panel

| Item | Description | Quantity | Cost | Total |
|---|---|---|---|---|
| USB2000+ | Ocean Optics USB 2000+ spectroradiometer | 2 | $2399.00 | $4798.00 |
| DET2-350-1000 | 2000-series detector, installed, with 350–1000 nm order sorting filter | 2 | $200.00 | $400.00 |
| GRATING #3 | Grating 3, installed, 350–1000 nm | 2 | N/C | N/C |
| SLIT-25 | Installed optical bench entrance aperture, 25-micron width | 2 | $158.00 | $316.00 |
| *** | Note: set baseline above 200 counts | | | |
| CC-3-UV-S | Cosine Corrector with Spectralon diffusing material | 1 | $136.00 | $136.00 |
| USB-ADP-PC | Adapter pkg. to connect spectrometer to PC (serial) | 2 | $94.00 | $188.00 |
| 074-21000-001 | Protective Cap, Blue | 10 | $1.50 | $15.00 |
| Custom Fibers | Custom, premium 5 meter 400 micron diameter fiber | 2 | $373.41 | $746.82 |
| AA-00822-000 | SRT-99-100 10” × 10” Reflectance target | 1 | $1200.00 | $1200.00 |
| | | | Total | $7799.82 |

Notes

The 350–1000 nm order sorting filter reduces or eliminates second-order effects.

Grating 2 or grating 3 may be used. We chose 3 because it provides a small improvement in the near-infrared response of the instrument. With either grating, the useable range of the instrument is approximately 375–950 nm.

The width of the slit determines the spectral resolution of the instrument. A 25-micron slit provides a spectral resolution that is slightly better than 1.5 nm. A 50-micron slit will allow more light to enter the instrument but will reduce the spectral resolution to about 3 nm. Slits >50 microns may cause the instrument to saturate when calibrating outdoors under sunny conditions.

The baseline count refers to the dark current through the detector array at room temperature. The dark current decreases as the temperature increases. If the dark current falls too low then the output from the detector array becomes unstable. This is most likely to happen outside on a hot day. Setting the count above 200 should prevent the instability, even on a very hot day.

The cosine corrector with Spectralon diffusing material is almost unbreakable, easy to clean, and can be submerged.

The adapter package is necessary to communicate with the instruments via a RS232 (serial) interface.

We recommend having spare caps to prevent dust from entering the spectroradiometer. The instruments should be capped when a fiber is not attached.

The length of the fibers is determined by the users. We have found that the minimum length should not be <3 m for most applications. We recommend using premium silicon monocoil fibers (unless the fiber length is >10 m) because they are more resistant to damage under field conditions. It is advisable to always have at least one spare fiber available when collecting data.

### CDAP software

CDAP software is available through a license issued by the University of Nebraska.

Current price list (January 2008):

Licensing for Nebraska public institutions/agencies = $1500 (includes executable code only)

Licensing for public institutions/agencies outside of Nebraska = $2000 (includes executable code only)

Licensing for non-public institutions/agencies = $2500

Instrument calibration and training package = $500

*Note that this is required for first-time users of the software*
Includes 2 days of training in software use at CALMIT, UNL
Includes 30 days of technical assistance (telephone support)

Long-term technical-assistance package = $500 per year

Unlimited telephone support
Access to web-posted software updates

Development of software modifications = $250 per day

For questions about this system, please contact:

Dr. Donald C. Rundquist
School of Natural Resources
University of Nebraska–Lincoln
307 Hardin Hall
Lincoln, NE 68583-0973
Email: drundquist1@unl.edu

## 2.7. Conclusions

This technique for chl-*a* retrieval from reflectance data requires neither further optimization of spectral band positions nor site-specific parameterization to accurately estimate chl-*a* in water bodies with widely varying bio-optical characteristics. Note that the technique, even when using wide spectral bands and optimized for the calibration dataset with chl-*a* ranging from 4.4 to 217.3 mg/m$^3$, allowed accurate chl-*a* prediction with no parameterization when applied to the four validation datasets, despite very different compositions of optically active constituents (chl-*a*, tripton, CDOM) in the water bodies and despite differences in the taxonomy of phytoplankton. Also important, the algorithms validated in this study do not require adjustments of the coefficients and do not need data on inherent optical properties of constituents, which can be variable and difficult to obtain. Additionally,

the relatively low cost associated with hand-held spectroradiometers and their ease of use offers widespread applications for monitoring the diverse conditions of coastal and inland waters.

These real-time monitoring tools may be useful as early warning systems for potential toxins in recreational waters and may provide useful information to water-management authorities. The principles used in this technique may also be extended to collect information over relatively large areas using airborne and spaceborne sensors. Coverage on a regional scale indicates when and where water quality parameters should be examined by detailed sampling and meticulous laboratory analysis.

## 2.8. References

Bauer, M.E., C.S.T. Daughtry, L.L. Biehl, E.T. Kanemasu and F.G. Hall. 1986. Field spectroscopy of agricultural crops. P. 65-75. *In* IEEE Transactions on Geoscience and Remote Sensing, GE-24:1.

Curran, P.J. and E.M.M. Novo. 1988. The relationship between suspended sediment concentration and remotely sensed spectral radiance: A review. J. Coas. Res. 4:351-368.

Dall'Olmo, G., A.A. Gitelson and D.C. Rundquist. 2003. Towards a unified approach for remote estimation of chlorophyll *a* in both terrestrial vegetation and turbid productive waters. Geophys. Res. Lett. 30:1038 [doi:10.1029/2003GL018065].

Dall'Olmo, G. and A.A. Gitelson. 2005. Effect of bio-optical parameter variability on the remote estimation of chlorophyll *a* concentration in turbid productive waters: experimental results. Appl. Opt. 44:412-422.

Dall'Olmo, G. and A. A. Gitelson. 2006. Effect of bio-optical parameter variability and uncertainties in reflectance measurements on the remote estimation of chlorophyll *a* concentration in turbid productive waters: modeling results, Appl. Optics 45(15):3577-3592.

Dekker, A. 1993. Detection of the optical water quality parameters for eutrophic waters by high resolution remote sensing. PhD dissertation, Free University, Amsterdam, The Netherlands.

Doxaran, D., J.M. Froidefond and P. Castaing. 2002. A reflectance band ratio used to estimate suspended matter concentrations in coastal sediment-dominated waters. Int. J. Remote Sens. 23:5079-5085.

Doxaran, D.R., C.N. Cherukuru and S.J. Lavender. 2005. Use of reflectance band ratios to estimate suspended and dissolved matter concentrations in estuarine waters. Int. J. Remote Sens. 26:1763-1769.

Gitelson, A.A. 1992. The peak near 700 nm on reflectance spectra of algae and water: relationships of its magnitude and position with chlorophyll concentration. Int. J. Remote Sens. 13:3367-3373.

Gitelson, A.A., J.F. Schalles and C.M. Hladik. 2007. Remote chlorophyll *a* retrieval in turbid, productive estuaries: Chesapeake Bay case study. Remote Sens. Environ. 109:464–472.

Gitelson, A.A., G. Dall'Olmo, W. Moses, D.C. Rundquist, T. Barrow, T.R. Fisher, D. Gurlin and J. Holz. 2008. Technique for remote chlorophyll *a* estimation in turbid productive waters. Remote Sens. Environ. 112: 3582–3593, doi:10.1016/ j.rse.2008.04.015.

Gitelson, A., D. Gurlin, W. Moses, and T. Barrow, "A bio-optical algorithm for the remote estimation of the chlorophyll *a* concentration in case 2 waters", Environmental Research Letters, 2009, in press.

Gordon, H. and A. Morel. 1983. Remote assessment of ocean color for interpretation of satellite visible imagery. A review. Lecture notes on coastal and estuarine studies. Springer-Verlag.

Han, L. and D. Rundquist, 1998. The impact of a wind-roughened water surface on remote measurements of turbidity. Int. J. Remote Sens. 19 (1):195–201.

Ohde, T. and H. Siegel. 2003. Derivation of immersion factors for the hyperspectral Trios radiance sensor. J. Opt. A–Pure Appl. Opt. 5(3):12–14.

# Chapter 3. Airborne hyperspectral remote sensing

In Chapter 2 we examined the use of high-spectral resolution sensors (field spectroradiometers) to measure the optical properties of lakes, typically from boats or other platforms located on the water surface. In this chapter, we discuss imaging spectrometers, also known as hyperspectral sensors.

Like field spectroradiometers, hyperspectral sensors operate in tens or even hundreds of discrete segments (bands) of the spectrum, but rather than just measuring upwelling radiance at a single point, hyperspectral sensors collect these data over a wider area in the form of a series of images, each associated with one narrow spectral band. These individual slices of spectral information can be conceptualized or visualized as a data cube (Fig. 3.1), which is the result of "stacking" the individual images for each discrete spectral band. Two dimensions of this cube are "spatial" (rows and columns of pixels), while the third dimension is "spectral" (the many narrow and contiguous spectral bands measured by the sensor). Thus, any location in the image can be selected to obtain a nearly continuous spectral profile for that pixel.

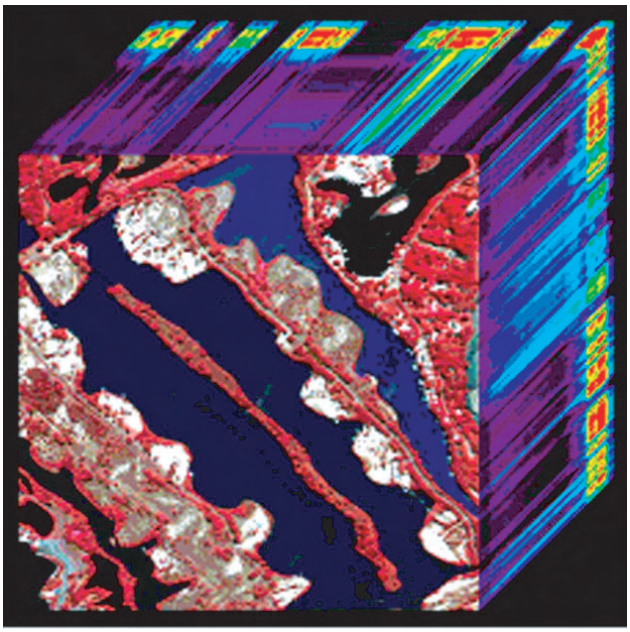

**Figure 3.1.** Example of a spectral cube.

The algorithms developed and discussed in the Chapter 2 can be applied to the data composing a hyperspectral image on a pixel-by-pixel basis to generate thematic images highlighting specific characteristics of the target. For example, an algorithm could be applied to the image data that calculates the chlorophyll *a* concentration based on each pixel's particular spectral signature. The end result would be a map of chlorophyll *a* distribution in a lake.

## 3.1. The AISA Eagle hyperspectral imager

The University of Nebraska's Center for Advanced Land Management Information Technologies (CALMIT) operates a specially modified Piper Saratoga aircraft (Fig. 3.2a) as the base platform for deploying the Airborne

Imaging Spectrometer for Applications (AISA) Eagle hyperspectral imager. The Eagle is the primary instrument in the suite of tools deployed onboard the aircraft.

The AISA (Airborne Imaging Spectrometer for Application) Eagle Visible/Near-Infrared (VNIR) remote hyperspectral sensor (Fig. 3.2b) is capable of collecting spectral-radiance data and compiling images in many parts of the blue, green, red and near-infrared portions of the electromagnetic spectrum. The Eagle is a complete push-broom system with a swath width of 1000 spatial pixels, a miniature Global Positioning System /Inertial Navigation Sensor and a data acquisition unit in a rugged PC with display unit and power supply.

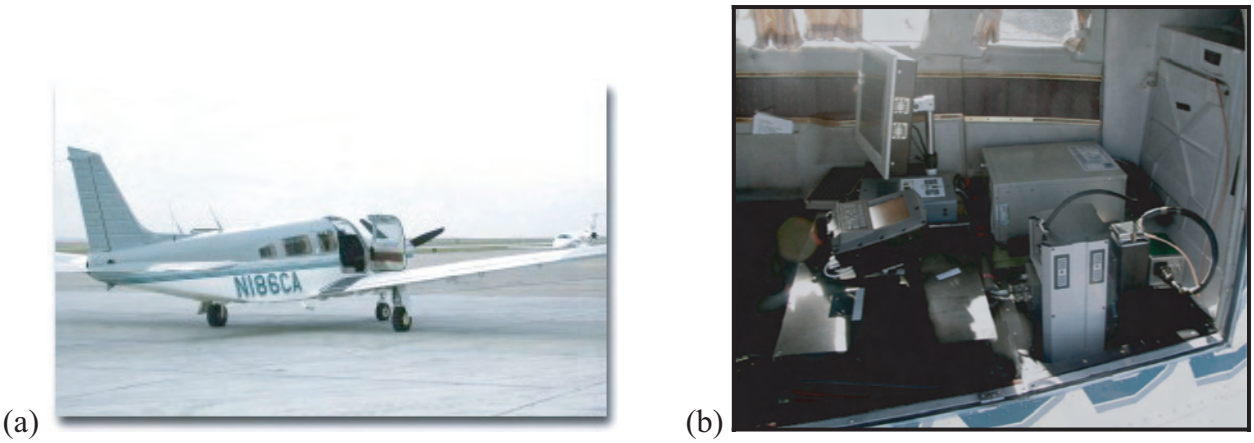


**Figure 3.2.** The AISA Eagle airborne hyperspectral sensor. (a) Piper Saratoga aircraft. (b) AISA Eagle VNIR sensor installed within the aircraft.

While upwelling radiance can be measured in as many as 512 discrete spectral bands, the instrument is seldom programmed for more than 100. Accompanying software enables the development of unique, project-specific band sets. As such, the band centers can be identified and channel widths adjusted to meet the project requirements. Aircraft position and attitude, upwelling radiance and downwelling solar irradiance are simultaneously recorded in the raw data product.

This hyperspectral imaging system has been deployed for use in numerous research collaborations with various public service, commercial and educational organizations. These missions have supported a wide variety of research topics including water quality, agriculture, environmental quality, invasive species and military applications. This chapter focuses on examples of AISA-Eagle hyperspectral imagery as used in water-quality monitoring.

## 3.2. Case study 1 – Fremont Lakes, Fremont, NE

The Fremont Lakes system is a series of groundwater-fed, sand-pit lakes located just west–southwest of the east-central Nebraska town of Fremont. About one-half of the lakes are located within Fremont State Lakes State Park and experience a high level of recreational use and limited shoreline development. The remaining lakes in the complex are private and experience a lesser degree of recreational use and a much greater level of shoreline development.

Lakes in the Fremont system exhibit varying trophic states throughout the spring, summer and fall. The purpose of this study was to (1) monitor the trophic states of the lakes and (2) spatially quantify algal and total suspended solid loads through the recreational season.

### AISA Eagle imagery

The following processed image and resulting image products were generated from a dataset acquired 5 August 2005 over Fremont Lakes. Acquisition parameters for the flight were:

- Spatial Resolution: 2 m
- Spectral Resolution: 97 bands
- Acquisition Altitude: 3,000 m AGL
- Acquisition Speed: 120 mph
- Flight Direction: SE–NW
- Time of Day: 10:45 am CDT
- Sky Conditions: Clear (<5% Clouds)
- Wind Direction/Speed: NW @ 15–20 mph

The initial processing produces a multilayered, map-quality image. (See Appendix C for details of image processing). As noted previously, because the image consists of the multiple spectral layers, a spectral curve can be generated from each and every individual pixel on the image (Fig. 3.3 and 3.4).

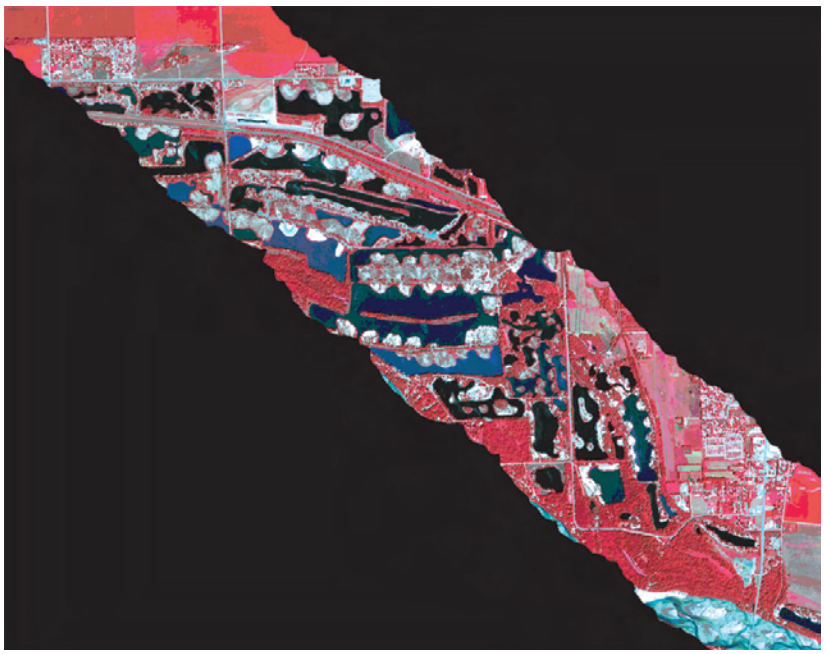

**Figure 3.3.** False-color composite image using three spectral bands of AISA Eagle data.

### Removal of unnecessary data

When possible, the size of the dataset is reduced to include only the target information. In the Fremont Lake case (Fig. 3.5), the dataset has been reduced to lake (water) pixels only (*i.e.*, land areas have been eliminated). Colors in this intermediate image product have no special meaning.

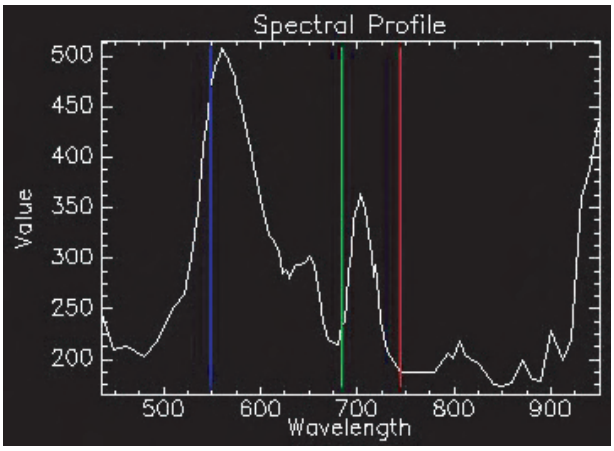


**Figure 3.4.** Spectral reflectance for one pixel in the hyperspectral image.

**Figure 3.5.** Pixels containing only water areas in the Fremont Lakes imagery.

## Application of algorithms

Thematic maps highlighting the relative density and spatial distribution of chlorophyll *a* (chl-*a*) and total suspended solids (TSS) are generated through the application of the algorithms discussed in Chapter 2. Specifically, they are:

- Chlorophyll $\propto [R^{-1}(\lambda_1) - R^{-1}(\lambda_2)] \times R(\lambda_3)$
- Total Suspended Solids $\propto [R(\lambda_3)/R(\lambda_4)]$

where $\lambda_1$ = 665–675 nm, $\lambda_2$ = 700–710 nm, $\lambda_3$ = 730–740 nm, $\lambda_4$ = 540–560 nm.

The algorithms were applied to every pixel comprising the water-masked image. Once the computations were complete, colors were assigned to different levels of calculated chlorophyll *a* in the surface waters under investigation.

Lake managers and/or decision makers now have thematic map products highlighting both the concentration and spatial distribution of chlorophyll *a* (Fig. 3.6) and total suspended solids (Fig. 3.7) at the time the imagery was collected. There is also a product that delivers chlorophyll *a* concentration in mg $m^{-3}$ (see Lake Minnetonka case study later in this chapter). The accuracy of the chlorophyll *a* estimation algorithm is discussed in Chapter 2.

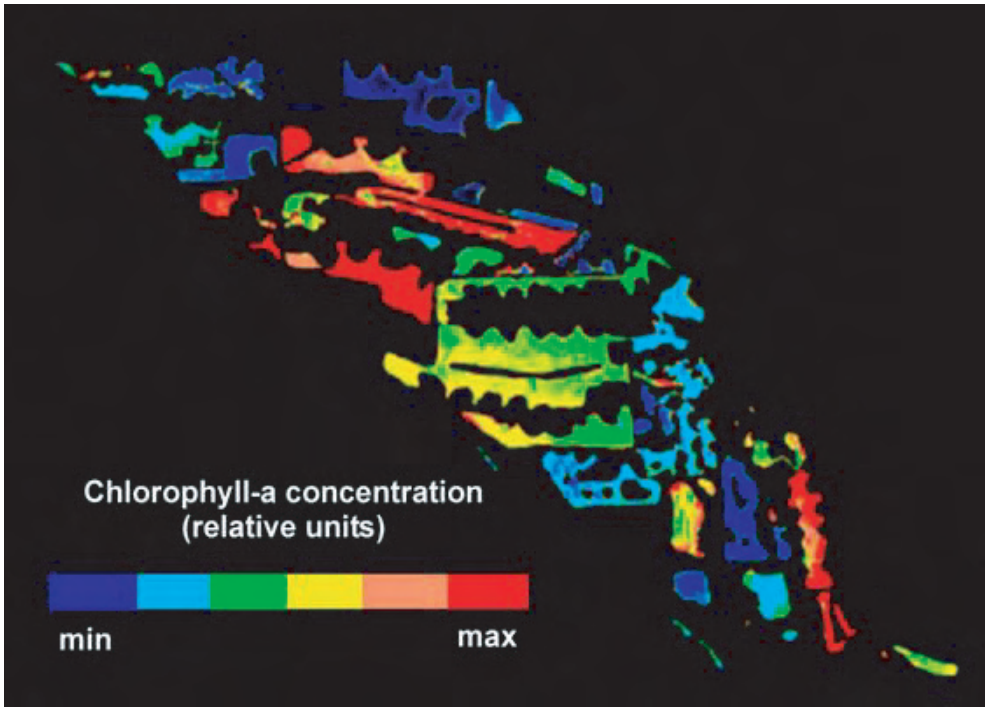


**Figure 3.6.** Thematic map highlighting distribution of chlorophyll *a*.

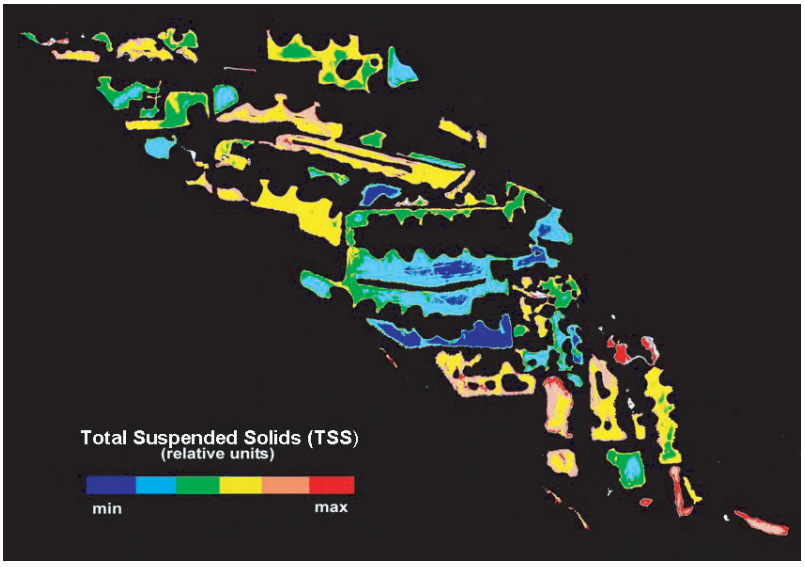


**Figure 3.7.** Thematic map highlighting distribution of total suspended solids.

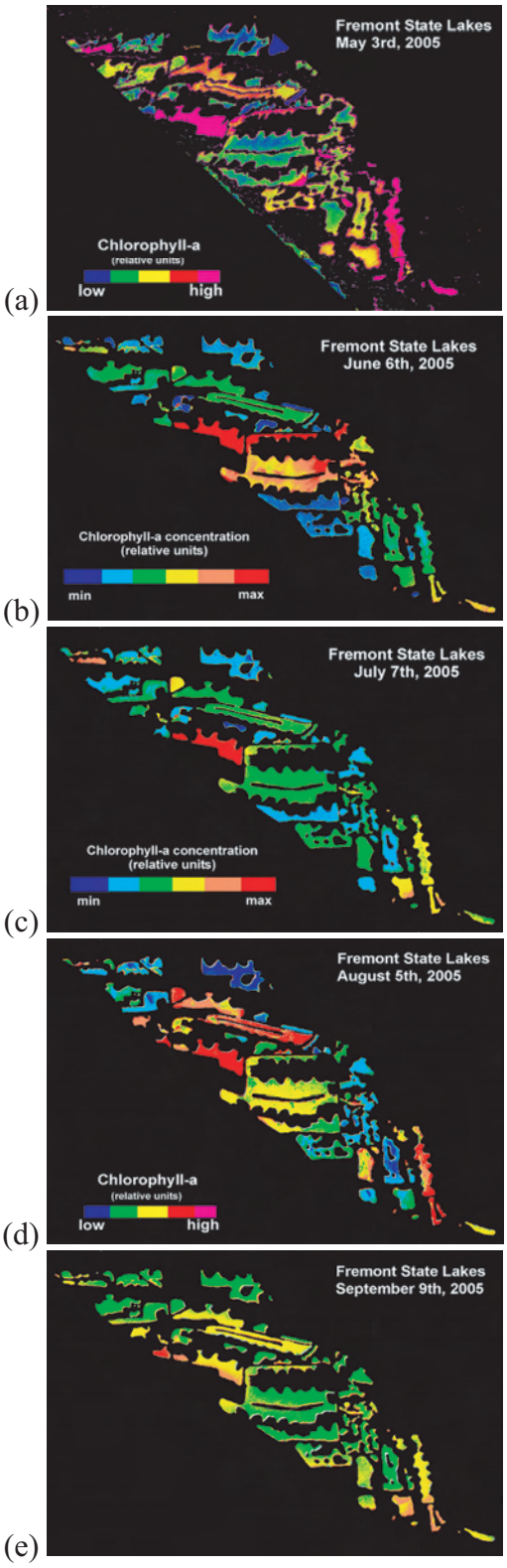


**Figure 3.8.** Maps of chlorophyll *a* concentration for the Fremont Lakes, 2005: (a) 3 May; (b) 6 June; (c) 7 July; (d) 5 August; (e) 9 September.

### Additional image product samples

The Fremont Lakes case study produced a multi-temporal look at the lake complex through the 2005 field season. Chlorophyll *a* maps were generated for each aerial-acquisition date (Fig. 3.8).

## 3.3. Case study 2 – Pawnee Lake, NE

Pawnee Lake is primarily a recreational lake located just west of Lincoln, Nebraska. Airborne hyperspectral images were collected on repeated flights from 10 April through 26 July 2006. This multi-temporal series is another example of the system's the ability to track spatial and temporal variability of a single lake (Fig. 3.9).

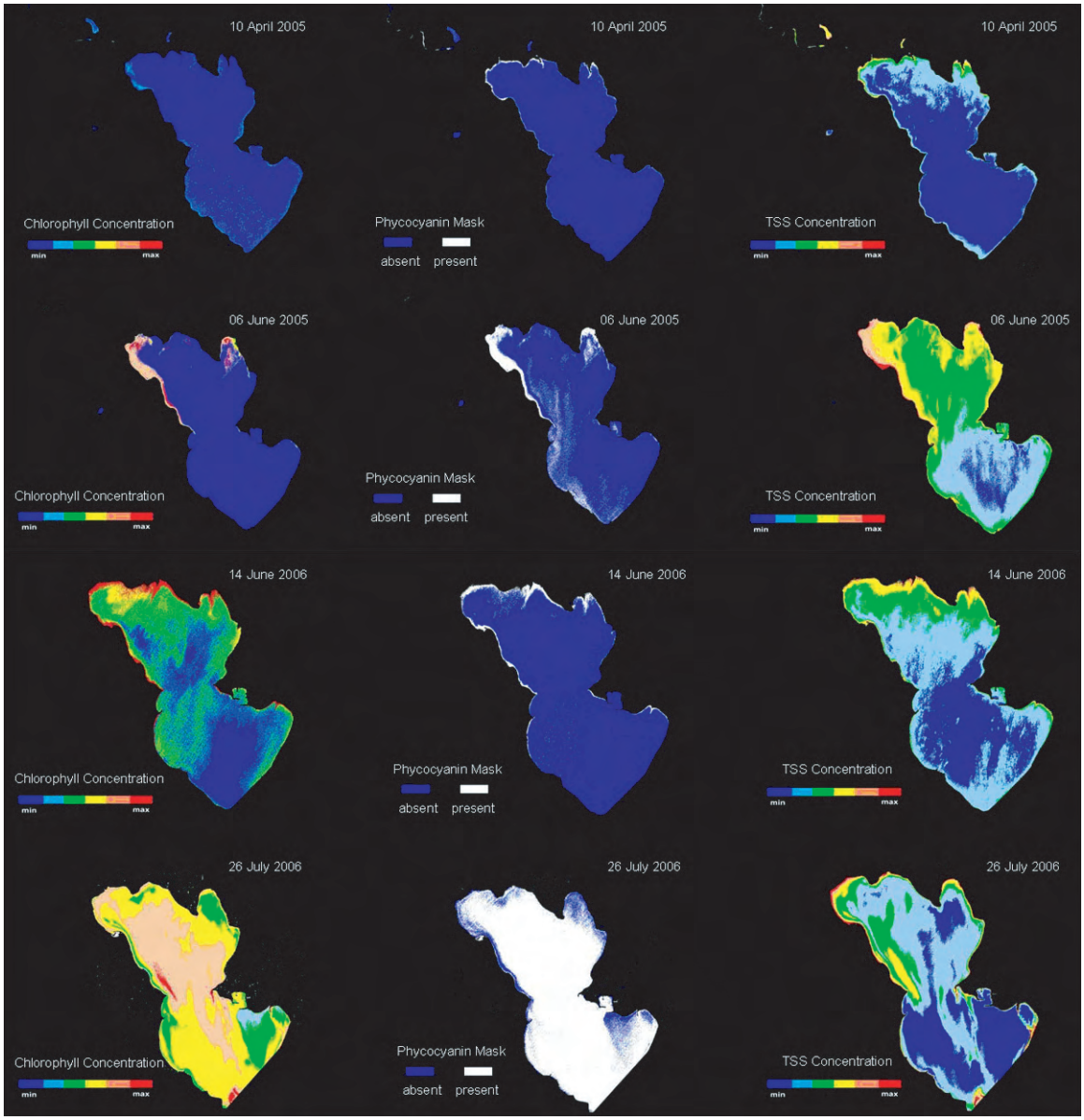


**Figure 3.9.** Multi-temporal series of chlorophyll, phycocyanin presence and total suspended solids concentration maps for Pawnee Lake, NE, April–July 2006.

## 3.4. Case study 3 – Lake Minnetonka, MN

The previous examples each involved data collected along a single flight line. This case study demonstrates the how the system can be used to generate thematic products resulting from a mosaic of multiple images.

Lake Minnetonka is a large complex of interconnected lakes located northwest of the city of Minneapolis. In a project of this size, the 14 flight lines were collected on two consecutive days. Flight lines were orientated NW–SE. (See Planning a Successful Mission) for detailed explanation of flight line development.) The image produced (Fig. 3.10) is a mosaic of several aerial images. The colors approximate those that would be seen by the human eye. Note that land areas have been masked out.

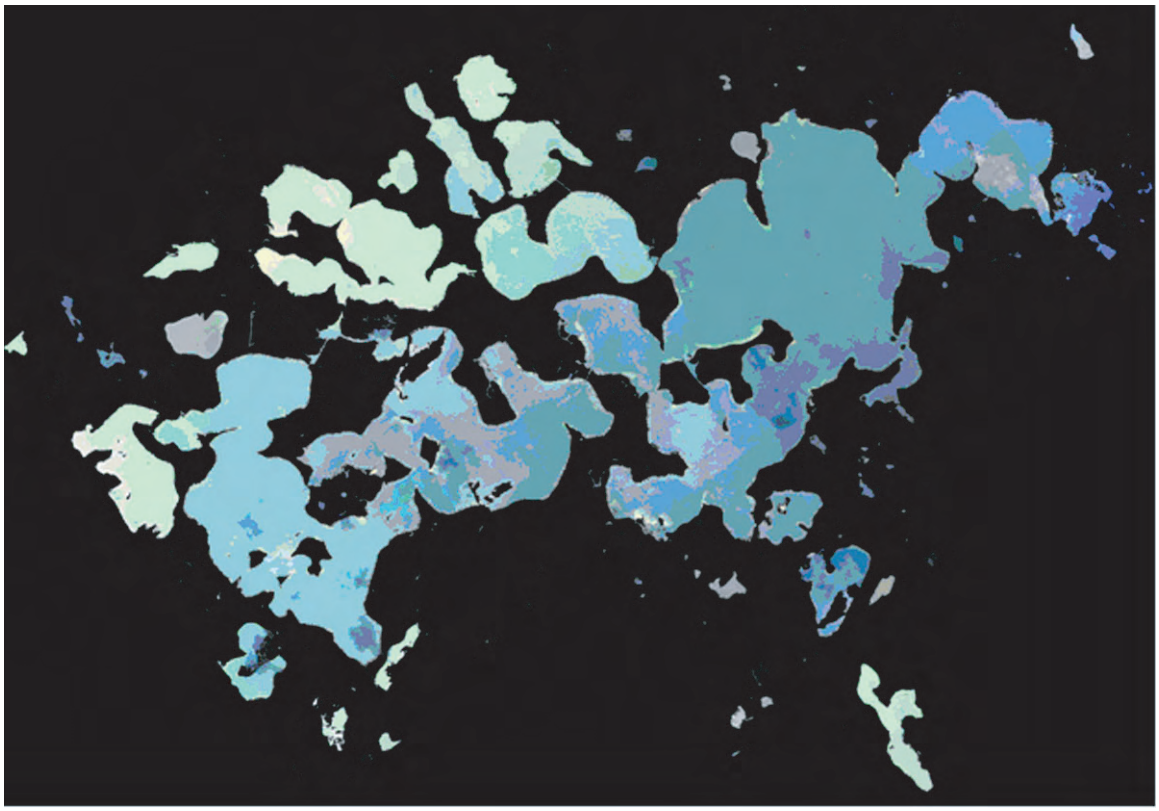

**Figure 3.10.** Lake Minnetonka, MN, August 2005. Mosaic used to generate a chlorophyll map (Fig. 3.11) and a phycocyanin map (Fig. 3.12).

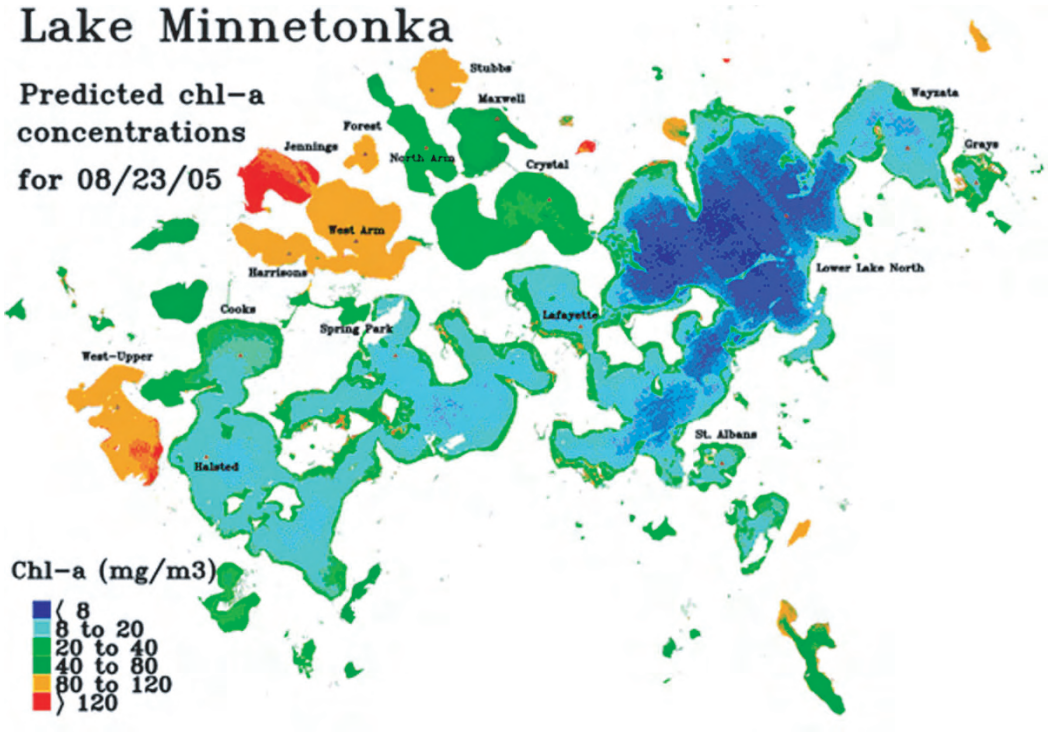


**Figure 3.11.** Chlorophyll map, Lake Minnetonka, MN, August 2005.

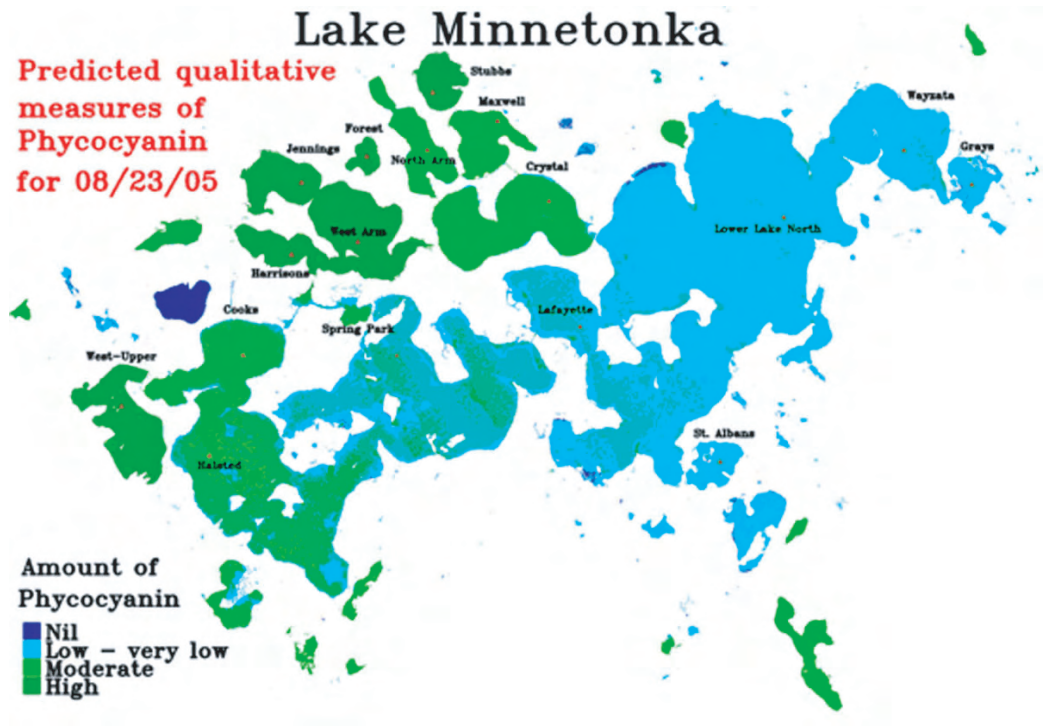


**Figure 3.12.** Phycocyanin Map, Lake Minnetonka, MN, August 2005.

Chlorophyll *a* concentration estimates derived from the AISA Eagle imagery were compared with laboratory measurements. They were strongly related, with determination coefficient $r^2 = 0.94$. The root mean squared error of chlorophyll estimation was below 6.5 mg $m^{-3}$ (Fig. 3.13).

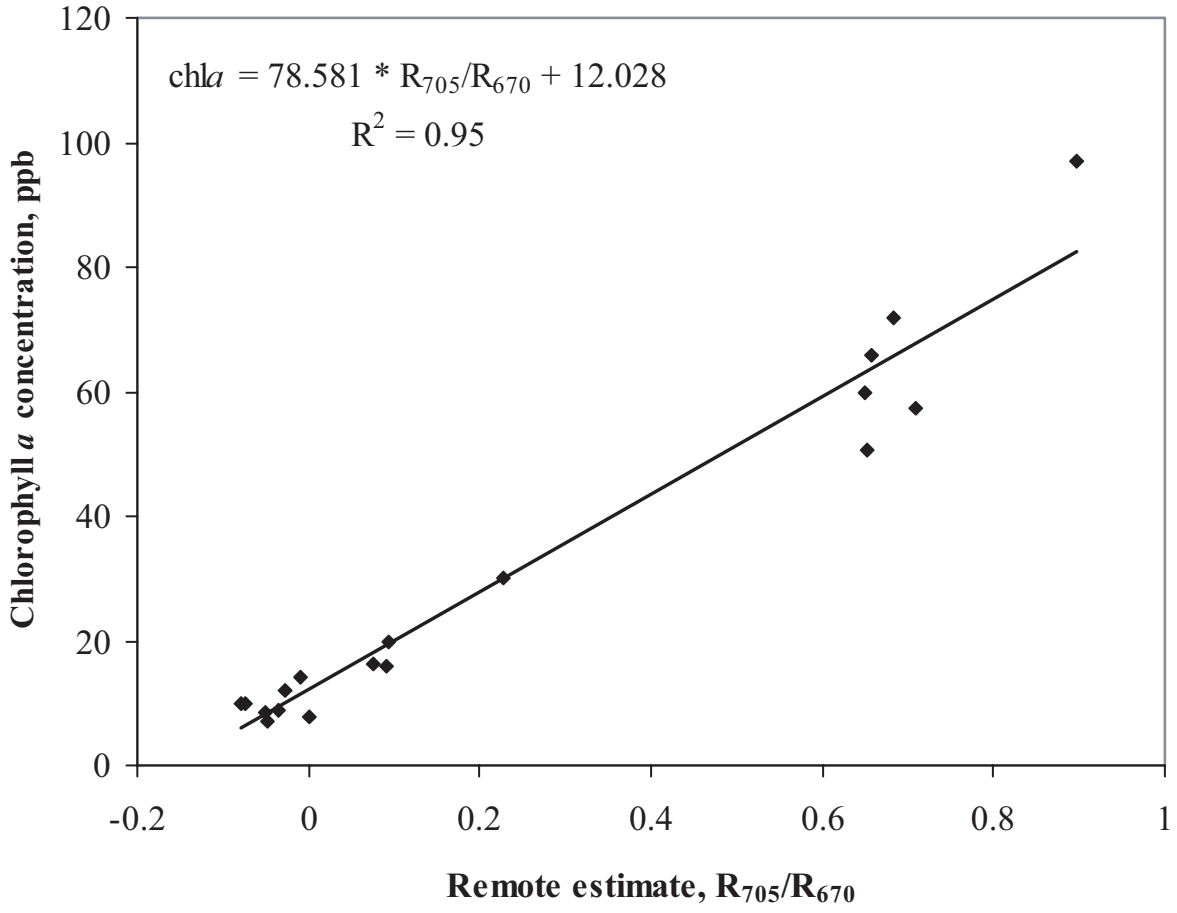


**Figure 3.13.** AISA estimates of chlorophyll *a* plotted vs. laboratory measurements of chlorophyll *a* concentrations.

## 3.5. Planning a successful mission

The key to success for any airborne remote sensing project is early communication with the flight-mission co-ordinator to clearly define the project objectives, operational parameters and final data product requirements. Project objectives drive the development of each mission plan. Due to the wide variety of targets and budgetary concerns, a compromise involving acquisition parameters is quite often required to obtain the optimum results. Operational parameter concerns can be grouped as:

- Area of interest
- Aircraft limitations
- Instrument configuration

Initial specifications of spatial resolution, band selection, and target size may have to be adjusted.

Other decisions related to the mission parameters that require decisions include:

- Length, direction and overlap of multiple flight lines
- Timing of flights
- Flight restrictions (Air Traffic Control)
- Acceptable weather conditions

The following sections cover issues related to the completion of an agreement between the research coordinator and the mission planner defining the final mission parameter requirements.

### Band selection

The CALMIT faculty and staff have spent considerable time developing an optimal set of band files for both aquatic and terrestrial targets. If desired, a custom band set can be generated for a specific project (see Appendix D for the recommended band set for aquatic targets).

### Flight line parameters and timing

Four interrelated issues require consideration in the development of an optimal set of flight lines for a remote sensing mission: swath width (corridor of coverage) based on spatial resolution; target size, orientation (flight-line direction), location; timing of the acquisition; and weather.

Flight-line swath width is driven by spatial resolution and is a function of the altitude flown by the aircraft. As altitude increases, swath width increases and the spatial resolution decreases. Flight line length is a function of spatial resolution required by the project and the band set used. The on-board computer can record a maximum of 2.0 GB of raw data for any single flight line. Selection of a high spatial resolution or a large set of spectral bands will limit the maximum length of flight lines. Compromises are addressed (below) to achieve optimum results when target size is an issue.

Flight direction issues are driven by the sun-target-sensor angle and increases in path length. Flying perpendicular to the solar azimuth creates the maximum amount of solar distortion across an image. Flying directly into or away from the solar azimuth reduces the effects to the minimum. This can be an important issue when working with terrestrial targets, but it is an especially critical element in the development of flight lines over an aquatic target. In that case, one must minimize the specular reflectance (sun-glint) of the water surface (Fig. 3.14).

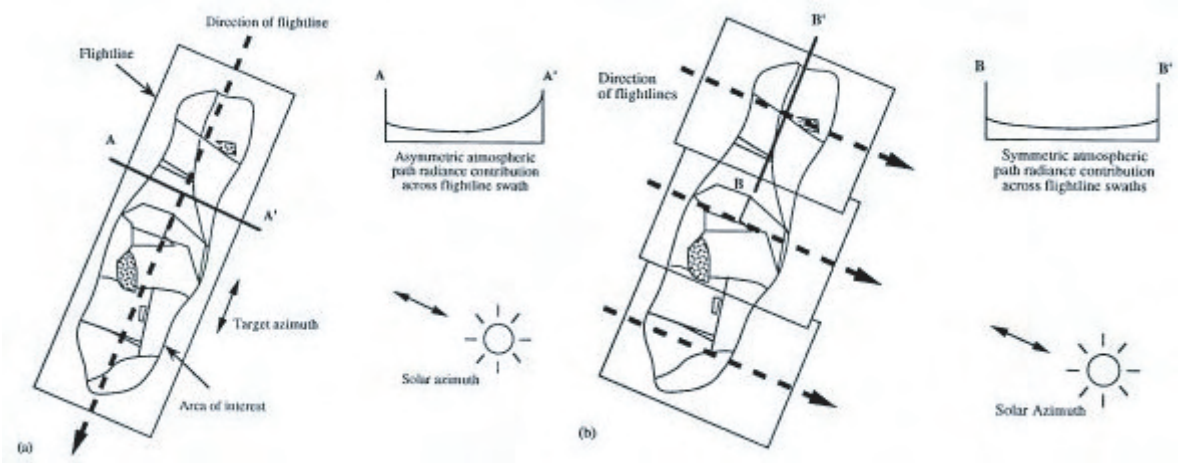


**Figure 3.14.** Directional affects related to solar azimuth: (a) flying perpendicular to the solar azimuth; (b) flying parallel to the solar azimuth.

Timing of flight lines is closely related to the directional determination. As a general rule, airborne image acquisitions should be conducted ± 2 h from solar noon. The high solar angles during this window of time provide the maximum amount of solar illumination, minimizes shadowing, and decreases atmospheric scattering. Further, morning lines should be flown in a NW–SE direction, noon-time lines should be flown N–S and afternoon lines should be flown NE–SW.

Some problems are associated with flight direction and time (Fig 3.15). The flight direction was NW–SE at 12:45 pm CDT, on 1 June 2006. and although clouds had no direct influence on the image, cloud shadows are clearly visible in the lower left of the image.

The decision to fly into or away from the sun is made by the pilot and instrument operator, based primarily on visibility and the wind direction and speed. The decision may also be driven by location and the presence of other air traffic. When developing flight lines for multi-temporal acquisitions, seasonal changes must be considered. Tide cycles may also be a consideration when the target is particularly affected by them.

When acquisition requires multiple flight lines over a single target, the flight lines should be laid out with a 20–30% side-lap to avoid data skips arising from changes in the aircraft's attitude (*i.e.*, roll, pitch and yaw). In

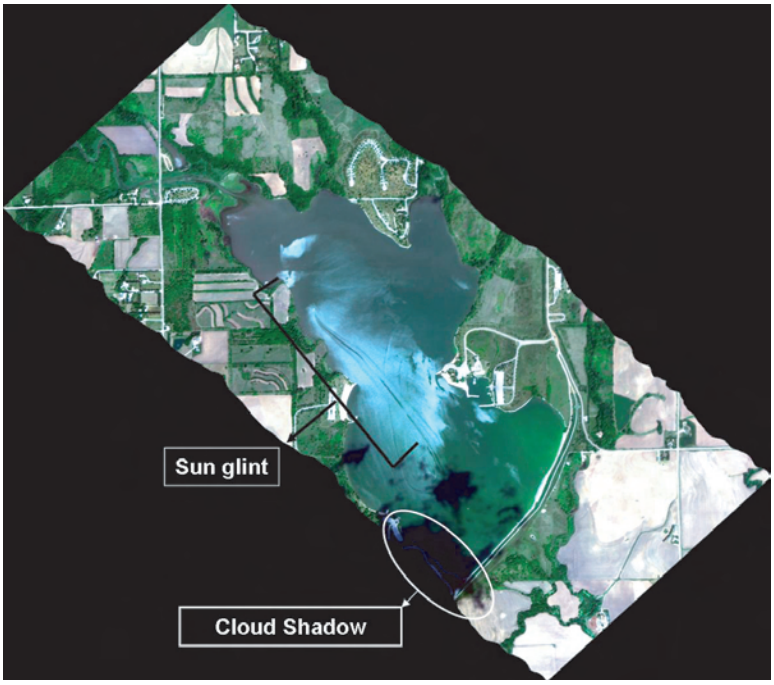


**Figure 3.15.** AISA Eagle image illustrating problems with sun-glint and cloud shadows.

general, multiple flight lines should all be acquired flying in the same direction to minimize image-to-image differences due to atmospheric distortion, aircraft crab-angle and ground speed.

Actual flight plans for each mission are filed the morning of each scheduled acquisition. The flight plans are developed with consideration for restricted, controlled, and military airspaces, among others. Missions requiring flights into or near restricted areas generally require FAA notification well ahead of the scheduled acquisition date, making it critical that the mission planning be initiated well in advance of the expected acquisition date. CALMIT flight crews have established a good working relationship with the FAA and can usually get flight approvals in these areas. Safety, image quality and data-collection efficiency are the goals of the flight crew.

Weather is the most unpredictable variable associated with an airborne acquisition. Long-range planning is best, but when mission success is weather dependent, flexibility is a must. For example, requirements of an aquatic project may dictate that acquisitions be completed with clear water conditions only. A successful acquisition cannot be completed after a heavy rain storm, although generally skies will be crystal clear the next morning.

As a general rule, missions will not be initiated without a reasonable chance of successful completion. As much as possible, airborne acquisitions will be carried out under as close to ideal conditions as possible. The flight crew monitors weather conditions in the areas of scheduled projects on a daily basis. Standard operating procedures will be to publish, via email, all projects scheduled for completion during a week. Daily flight decisions and contact with project PIs are made the night before a scheduled mission. If conditions warrant, final notification will occur early morning (~5:00–5:30 am) on the day of the acquisition.

Coordination of an airborne acquisition with ground-truthing activities requires good lines of communication and flexibility. The flight crew will be in contact with the project PI leading up to a potential acquisition. Given the tentative nature of the weather, ground-truthing parties should set aside a window of time for completion for their part of the project. Setting a definitive date for an acquisition with no flexibility is a recipe for failure. Additionally, completion of ground-truthing activities will generally take much longer than the collection of the airborne data and may well take more than a single day.

End users who plan to do additional processing must recognize the large volume of data generated by the system. While computer hardware and software capabilities have improved, the extremely high data volumes generated by hyperspectral sensors require a higher level of computational resources than most other remote sensing systems.

With these critical elements and questions in mind, a formal mission request must be accompanied by a completed Mission Planning Form (Appendix E). While some of the individual parameters may be adjusted as the plan is developed, the basic questions need to be addressed to develop a comprehensive mission plan.

## 3.5. Cost estimation

Because each mission brings its own unique set of requirements and parameters, each will present a unique set of budget outcomes. Factors considered in the development of each project may include:

- Ferry time
- Acquisition time
- Per diem for flight crew
- Number of flight lines
- Level 1 processing
- Level 2 processing
- Level 3 processing
- Additional processing

No two projects will have the same budgetary considerations, so providing an exact cost for a hypothetical project is difficult. An accurate cost estimate is generated for each project based on actual parameters and flight requirements.

A review of all projects completed over the course of the last four years, ranging from local missions of a single flight line through missions with more than 30 flight lines located 1100 miles from Lincoln, shows the average cost was $\$350/mi^2$. This rate is biased on the high side due to the number of projects completed at distances from Lincoln with a high number of flight lines. Further information can be obtained by contacting CALMIT (see Appendix E for details).

# Chapter 4. Satellite remote sensing I: Landsat and other moderate-resolution systems

## 4.1. Introduction

The first category of satellite remote sensing systems discussed in this report consists of those capable of providing routine, operational monitoring at local to regional scales. These systems generally share the following characteristics:

- Moderate spatial resolution (nominally 10 m to 100 m)
- Spectral resolution of a few relatively broad spectral bands, typically in the visible and the near-infrared wavelengths with some systems employing additional panchromatic, middle infrared, and/or thermal infrared bands
- Moderate coverage area (60–200 km or wider swath)
- Regular coverage (5–26 day repeat, but constrained by cloud cover)
- Low to high cost for imagery.

These systems were designed for monitoring local and regional-scale environmental and surface conditions. Their primary advantages for lake management applications are regular coverage by some of the systems, relatively wide spatial extent of coverage and spatial resolution suitable for monitoring all lakes 4 ha and larger; the primary disadvantage is the limited spectral resolution (compared to hyperspectral systems). The primary system used for monitoring land, vegetation and water resources has been Landsat-5 and -7.

The launch of the Earth Resources Technology Satellite in 1972 (later renamed Landsat-1) introduced a new era of terrestrial satellite remote sensing. Since then, the Landsat series of satellites has been regularly collecting moderate resolution multispectral imagery around the world. Although the Landsat spectral bands were selected for terrestrial features, several studies have demonstrated a strong relationship between Landsat Multispectral Scanner (MSS) and Thematic Mapper (TM) data and *in situ* observations of water clarity and chlorophyll *a* (*e.g.*, Lillesand *et al.* 1983, Lathrop 1992, Mayo *et al.* 1995, Kloiber *et al.* 2002b).

Two Landsat satellites are currently operating: Landsat-5 (launched in 1984) carries the TM instrument, and Landsat-7 (launched in 1999) carries the Enhanced Thematic Mapper Plus (ETM+). Since July 2003, Landsat-7 has been operating with the scan-line corrector (SLC) off due to a malfunction. However, Olmanson *et al.* (2008) found that Landsat-7 ETM+ (SLC off) imagery worked as well for water clarity assessment as earlier (intact) ETM+ imagery because only a representative sample of pixels is needed from each lake, and the missing data generally did not affect the results. Each satellite has a 16-day repeat cycle, so Landsat images are collected every 8 days for many portions of the world, including North America. The data are archived at and available from the US Geological Survey Earth Resources Observation and Science Center (USGS EROS Center) and other locations.

Other moderate resolution satellites that could be or have been used for water quality assessment include SPOT (Satellite Pour l'Observation de la Terre) from France, IRS (Indian Remote Sensing Satellite) AWiFS and LISS-3 from India and RapidEye system from Germany. We compiled the basic specifications of the primary satellite systems that have the necessary combination of properties (Table 4.1).

**Table 4.1.** Specifications of satellite systems suitable for lake monitoring.

| Satellite / Sensor | Spectral Bands (µm) | Spatial Resolution (m) | Radiometric Resolution (bits) | Swath Width (km) | Repeat Orbit (days) | Cost per Image ($) |
|---|---|---|---|---|---|---|
| **Landsat-7** ETM+ | 0.52–0.90 | 15 | 8 | 180 | 16 | Available free of charge |
| | 0.45–0.52 | 30 | | | | |
| | 0.52–0.60 | | | | | |
| | 0.63–0.69 | | | | | |
| | 0.75–0.90 | | | | | |
| | 1.55–1.75 | | | | | |
| | 2.09–2.35 | | | | | |
| | 10.4–12.5 | 60 | | | | |
| **Landsat-5** TM | 0.45–0.52 | 30 | 8 | 180 | 16 | Available free of charge |
| | 0.52–0.60 | | | | | |
| | 0.63–0.69 | | | | | |
| | 0.76–0.90 | | | | | |
| | 1.55–1.75 | | | | | |
| | 2.08–2.35 | | | | | |
| | 10.4–12.5 | 120 | | | | |
| **SPOT-5** HRG | 0.48–0.71 | 2.5 or 5 | 8 | 60 | 26, but 4 - 5 days with off-nadir viewing | 6,750 |
| | 0.50–0.59 | 10 | | | | 3,375 |
| | 0.61–0.68 | | | | | |
| | 0.78–0.89 | | | | | |
| | 1.58–1.75 | 20 | | | | |
| **Resourcesat-1** (IRS-P6) LISS-3 | 0.52–0.59 | 23.5 | 7 | 141 | 24 | 2,275 |
| | 0.62–0.68 | | | | | |
| | 0.77–0.86 | | | | | |
| | 1.55–1.70 | | | | | |
| AWiFS | 0.52–0.59 | 56 | 10 | 740 | 5 | 600 |
| | 0.62–0.68 | | | | | |
| | 0.77–0.86 | | | | | |
| | 1.55–1.70 | | | | | |
| **RapidEye** System of 5 satellites | 0.44–0.51 | 5 | 12 | 77 | 5.5 days with daily off-nadir viewing | 7,500 |
| | 0.52–0.59 | | | | | |
| | 0.63–0.68 | | | | | |
| | 0.69–0.73 | | | | | |
| | 0.76–0.85 | | | | | |

Looking ahead, the Landsat Data Continuity Mission (LDCM) scheduled for launch in 2012 will provide continued acquisition of data consistent with the Landsat ETM+. Although the data will be available at no cost, only one satellite will provide coverage at 16-day intervals.

Each of these systems has its own advantages, such as higher spatial resolution, wider swath width or more spectral bands; however, their usefulness for regional lake assessments is limited by several disadvantages, including

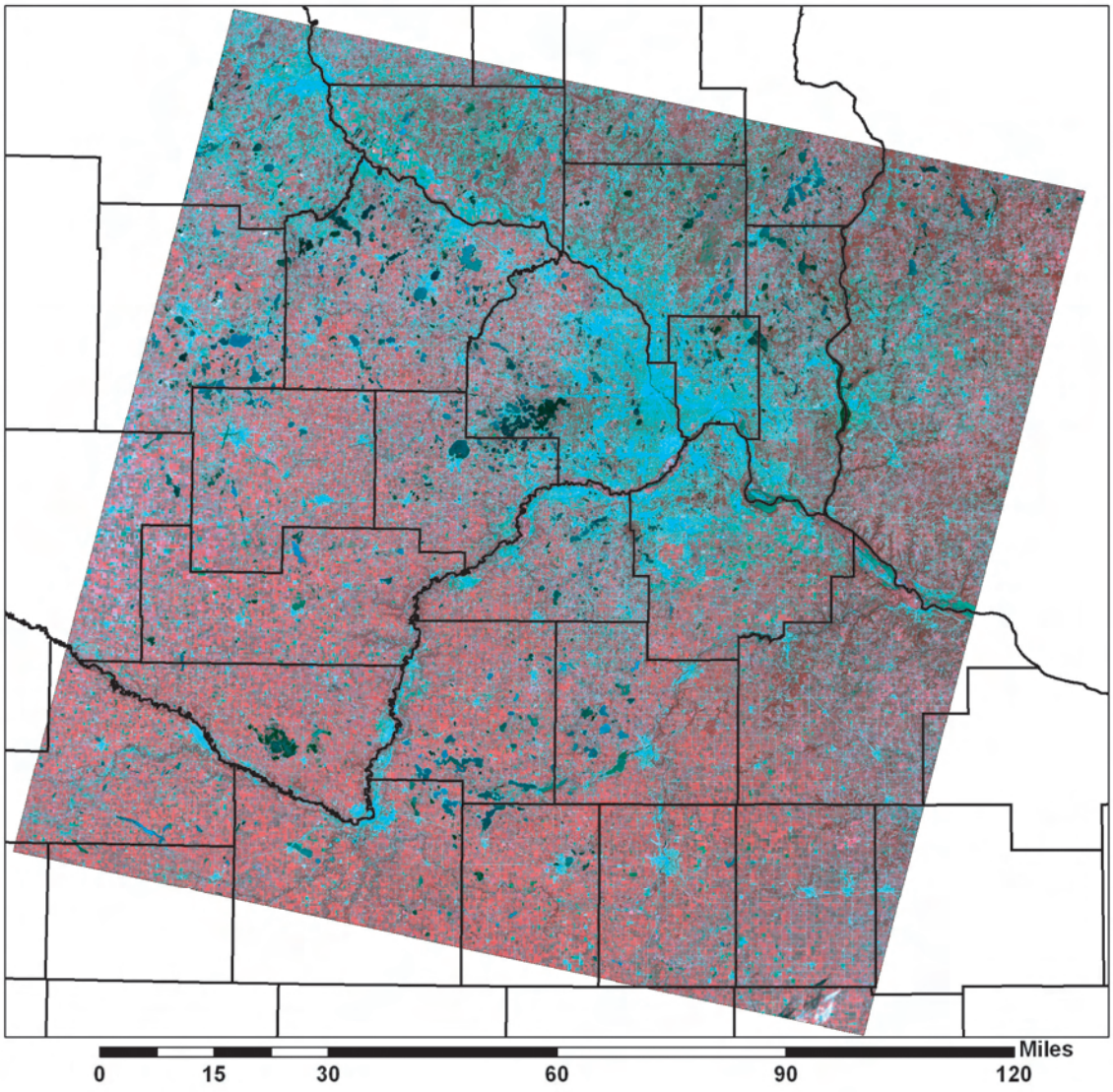


**Figure 4.1.** Landsat TM imagery of east-central Minnesota, including the seven-county Twin Cities Metropolitan Area.

the lack of a blue band (useful for water clarity assessment) and/or middle infrared and thermal bands (which can improve image processing), limited coverage, higher cost, or the necessity for "tasking" (scheduling image acquisitions in advance). Although the potential is great for a better system than Landsat, its spectral bands, radiometric resolution, spatial resolution, temporal coverage, data availability and relatively low cost make it particularly useful for regional assessment of inland lakes. The Landsat geographic coverage of 31,000 $km^2$/image allows for the simultaneous assessment of thousands of lakes in lake-rich areas. The spatial resolution of 30 m is suitable for all lakes down to about 4 ha and enables mapping in-lake variability.

This chapter describes several studies that used Landsat imagery to monitor environmental conditions in lakes. The primary sensor on Landsats-1, -2 and -3 was the Multispectral Scanner (MSS). These satellites had an 18-day repeat cycle, spatial resolution of 79 m, and four spectral bands ranging from visible green to near-infrared (NIR) wavelengths. Landsat-3 added a thermal infrared (TIR) band. Landsat-4 and -5 have a 16-day repeat cycle, an improved spatial resolution of 30 m, and included both the MSS and the TM sensor. The TM sensor has seven bands from visible blue to thermal infrared with improved spatial resolution of 30 m for the visible, near, and

middle infrared bands, and 120 m for the thermal infrared band. Landsat-6 failed to reach orbit at launch. The ETM+ sensor on Landsat-7 is similar to the TM but includes a 15-m panchromatic band, 60-m resolution for the thermal band, and improved radiometric calibration. However, in most respects, TM and ETM+ are similar and either can be used, such as for the imagery over the Twin Cities Metropolitan Area, Minneapolis-St. Paul, Minnesota (Fig. 4.1) and the Lake Minnetonka area (Fig. 4.2).

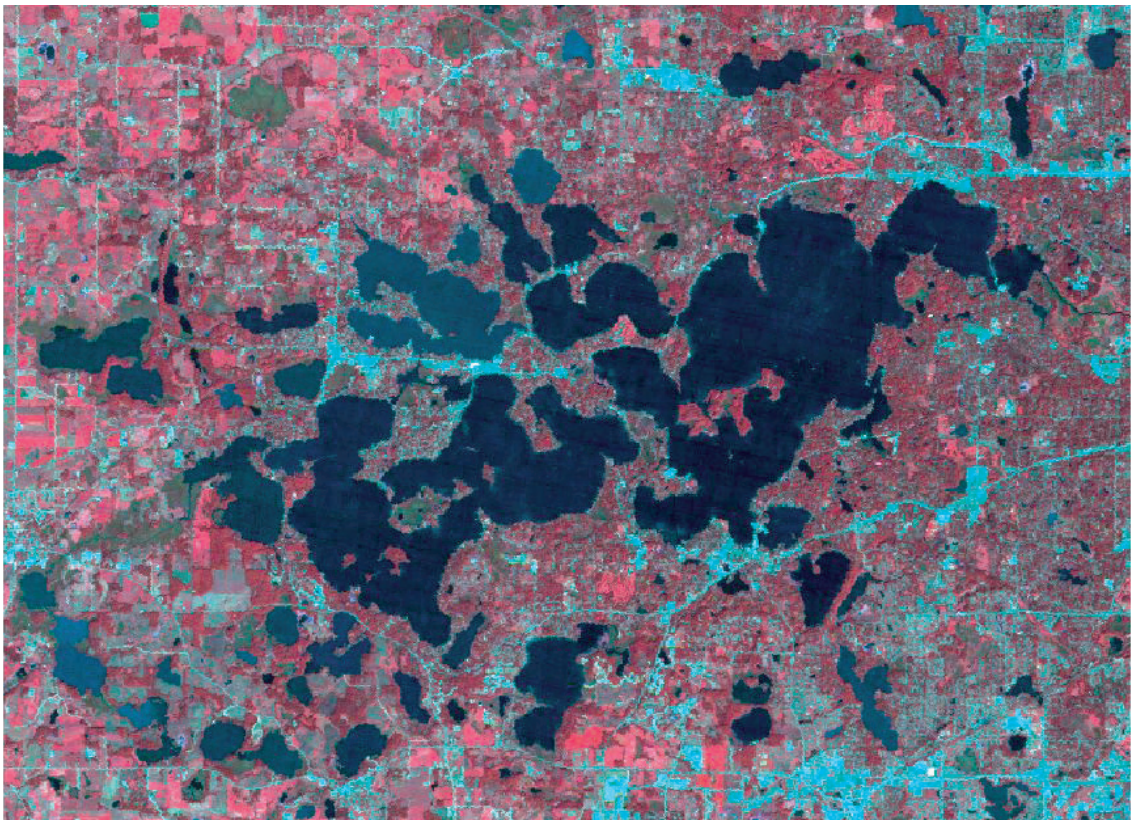

**Figure 4.2.** Landsat TM imagery of the Lake Minnetonka area near Minneapolis, MN.

## 4.2. Acquiring Landsat imagery

Further information on the Landsat systems and data products is available at:

http://landsat.gsfc.nasa.gov/
http://landsat.usgs.gov/index.php

All Landsat data acquired over North America have been archived and are available from the USGS EROS Data Center.

http://earthexplorer.usgs.gov/
http://glovis.usgs.gov/

## 4.3. Case study 1 – Statewide water clarity assessments for Minnesota, Wisconsin and Michigan

Effective environmental planning and management requires long term water quality information on a wide regional scale. Unfortunately only a limited number of lakes are regularly monitored by conventional observations, and historical water quality data for most lakes are deficient. Although we cannot go back in time and collect additional water quality information using conventional field methods to fill gaps from previous efforts, the Landsat data collected and archived regularly since the early 1970s enable historical water quality information to be extracted from the Landsat images. The extraction of historic and current water quality data from satellite images, coupled with existing data collection efforts, may facilitate the development of comprehensive regional databases used to evaluate regional differences and water quality trends over time. If used in combination with land-use data, this information can help determine the impacts of different land-use practices on lake condition (Fig. 4.3). Results of such analyses will help local and state agencies make informed decisions about development policy and improve the management of lake resources.

Development of comprehensive water quality databases is well underway in Minnesota, Wisconsin and Michigan, and all three states have completed Landsat statewide water clarity assessments (Fig. 4.4). The methods used for these assessments will be described in the next section. The University of Minnesota Remote Sensing and Geospatial Analysis Laboratory (RSL) in collaboration with the Minnesota Pollution Control Agency (MPCA) has completed a historical water clarity database of more than 10,000 lakes that cover the entire state for ~1985, ~1990, ~1995, ~2000 and ~2005 time periods (see http://water.umn.edu/ and Olmanson *et al.* 2008). The correlation between satellite data and field measurements of Secchi depth was strong (average $R^2$ of 0.83 and range 0.71–0.96) for more than 100 images analyzed. These water clarity atlases are currently being used to assess spatial patterns and temporal trends in lake water clarity based on surrounding land use and cover by using a geographical information system (GIS) to link the lake clarity data with land use features. The RSL is currently working on additional water clarity assessments which include using MSS imagery for the ~1975 time period and more recent 2006, 2007 and 2008 Landsat TM and ETM+ imagery. The data can be accessed in a LakeBrowser application at http://water.umn.edu.

In Wisconsin, a series of statewide assessments have been produced by cooperation between the University of Wisconsin (UW) and the Wisconsin Department of Natural Resources (WDNR). The first such assessment used Landsat MSS imagery from ~1980 to map water clarity in more than 3000 lakes (Scarpace *et al.* 1979, Martin *et al.* 1983). The higher spatial resolution of Landsat TM and ETM+ allowed this number to increase to ~8000 lakes in similar assessments in the ~1992, ~2000, and ~2005 time periods (Chipman *et al.* 2004, Peckham and Lillesand 2006).

In Wisconsin's 2000 assessment, Landsat TM and ETM+ were used in combination to estimate water clarity in 8645 lakes in 1999–2001 (see http://www.lakesat.org). The median $R^2$ for the regression models of Secchi depth and the spectral measurements was 0.79 for the 17 images analyzed. In an independent validation of 233 lakes the root mean squared error (RMSE) ranged from 0.61–0.89 m (Chipman *et al.* 2004).

Following the 2000 statewide assessment, the WDNR took over full responsibility for this program. During the transition period, workshops, meetings and other training processes facilitated the transfer of this technology from UW to the WDNR, and the completion of the 2005 assessment demonstrated the success of this approach. Currently, the WDNR continues to acquire satellite imagery and field data to support ongoing Landsat-based lake monitoring.

In Michigan, similar methods have been used to conduct a Landsat water clarity assessment for the 2005 time period (http://mi.water.usgs.gov:80/splan1/sp00301/remotesensing.php). A regional view of satellite-mapped water clarity in the region's lakes was produced for the 2000 time period, including final results from Minnesota and Wisconsin, and preliminary sample results for selected areas in Michigan (Fig 4.4). The existence of these

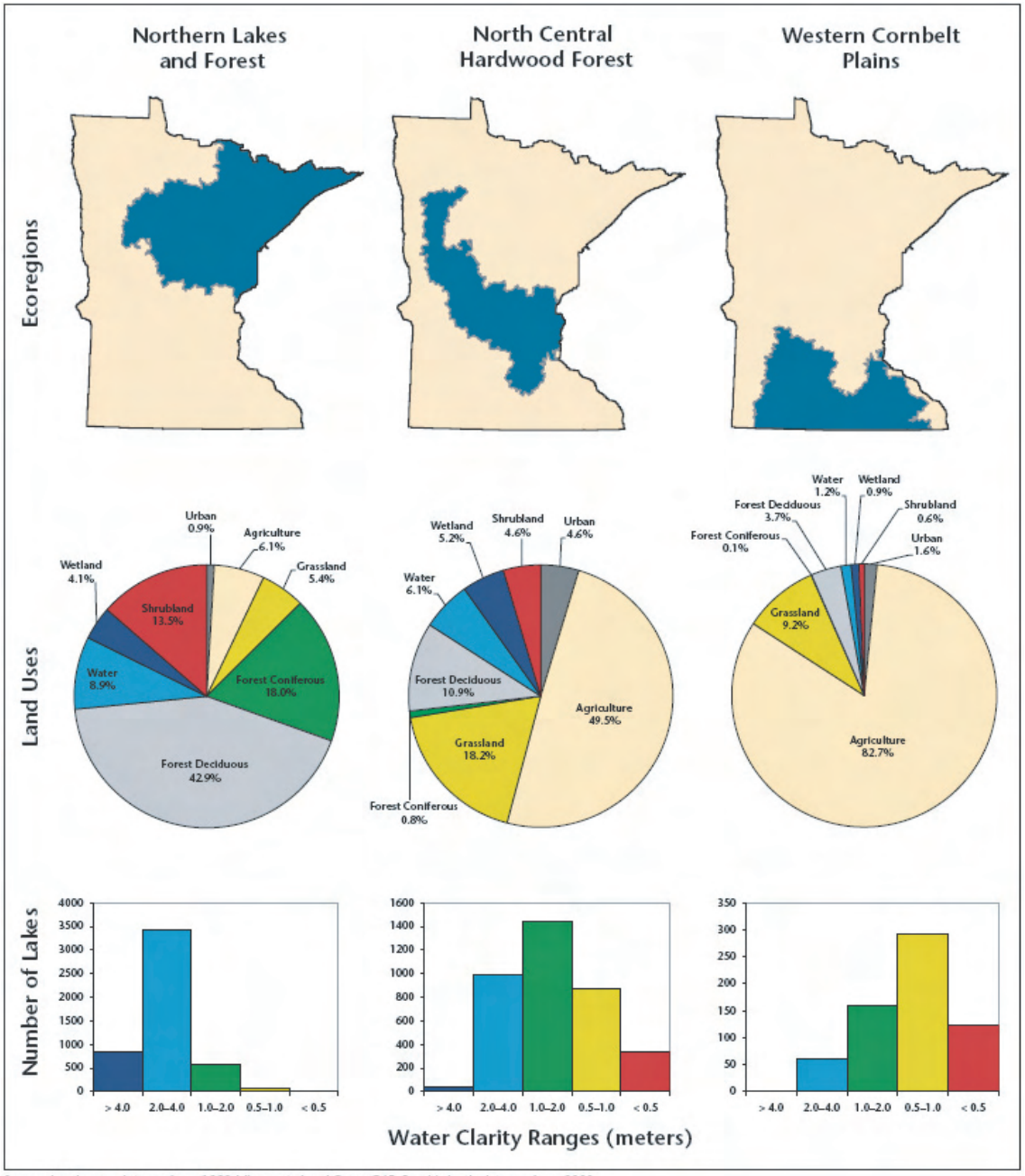


Source: Land-cover data are from 1990 Minnesota Land Cover GAP. Secchi depth data are from 2000.

Note: One (1) meter equals 3.3 feet.

**Figure 4.3.** Land use/land cover distribution and water clarity in three Minnesota ecoregions (Fig. 3 in Brezonik *et al.* 2007). Reprinted with permission of the University of Minnesota's Center for Urban and Regional Affairs (CURA).

statewide assessments covering thousands of lakes on multiple dates in the lake-rich states of the Upper Midwest region should provide an invaluable resource for future research on the causes and effects of spatial and temporal variations in lake water clarity regionally.

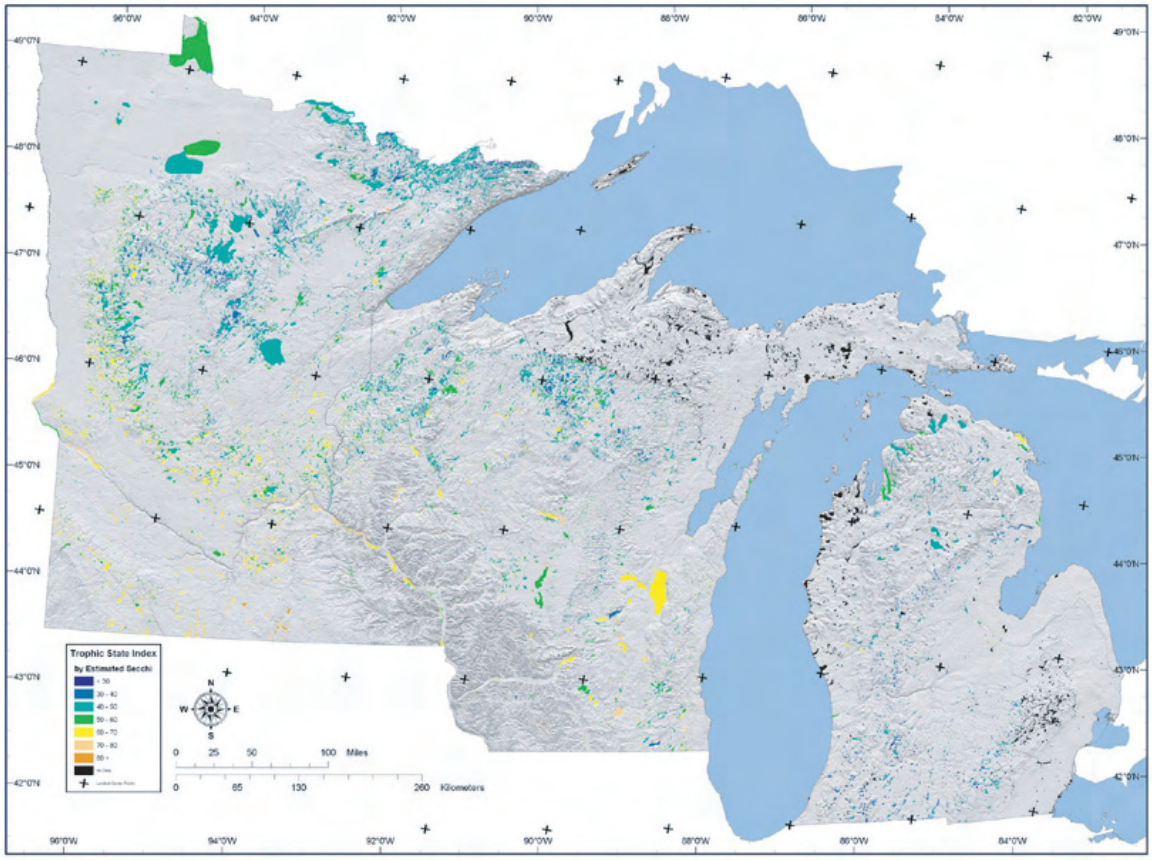


**Figure 4.4.** Three-state Landsat-based 2000 water clarity map for Minnesota, Wisconsin and Michigan. Results for Michigan are preliminary, and only limited areas are shown. (map courtesy of Sam Batzli, University of Wisconsin-Madison Environmental Remote Sensing Center).

## 4.4. Case Study 2 – Pilot water clarity assessments for Illinois, Indiana and Ohio

As part of the NALMS EPA remote sensing project, the University of Minnesota Remote Sensing and Geospatial Analysis Laboratory completed Landsat water clarity assessments of lakes in Illinois, Indiana and Ohio using one path of Landsat imagery for each state (Fig. 4.5). The paths of Landsat imagery cover a large proportion of the lakes in each state. *In situ* data used for calibration of the Landsat data were provided by the state cooperators: Illinois Environmental Protection Agency, Northeastern Illinois Planning Commission, Indiana University, Ohio DNR, and Kent State University. The water clarity assessments for each state have been made available to state, regional and local agencies and the general public (http://www.water.umn.edu/nalms/), and the data are made available at a pixel-level basis in a format suitable for use with interactive mapping platforms such as Google Earth.

### Overview

The overall objective of this project was to determine whether methods proven effective in Minnesota and Wisconsin (Kloiber *et al.* 2002b, Chipman *et al.* 2004, Olmanson *et al.* 2008) to assess key management indicators of trophic state are effective in other Midwest states. Three common water quality variables that indicate lake trophic state are total phosphorus (TP), chlorophyll *a* (chl-*a*) and Secchi disk transparency (SD). Lake managers use these variables, along with a variety of transformations such as Carlson (1977) trophic state index (TSI). Secchi depth is usually the most commonly collected water quality variable and is strongly related to Landsat

TM/ETM+ blue and red bands (Kloiber *et al.* 2002a). This project involved calibrating Landsat TM and ETM+ imagery with field-collected SD measurements and applying that relationship to estimate SD for all lakes in an image. The results are then mapped as distributions of SD or transformed to Carlson's TSI based on transparency: TSI(SD) = 60 – 14.41 ln(SD).

Differences in lake SD may be due to factors other than algal turbidity (as indicated by chlorophyll levels). Most significant of these (nontrophic-state) factors are non-algal turbidity (including soil-derived clays and suspended sediment) and humic color. Therefore, the results are based on SD calibrations as satellite-estimated SD or TSI(SD), which identifies the value as an index based on transparency, rather than the common term, TSI.

## Methods

The procedures used for this project are described in Kloiber *et al.* (2002a), and step-by-step image processing procedures are outlined in Olmanson *et al.* (2001). The procedures described are practical and efficient methods that apply empirical relationships to Landsat imagery for routine, regional-scale water clarity assessments of lakes. Some modifications to the methodology were made when appropriate as experience and advances in software and computer hardware have improved and image processing procedures have simplified.

### *Satellite imagery and lake reference data*

For this assessment we targeted recent clear paths of Landsat imagery from a late summer index period. Clear imagery is critical for water clarity assessments. Clouds, cloud shadows and haze affect the spectral radiometric response recorded and if used for water clarity assessments will give erroneous results (Olmanson *et al.* 2008). Using paths of Landsat imagery (2–5 consecutive images) as an alternative to individual images has many advantages. It decreases processing time and increases accuracy of the assessment because all images can be processed at the same time, and the larger area allows a larger number of data points and usually increases the range of water clarity conditions of the calibration data. Stadelmann *et al.* (2001) found images selected from a late summer index period (July 15–September 15) would work well for remote sensing of water clarity in Minnesota. For this project we extended the window a few days (under the assumption that the window could be increased in lower latitudes) in Indiana to acquire some recent clear imagery. The major advantages to using images from this late summer index period is that short-term variability of lake water clarity is at a seasonal minimum and most lakes have seasonal maximum algal concentrations and minimum water clarity.

In lakes, water clarity commonly is measured by a Secchi disk (a 20-cm [8-inch] diameter, white and black, white, or black disk) lowered into the water until it can no longer be seen. The depth of disappearance is called the Secchi depth. Algae and algal-derived particles, organic matter (humic color), and soil-derived clay and silt particles all affect water clarity. In glacial lakes, soil-derived turbidity usually is not important, and water clarity most commonly is related to algal abundance. Thus, Secchi depth is an indirect measure of a lake's trophic state, its status in terms of nutrient concentrations and biological productivity. In some lakes (*e.g.*, reservoirs), soil-derived turbidity is a major component of water clarity and cannot be used as an indirect measure of trophic state. However, water clarity is a useful measure of water quality because it relates directly to human-use perceptions of quality (Heiskary and Walker 1988). Because of its simplicity, Secchi depth is one of the most frequently measured properties of lakes and amenable to citizen monitoring programs.

The availability of lake reference data varied in each participating state. To calibrate the imagery we used water clarity data collected as near to the imagery date as data availability allowed.

For Illinois we used Landsat TM imagery from 31 July 2006, path 23/rows 31–35, which was mostly clear with a few clouds south of Chicago (Fig. 4.5). Water clarity data were supplied by the Illinois Environmental Protection Agency and Northeastern Illinois Planning Commission. Data availability was good with data for 59 lakes collected within 7 days of the image date.

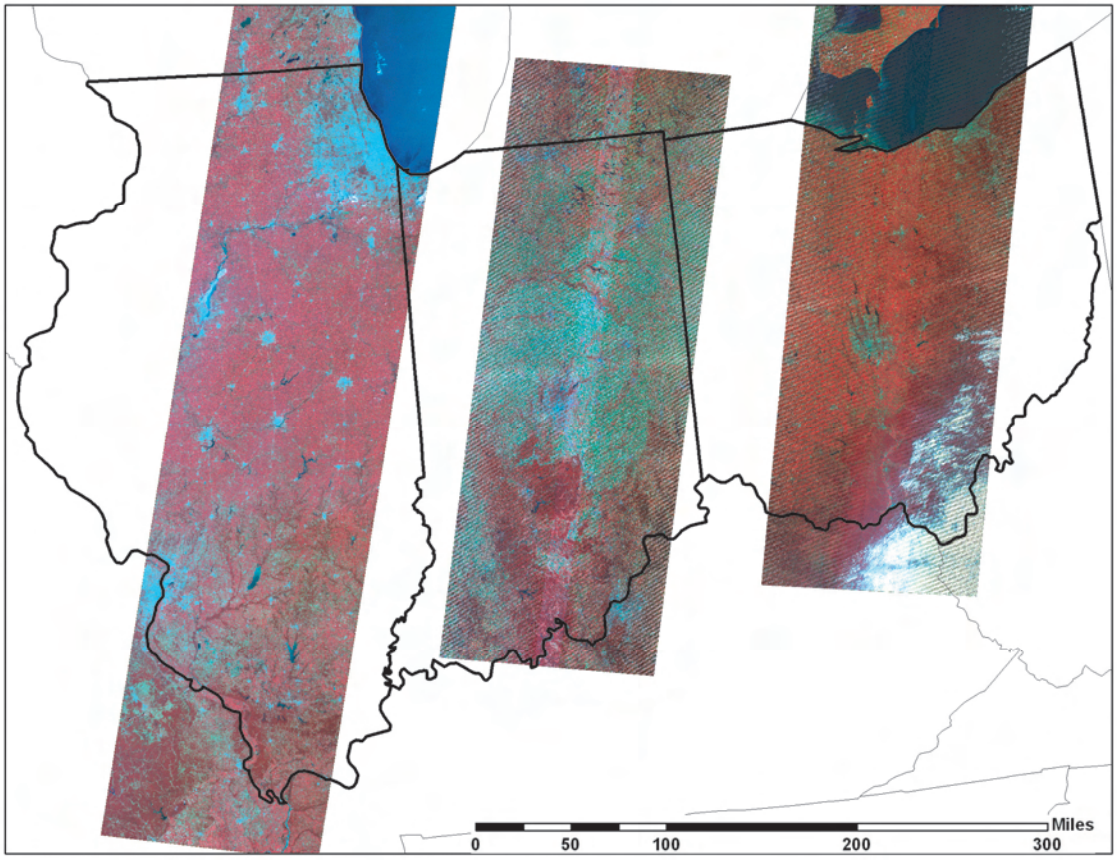


**Figure 4.5.** Landsat TM and ETM+ imagery used for water clarity assessments in Illinois, Indiana, and Ohio. (See text for specific path/row numbers and image acquisition dates).

For Indiana we used Landsat ETM+ SLC off imagery from 21 September 2004, path 21/rows 31–33, which was mostly clear with some minor cloud cover (Fig. 4.5). Water clarity data were supplied by Indiana University, and data availability was good with data for 34 lakes collected within 8 days of the image date.

Finally, for Ohio we used Landsat ETM+ SLC off imagery from 12 August 2006, path 19/rows 31–33, which was mostly clear with some cloud cover in the southeastern portion of the image (Fig. 4.5). Water clarity data were supplied by the Ohio DNR and Kent State University. Data availability was relatively sparse, with data for only nine lakes within 10 days of the image date.

### *Classification procedures*

This section summarizes our image classification procedures; more detail is provided by Olmanson *et al.* (2001), and the rationale for the procedures is described by Kloiber *et al.* (2002a). We used ERDAS Imagine, image processing software, and ESRI ArcGIS, geographical information system (GIS) software for the image processing steps. Acquiring a representative sample from the image for each lake was our primary objective. Ideally, the sample should represent the center portion of the lake where reflectance from vegetation, the shoreline, or the lake bottom does not affect the spectral response.

As with most image processing, preprocessing the imagery is needed to assure good results. This included rectifying the imagery using approximately 40 well-distributed ground control points (GCP). The geometrically corrected images had a positional accuracy (RMSE) on the order of ±0.25 pixels, or 7.5 m. The next step was to

remove from the image any areas covered with clouds or haze. We did not perform atmospheric correction or normalization of the imagery for the regression method used.

Once the preprocessing of the imagery is completed, processing for water clarity assessments begins by first producing a "water-only" image by performing an unsupervised classification (clustering) in ERDAS Imagine. Because water features tend to have very different spectral characteristics from terrestrial features, water is one or more distinct classes that can be easily identify. We then masked out terrestrial features creating a water-only image and performed a second unsupervised classification on the water-only image to generated spectral signatures of each class. We used these signatures, along with the location of where the pixels occur, to differentiate classes containing clear water, turbid water and shallow water (where sediment and/or macrophytes affect spectral response). Based on this analysis, we masked off the affected pixels. Next, the spectral-radiometric data from the "open-water" image were obtained to develop relationships with measured SD. Samples from each lake can be digitized manually, or a polygon layer can be used to help automate the process, as described in Olmanson *et al.* (2001). For this project we digitized sample locations. The signature editor in ERDAS Imagine was used to extract the spectral-radiometric data from the image for all the lakes with field data.

We calibrated the Landsat imagery using the SD measurements collected within a few days of the image acquisition date. The window used depended on the availability of SD data and was increased to 10 days in Ohio where data were sparse. Using log-transformed SD data as the dependent variable and Landsat Thematic Mapper band 1 (TM1) and the TM1:TM3 ratio as independent variables, we performed a multiple regression. The general predictive equation used for water clarity estimation is:

$$\ln(SD) = a(TM1/TM3) + b(TM1) + c$$

where a, b and c are coefficients fit to the calibration data by the regression analysis; ln(SD) is the natural logarithm of the Secchi depth for a given lake; and TM1 and TM3 are the brightness values measured by the Landsat sensor in the blue and red bands, respectively.

A model was developed for the Landsat images and then applied to the open water pixels of each image to create a pixel-level water clarity map. The pixel-level method was used for this project due to the absence of a lake polygon layer appropriate for image processing. The pixel-level method has an advantage over lake-level maps because intra-lake differences can be distinguished, especially apparent in reservoirs where sediment settles out as water movement slows.

## Results and discussion

For this assessment we used 11 Landsat images from three different dates (one path for each of the three states). For Indiana and Ohio a model was developed for each path of imagery from the same date. For Illinois two models were developed. The model for rows 31 and 32 represented lakes in northern Illinois, which are pre-

**Table 4.2.** Lake clarity classification statistics for Illinois, Indiana and Ohio.

| State | N | SD Range (m) | $R^2$ | SEE | Number of Lakes Assessed* |
|---|---|---|---|---|---|
| Illinois N | 23 | 0.3–4.1 | 0.87 | 0.30 | ~526 |
| Illinois S | 36 | 0.2–4.6 | 0.81 | 0.33 | ~931 |
| Indiana | 31 | 0.2–7.6 | 0.78 | 0.28 | ~1067 |
| Ohio | 9 | 0.4–4.7 | 0.80 | 0.40 | ~430 |

* Lakes over 6 ha within state boundary.

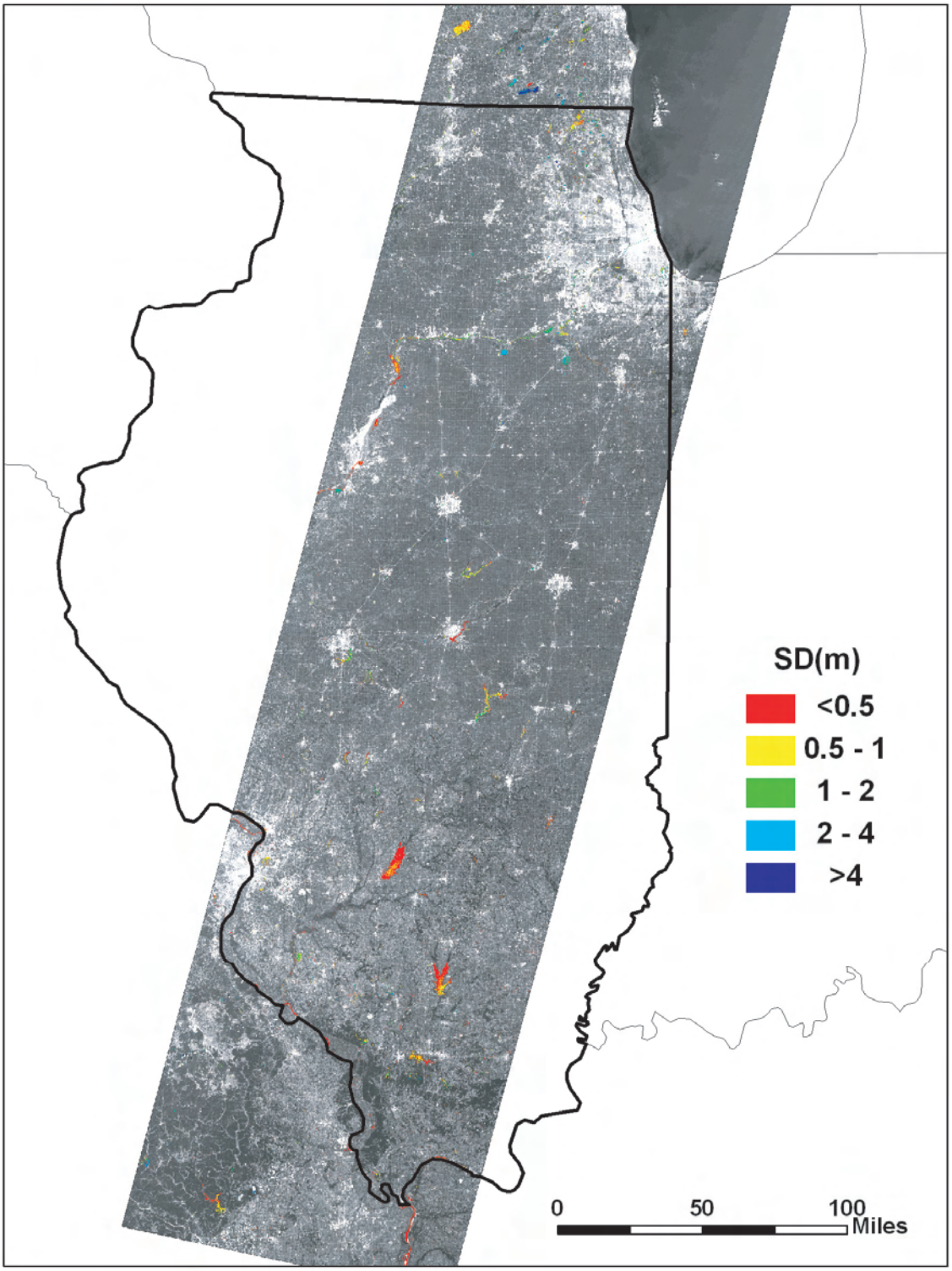


**Figure 4.6.** 31 July 2006 Landsat lake clarity map of Illinois lakes with Landsat TM band 2 as the background.

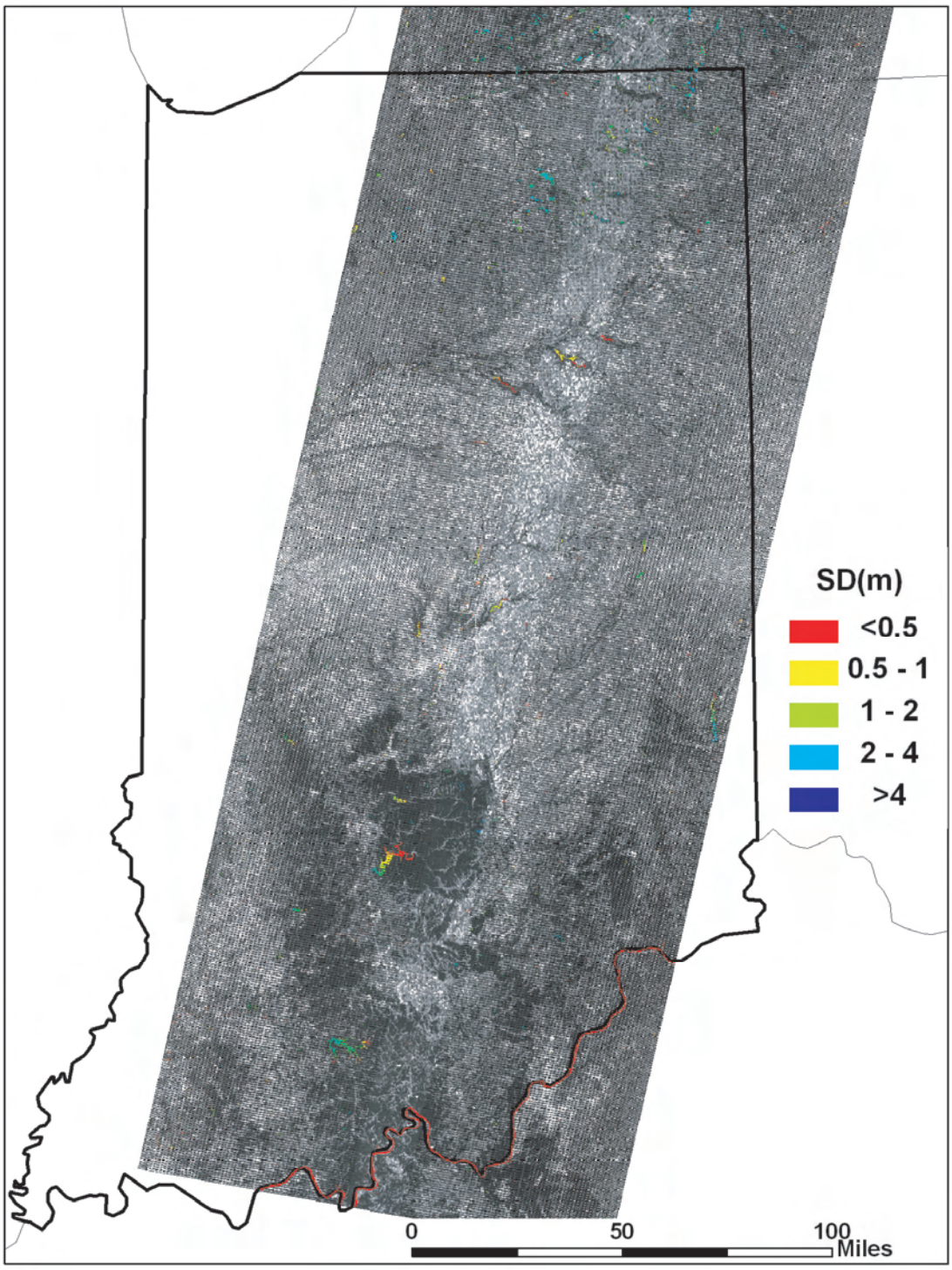


**Figure 4.7.** 21 September 2004 Landsat lake clarity map of Indiana lakes with Landsat ETM+ band 2 as the background.

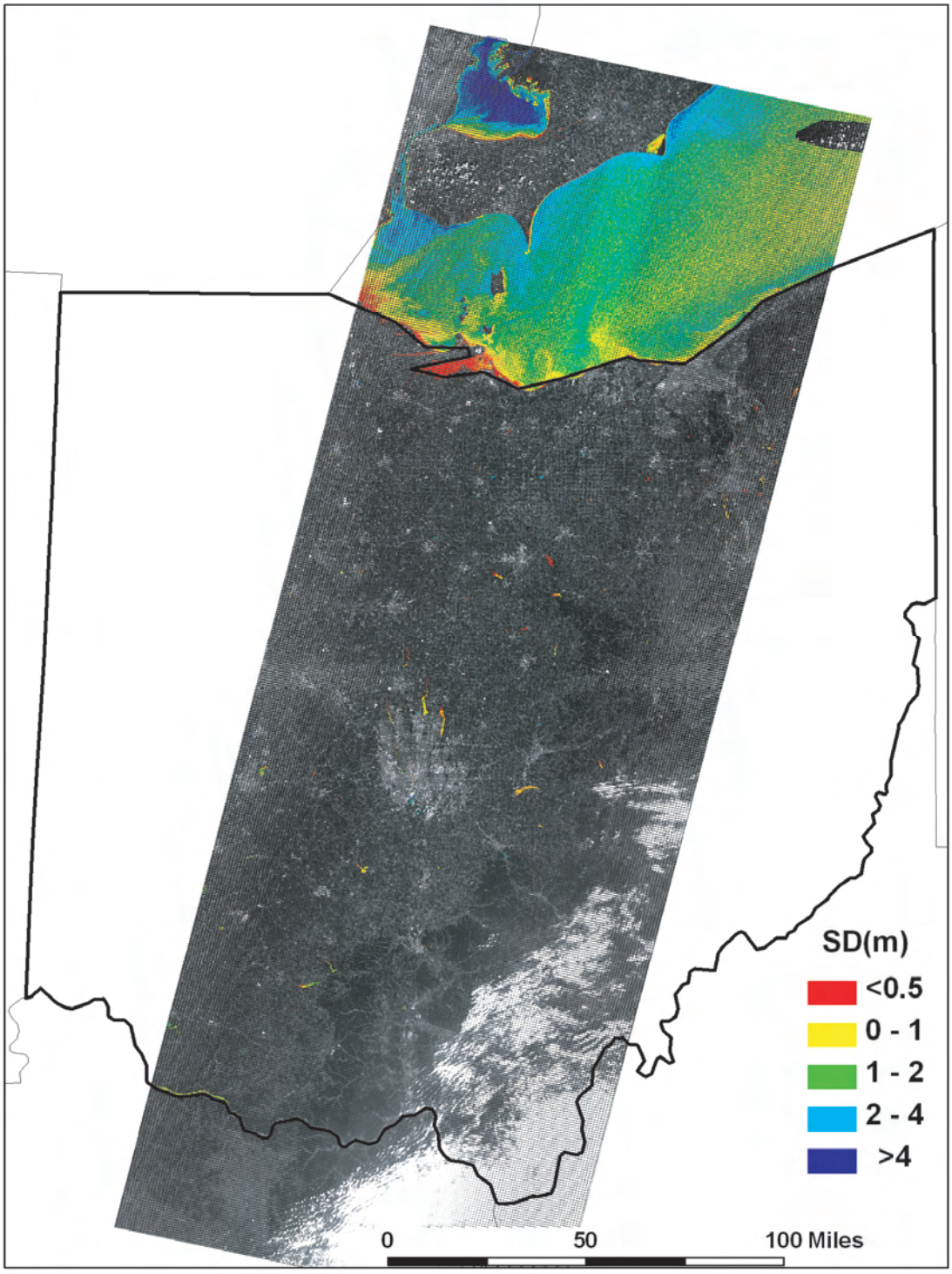


**Figure 4.8.** 12 August 2006 Landsat lake clarity map of Ohio lakes with Landsat ETM+ band 2 as the background.

dominantly algae-dominated lakes. The model for rows 33, 34 and 35 represented lakes in central and southern Illinois, which are more sediment-dominated lakes. Each of the models showed strong relationships between the water clarity data and the spectral-radiometric response of the Landsat data. The number of data points (n), coefficient of determination ($R^2$), standard error of estimate (SEE) and the number of lakes assessed per path of images were recorded (Table 4.2). Values of R2 (a measure of goodness of fit) for the regression relationships to establish the coefficients of the predictive equation range 0.78–0.87 with an average of 0.81, meaning that they explain 78–87% of the variance in the relationship. Given that ground-based measurements of Secchi depth are

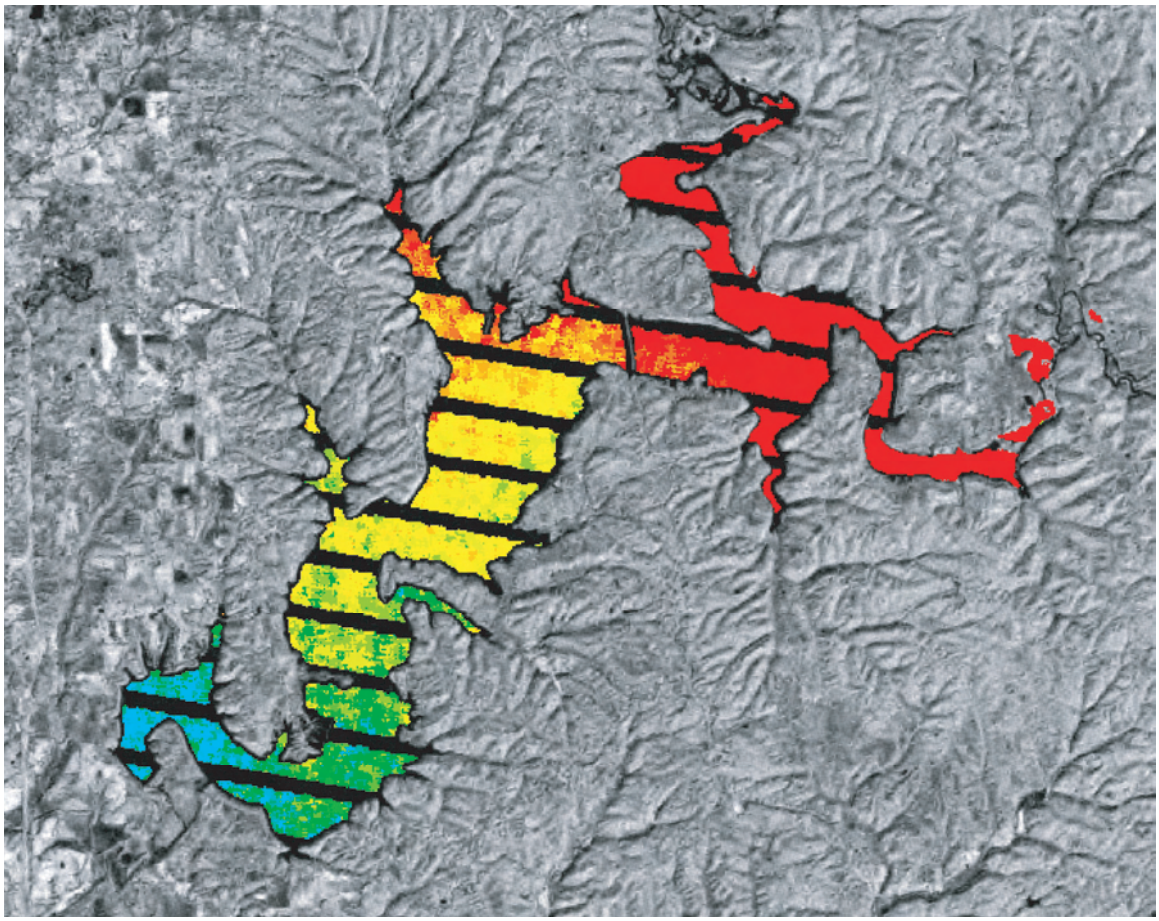

**Figure 4.9.** Example of variable water clarity in Lake Monroe near Bloomington, IN. The black lines across the lake are missing data due to the scan line corrector problem with Landsat-7 ETM+ data.

themselves subject to some imprecision, we consider this to be quite acceptable. For this project we assessed the water clarity of more than 3000 lakes: 1400 in Illinois (Fig. 4.6), 1100 in Indiana (Fig. 4.7), 400 in Ohio (Fig. 4.8), and additional lakes outside of these state boundaries.

The maps indicate differences in water clarity among lakes in these states. Reservoirs, which are common in central and southern Illinois, Indiana and Ohio, typically have variable water clarity where the sediment settles as water moves into the reservoir (Fig. 4.9). Distribution of water clarity of lakes >6 ha within each state boundary (Fig. 4.10) show that Indiana has some of the better water clarity of the three states. The water clarity is distributed in a typical bell curve with a median water clarity of 1.32 m. Illinois has a median water clarity of 0.87 m, with water clarity skewed toward the lower water clarity classes. Ohio has the lowest water clarity with a median of 0.62 m and is highly skewed toward the lower water clarity classes.

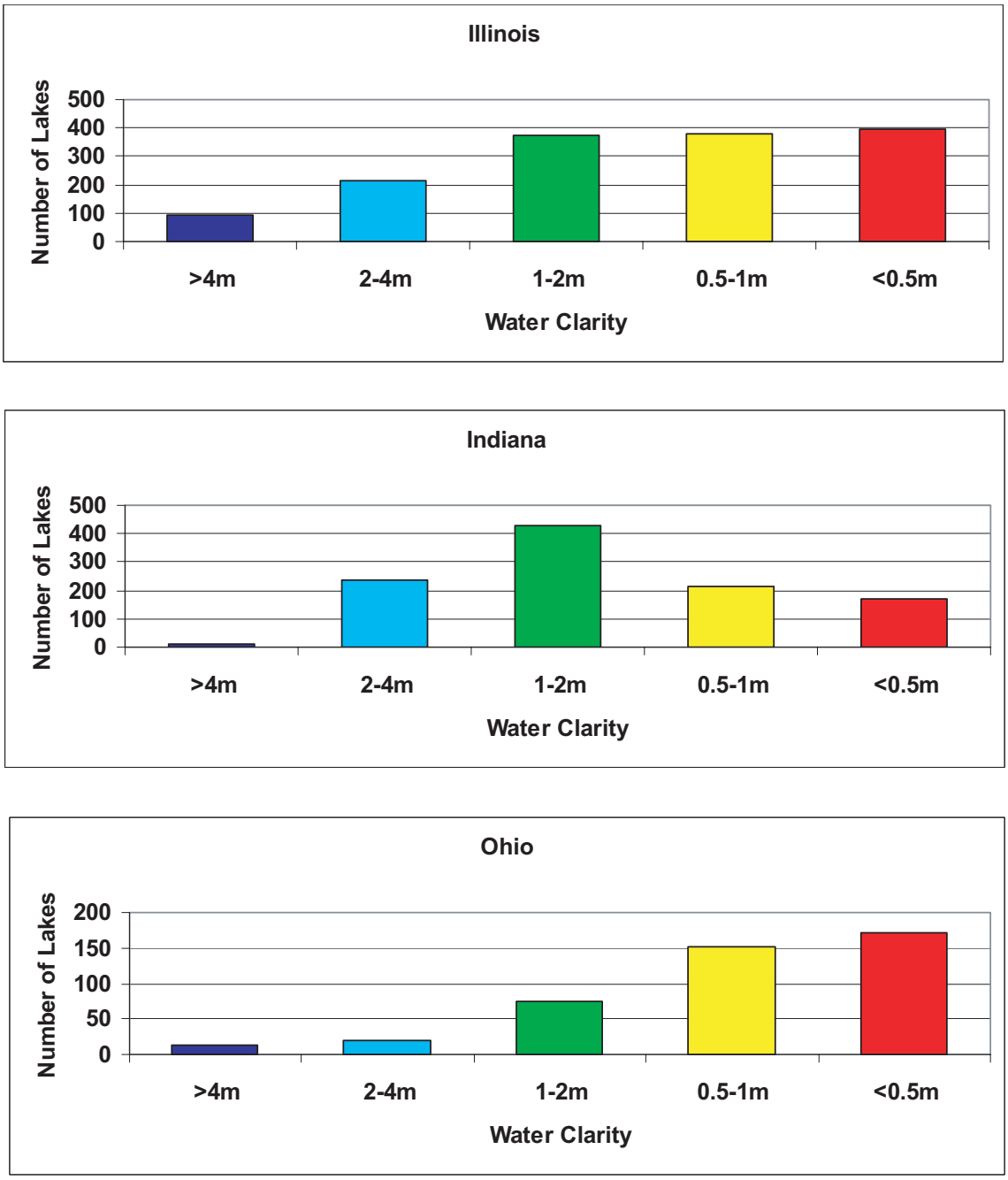


**Figure 4.10.** Water clarity distribution of Illinois, Indiana and Ohio lakes >6 ha.

## 4.5. Costs and resource requirements

The costs required to conduct a statewide or regional assessment of water clarity using satellite imagery include the cost of the imagery itself, the GIS and image processing software used, any additional field data that need to be acquired, and the personnel time required for the project. As discussed in the introduction to this chapter, a number of "moderate-resolution" satellite systems could be used for this type of effort, and the costs per image vary widely. We focused on the use of Landsat imagery, which has several distinct advantages, including low

cost since all Landsat imagery is provided at no cost over the Internet; however, the other costs listed above still need to be considered.

The work described in these case studies primarily involved the use of the ERDAS Imagine image processing software and ESRI ArcGIS software. Other similar software systems (*e.g.*, RSI ENVI) could also be used. If this software is not already available in-house, the costs of licenses will need to be considered. License costs can vary widely depending on several factors, including vendor pricing policies, type of organization (*e.g.*, educational vs. commercial) and number of licenses. Typically, costs may run from $500–5000 per year. Less-expensive (or free) image processing and GIS software systems are available but may not have all the functionality needed for the complete data processing stream utilized in these assessments.

A lengthy training period may be required for analysts new to this field (or new to the software involved). Once the analyst is familiar with the procedures and all data (imagery and field data) have been compiled, a sequence of Landsat images located along a single path can be analyzed in one or two days. For example, prior to the 2005 Wisconsin statewide assessment, a training workshop for Wisconsin Department of Natural Resources employees was conducted at the University of Wisconsin. Each trainee was given an individual Landsat image and pre-collected field data; during the day and a half of the workshop, the analyses of four of the five scenes were completed and the fifth was nearly completed. Note that in this case the trainees were guided at each step of the process by detailed instructions tailored to match the specific details of Wisconsin's field data and GIS resources. For a state or other agency just beginning work on a satellite lake assessment, the time required to develop specific procedures and complete analysis of imagery might well take several months, depending on the employees' prior experience with GIS and image processing software.

The methods discussed in this chapter require at least some field data to develop regression models relating water clarity to satellite-measured radiance data. Ideally, a large number of sampled lakes (>50) should be included in each image, with water clarity samples collected close to the date of the satellite overpass. Where only a few samples are available in an image area (<20 sampled lakes), extending the "window" of field data acquisition to accept data collected within 10 days of the image date may be necessary. In general, assessments of images based on small numbers of field-sampled lakes will have lower accuracy. For many U.S. states, existing lake monitoring programs can be used to acquire sufficient data for this purpose.

## 4.6. References

Brezonik, P.L., L.G. Olmanson, M.E. Bauer and S.M. Kloiber. 2007. Measuring water clarity and quality in Minnesota lakes and rivers: A census-based approach using remote-sensing techniques. CURA Reporter 37(2):3-13.

Carlson, R.E. 1977. A trophic state index for lakes. Limnol. Oceanogr. 22:361-369.

Chipman, J.W., T.M. Lillesand, J.E. Schmaltz, J.E. Leale and M.J. Nordheim. 2004. Mapping lake water clarity with Landsat images in Wisconsin, USA. Can. J. Remote Sens. 30:1-7.

Heiskary, S.A. and W.W. Walker Jr. 1988. Developing phosphorus criteria for Minnesota lakes. Lake Reserv. Manage. 4:1-9.

Kloiber, S.M., P.L. Brezonik, L.G. Olmanson and M.E. Bauer. 2002a. A procedure for regional lake water clarity assessment using Landsat multispectral data. Remote Sens. Environ. 82(1):38-47.

Kloiber, S.M., P.L. Brezonik and M.E. Bauer. 2002b. Application of Landsat imagery to regional-scale assessments of lake clarity. Water Res. 36:4330-4340.

Lathrop, R.G. 1992. Landsat Thematic Mapper monitoring of turbid inland water quality. Photogram. Eng. Rem. S. 58:465-470.

Lillesand, T.M., W.L. Johnson, R.L. Deuell, O.M. Lindstrom and D. E. Meisner. 1983. Use of Landsat data to predict the trophic state of Minnesota lakes. Photogram. Eng. Rem. S. 49:219-229.

Martin, R.H., E.O. Boebel, R.C. Dunst, O.D. Williams, M.V. Olsen, R.W. Merideth Jr. and F.L. Scarpace. 1983. Wisconsin lakes – a trophic assessment using Landsat digital data. Wisconsin Department of Natural Resources, Wisconsin Lake Classification Survey Project. Report S00536601. 294 p.

Mayo, M., A. Gitelson, Y.Z. Yacobi and Z. Ben-Avraham. 1995. Chlorophyll distribution in Lake Kinneret determined from Landsat Thematic Mapper data. Int. J. Remote Sens. 16 (1):175-182.

Olmanson, L.G., S.M. Kloiber, M.E. Bauer and P.L. Brezonik. 2001. Image processing protocol for regional assessments of lake water quality. Water Resources Center and Remote Sensing Laboratory, University of Minnesota, St. Paul, MN, 55108, October 2001.

Olmanson, L.G., M.E. Bauer and P.L. Brezonik.2008). A 20-year Landsat water clarity census of Minnesota's 10,000 lakes. Remote Sens. Environ. 112(11):4086-4097.

Peckham, S.D and T.M. Lillesand. 2006. Detection of spatial and temporal trends in Wisconsin lake water clarity using Landsat-derived estimates of Secchi depth. Lake Reserv. Manage. 22(4):331-341.

Scarpace, F.L., K.W. Holmquist and L.T. Fisher. 1979. Landsat analysis of lake quality. Photogram. Eng. Rem. S. 45(5):623-633.

Stadelmann, T.H., P.L. Brezonik and S. Kloiber. 2001. Seasonal patterns of chlorophyll *a* and Secchi disk transparency in lakes of east-central Minnesota: Implications for design of ground- and satellite-based monitoring programs. Lake Reserv. Manage. 17 (4):299-314.

# Chapter 5. Satellite remote sensing II: High-resolution systems

## 5.1. Introduction

The next category of satellite remote sensing systems to be discussed in this report consists of systems capable of providing routine, operational monitoring at local scales. These systems generally share the following characteristics:

- High spatial resolution (nominally 0.4–2.5 m for a panchromatic band and 1.6–10 m for multispectral bands)
- Spectral resolution of a few relatively broad spectral bands, typically in the visible and the near infrared (IR) wavelengths, with most systems also employing a higher spatial resolution panchromatic band (which can be used for spatial resolution enhancement of multispectral bands)
- Local coverage area (8–77 km swath)
- Regular coverage, due to pointable sensors (daily off-nadir coverage for some systems and 3.5–26 day repeat at nadir, but constrained by cloud cover)
- High to very high cost for imagery

These systems have been designed for both national security purposes and for monitoring local-scale environmental and anthropogenic land surface conditions. High resolution satellite imagery is commonly seen on news programs and is used in Google Earth. The primary systems used for monitoring land, vegetation and water resources have been GeoEye's IKONOS and Digital Globe's QuickBird. The major advantages of these systems for lake management applications are regular coverage and spatial resolution suitable for monitoring water quality and aquatic vegetation in small lakes, ponds and wetlands as small as 0.1 ha. The spatial resolution of Landsat TM with IKONOS and QuickBird imagery were compared using an image near the intersection of Yankee Doodle Road and Pilot Knob Road in Eagan Minnesota (Fig 5.1). The primary disadvantages are the limited spectral resolution (compared to hyperspectral systems), the small coverage area and the high cost of imagery. The spatial coverage of a Landsat TM image with an IKONOS image was also compared (Fig. 5.2). To cover an equivalent area of one Landsat image with IKONOS imagery would require over 250 IKONOS images and cost more than $600,000. The cost strongly suggests that these systems are best suited for local applications.

While high-resolution imagery such as aerial photography has been available for many years, the launch of the IKONOS-2 by Space Imaging, Inc. (now GeoEye) in September 1999 introduced the first commercially-available, high-resolution digital satellite imagery. Multispectral digital imagery approaching the spatial resolution of aerial photography has opened up many new applications beyond that achievable with aerial photography. QuickBird and IKONOS imagery both have four multispectral bands similar to Landsat TM bands 1–4, along with higher spatial resolution, making it possible to apply commonly used methods for the assessment of smaller lakes, ponds and wetlands. Two applications include water clarity assessment and aquatic plant assessment, which were both investigated by Sawaya *et al.* (2003) and are included in the case study section of this chapter. Other applications pertinent to water resources that benefit from high spatial resolution include, but are not limited to, detailed land cover classification, impervious surface mapping and shoreland mapping.

A few high resolution satellites are currently operating that can be used for water resource assessment. GeoEye operates the IKONOS and GeoEye-1 satellites and, until recently, the Orbview-3 satellite, which malfunctioned in March 2007. Digital Globe operates the QuickBird satellite and, plans to launch Worldview II in 2009 with

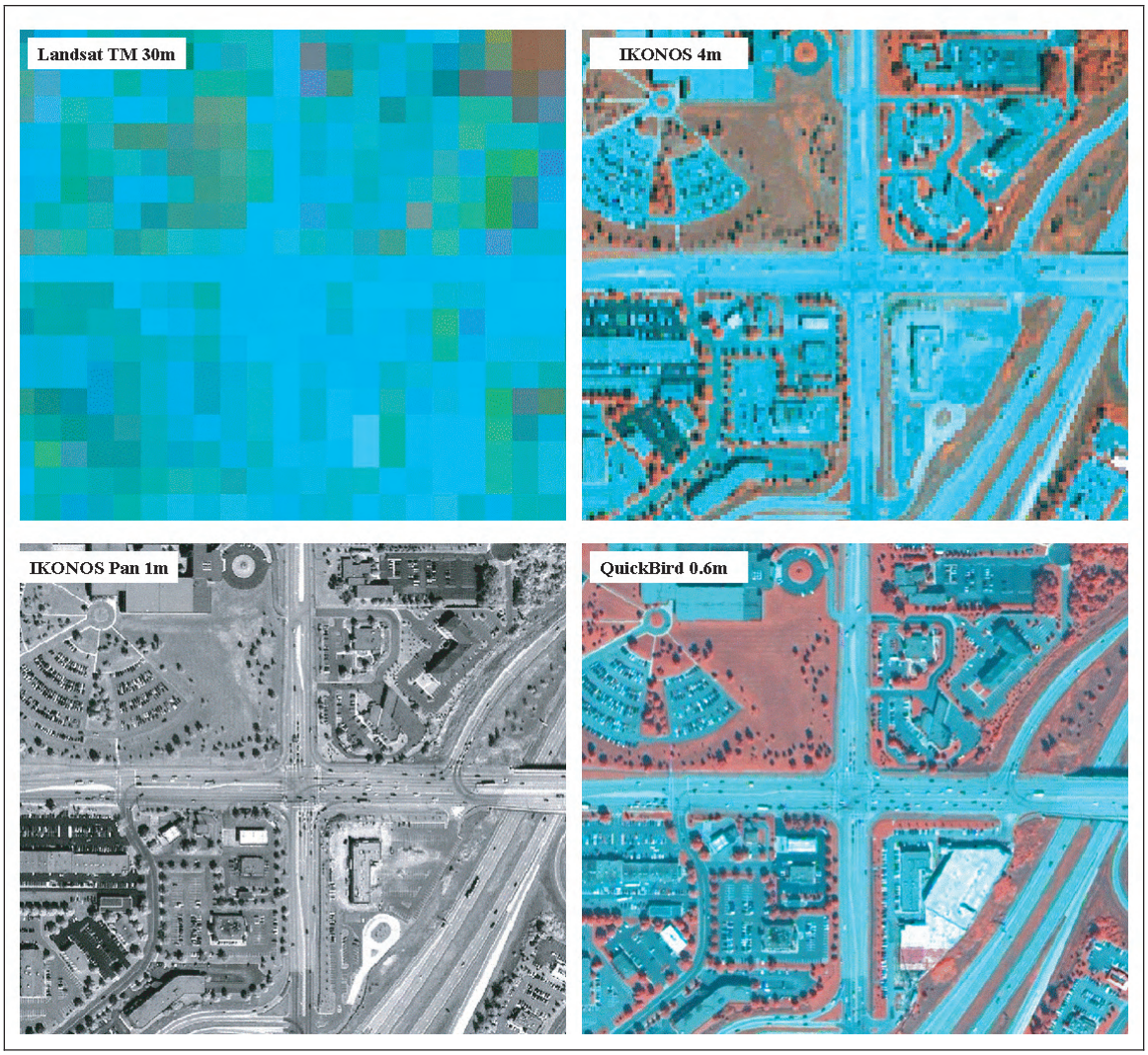


**Figure 5.1.** Comparison of spatial resolution of 30 m Landsat TM, 4 m IKONOS multispectral, 1 m IKONOS panchromatic and 0.6 m pan-sharpened multispectral QuickBird imagery (IKONOS imagery © GeoEye, QuickBird imagery © Digital Globe).

0.5-m resolution and 4 additional spectral bands. Indian Remote Sensing Satellite (IRS) Resourcesat-1 LISS-4 from India has three 5.8-m multispectral bands with a 24 km swath. SPOT (Satellite Pour l'Observation de la Terre)-5 from France has a 2.5-m panchromatic band and three 10-m multispectral bands. The RapidEye satellite constellation from Germany, launch in 2008, has five satellites with 5-m daily off-nadir coverage and 5.5 days at nadir, and an additional red edge spectral band. Although the spatial resolution of SPOT-5 and RapidEye are less than some of the other systems, the spatial coverage provided by a larger swath width is an advantage for larger study areas. The basic specifications of the primary satellite systems that have the necessary combination of properties (Table 5.1) and the spatial footprint of select high resolution systems are shown (Fig. 5.3).

Although the spectral bands of currently available high resolution imagery were selected for terrestrial features, Sawaya *et al.* (2003) demonstrated a strong relationship between IKONOS spectral data and in situ observations of water clarity similar to those found with Landsat TM data. Looking to the future, the Digital Globe's Worldview II satellite, scheduled for launch in 2009, will include four new spectral bands (red edge, coastal, yellow, and an additional near-infrared band). These bands may prove to be very beneficial to water resource applications and may provide significant improvement in assessment capabilities and accuracy.

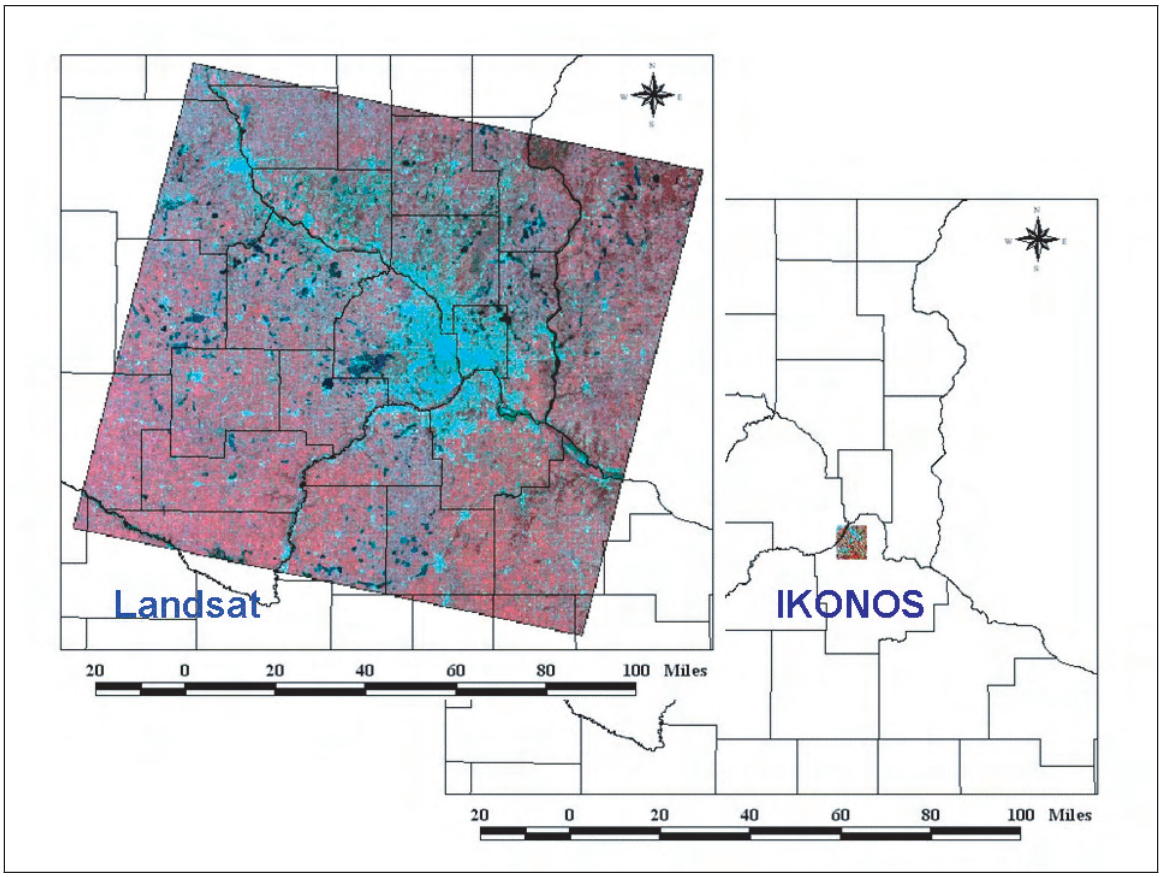


**Figure 5.2.** Comparison of spatial coverage of Landsat TM and IKONOS images.

While systems with higher spatial resolution have many advantages, the lack of a blue band in some of the systems (useful for water clarity assessment) and/or middle infrared and thermal bands (which can improve image classification accuracy) limits their usefulness for lake monitoring applications. Other factors that may limit the suitability of these systems for regional-scale lake assessments include limited geographic coverage, the necessity for "tasking" (scheduling data acquisitions in advance) and the high cost of imagery. Since imagery is not regularly acquired the archive of imagery for these sensors are quite limited, significantly hindering the use of these sensors for "retrospective" assessments. However, for local to subregional assessments where the imagery can be ordered in advance, the higher spatial resolution can provide detailed information that cannot be reasonably achieved with other satellite sensors.

Note that in many regions cloud cover will further limit the ability to collect usable imagery during a customer's desired tasking "window." Most companies consider "acceptable" imagery to be imagery with up to 20% cloud cover. If cloud cover exceeds this threshold and the data provider is unable to collect imagery during the specified tasking period, the image acquisition may be canceled or postponed; however, images with up to 20% cloud cover may be deemed acceptable by the terms of the acquisition agreement. Note that where land surface is visible the calculated percent cloud cover in an image may not include thin clouds, cloud shadows or haze. Thus, even if an image is deemed to have an acceptable level of cloud cover by the data provider, the acquired imagery may not be suitable for some applications such as water clarity assessment where the clouds, cloud shadows and haze will affect the spectral radiometric response of the imagery. Two images of the Lake Minnetonka area near Minneapolis, Minnesota, show haze and cloud cover considered "less than 10% cloud cover" (Fig. 5.4). While imagery with less than 10% cloud cover is usually clear or has only minor cloud cover, a contingency plan may

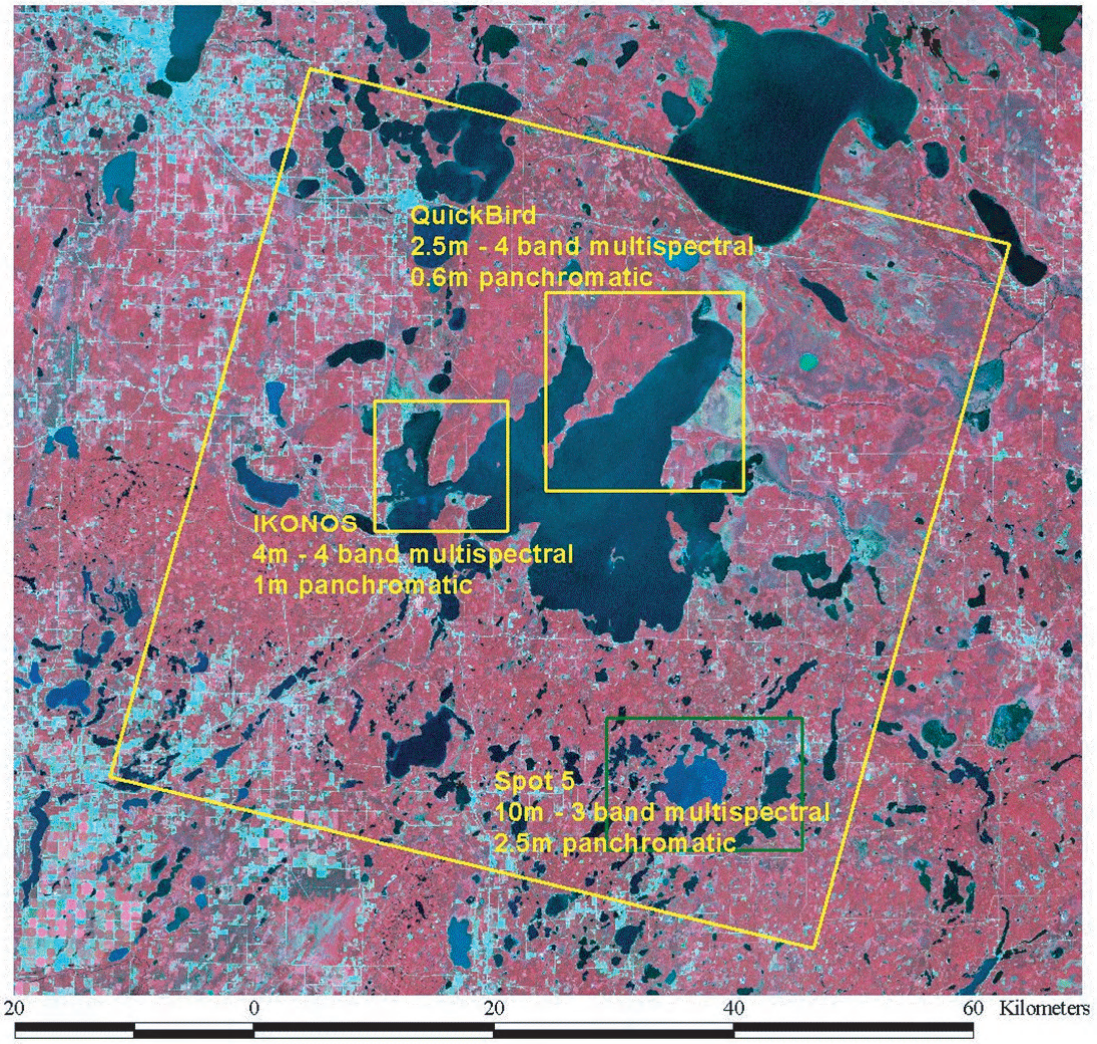


**Figure 5.3.** Comparison of spatial coverage of IKONOS, QuickBird and SPOT-5 imagery with portion of Landsat TM image in background (a full Landsat TM image is 170 × 183 km).

be necessary to compensate for imagery that is unsuitable for specific tasks. This may be especially problematic in cases where a large and expensive field-sampling campaign has been planned to coincide with the satellite tasking request.

## 5.2. Acquiring high resolution imagery

Further information describing data products and ordering is available at the following websites for the various systems:

IKONOS: http://www.geoeye.com/

QuickBird: http://www.digitalglobe.com/

SPOT 5: http://www.spot.com/

IRS-LISS-4: http://www.isro.org/

RapidEye: http://www.rapideye.de/

**Table 5.1.** Specifications of high resolution satellite systems suitable for lake monitoring.

| Satellite / Sensor | Spectral Bands (μm) | Spatial Resolution (m) | Radiometric Resolution (bits) | Swath Width (km) | Repeat Orbit (days) | Cost per Image ($)* |
|---|---|---|---|---|---|---|
| **IKONOS** | 0.56–0.93 | 0.82 | 11 | 11.3 | 3.5 | 2,400 |
| | 0.44–0.52 | 3.2 | | | | |
| | 0.51–0.60 | | | | | |
| | 0.63–0.70 | | | | | |
| | 0.76–0.85 | | | | | |
| **GeoEye-1** | 0.45–0.80 | 0.41 | 11 | 15.2 | 26, but 4 - 5 days with off-nadir viewing | 5,700 |
| | 0.45–0.51 | 1.65 | | | | |
| | 0.51–0.58 | | | | | |
| | 0.65–0.69 | | | | | |
| | 0.78–0.92 | | | | | |
| **QuickBird** | 0.45–0.90 | 0.61 | 11 | 16.5 | 3 | 6,256 |
| | 0.45–0.52 | 2.44 | | | | |
| | 0.51–0.60 | | | | | |
| | 0.63–0.69 | | | | | |
| | 0.76–0.90 | | | | | |
| **SPOT-5** HRG | 0.49–0.69 | 2.5 or 5 | 8 | 60 | 26, but 4–5 days with off-nadir viewing | 6,750 |
| | 0.49–0.61 | 10 | | | | 3,375 |
| | 0.61–0.68 | | | | | |
| | 0.78–0.89 | | | | | |
| | 1.58–1.75 | 20 | | | | |
| **RapidEye** System of 5 satellites | 0.44–0.51 | 5 | 12 | 77 | 5.5 days with daily off-nadir viewing | 7,500 |
| | 0.52–0.59 | | | | | |
| | 0.63–0.68 | | | | | |
| | 0.69–0.73 | | | | | |
| | 0.76–0.85 | | | | | |
| **Resourcesat-1** (IRS-P6) LISS-4 | 0.52 - 0.59 | 5.8 | 7 | 23.9 | 5 | 1,970 |
| | 0.62 - 0.68 | | | | | |
| | 0.77 - 0.86 | | | | | |

* Prices current as of publication. Pricing may vary.

## 5.3. Case studies – Overview

This section describes research that used IKONOS and QuickBird imagery to monitor environmental conditions in lakes, ponds and wetlands, previously reported by Sawaya *et al.* (2003) in Remote Sensing of Environment. The case studies are reprinted with minor edits, updates and some additional figures with permission from the publisher.

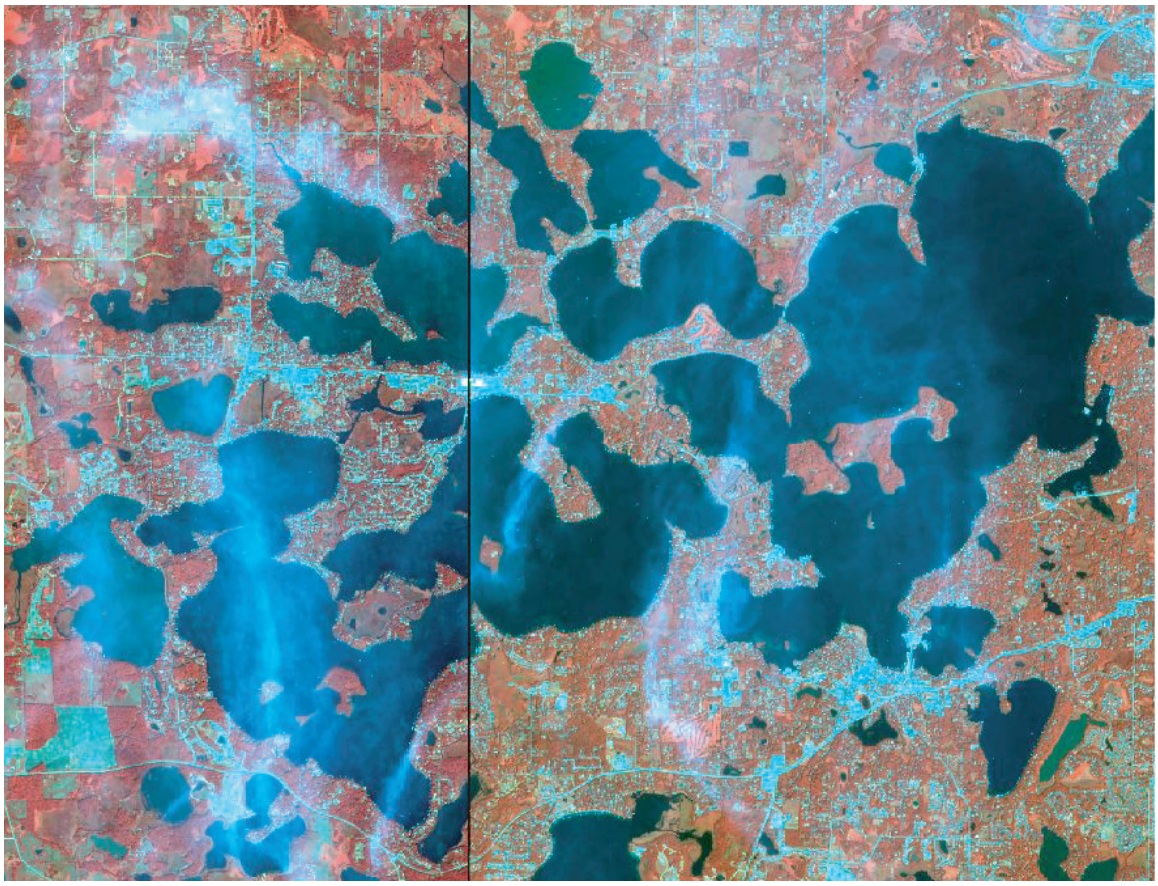

**Figure 5.4.** 1 September 2001 IKONOS imagery of the Lake Minnetonka area near Minneapolis, MN. Note the haze and thin clouds on image with "less than 10% cloud cover" (IKONOS Imagery © GeoEye).

The first case study demonstrates the use of IKONOS imagery for water clarity assessment of the small lakes, ponds and wetlands in Eagan, Minnesota, and compares those results to a Landsat TM water clarity assessment (Fig. 5.5).

The second case study is an aquatic vegetation survey of Swan Lake in Nicollet County, Minnesota (Fig. 5.6) and aquatic vegetation surveys of three lakes in the Lake Minnetonka area near Minneapolis, Minnesota (Fig. 5.7).

## 5.4. Case study 1 – Lake water clarity classification with IKONOS (from Sawaya *et al.* 2003)

IKONOS imagery has four multispectral bands similar to Landsat TM bands 1–4 and high spatial resolution, making it a good candidate for applying previous methods to the assessment of smaller lakes and ponds. In this study, we used a 4 September 2001 IKONOS high-resolution satellite image to assess the water clarity of smaller lakes and ponds for a city scale analysis of water clarity. These results are compared to a lake water clarity classification using a 30 August 2001 Landsat TM image. Assessment of smaller lakes and ponds is important because they tend to be more susceptible to impacts than larger lakes.

The overall objective of our research was to estimate variables related to key management indicators, such as the trophic state indices of Carlson (1977). The three common water quality variables that indicate lake trophic

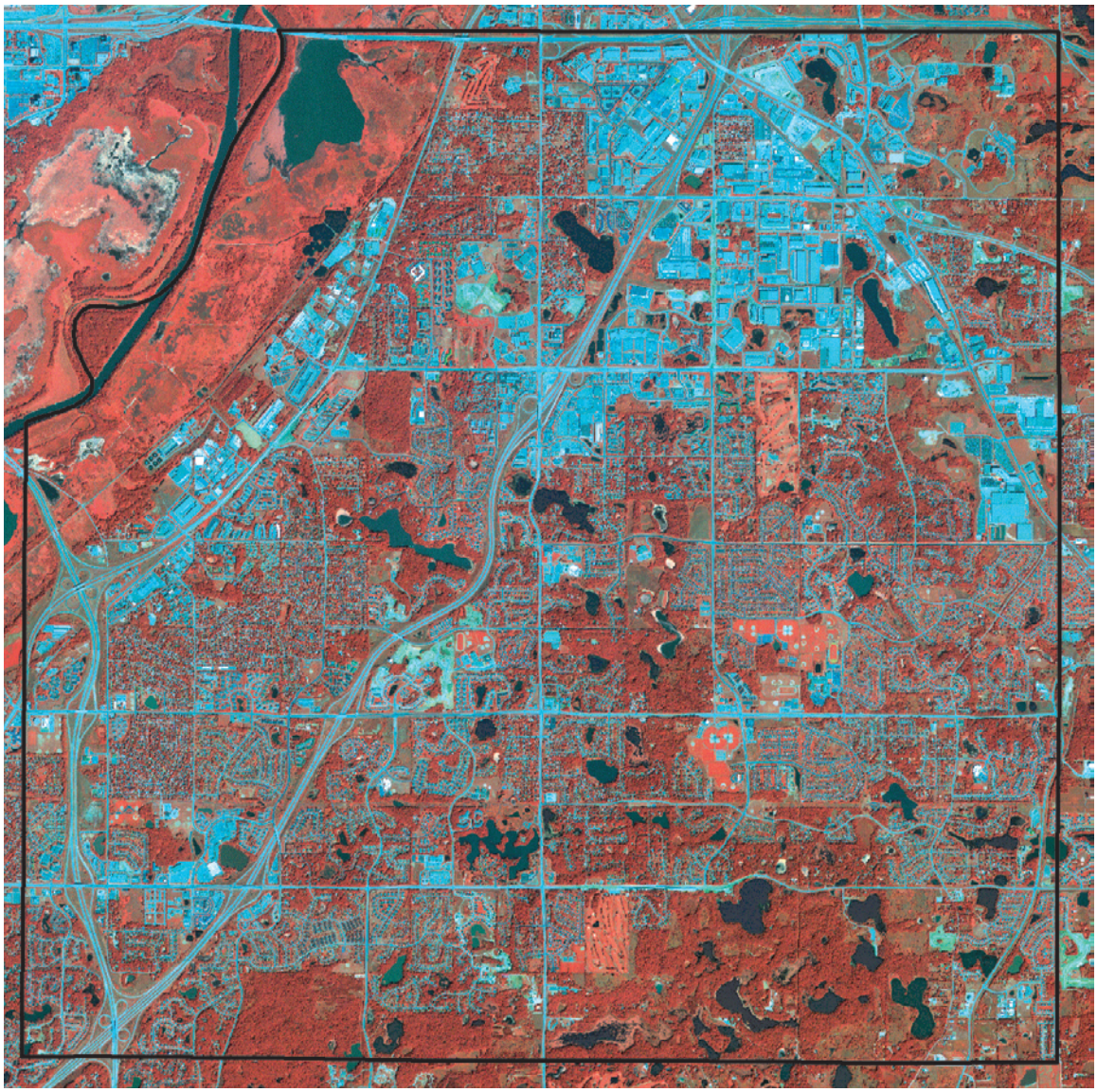

**Figure 5.5.** 4 September 2001 IKONOS image of the City of Eagan, MN. (IKONOS Imagery © GeoEye).

state are total phosphorus (TP), chlorophyll *a* (chl-*a*), and Secchi disk transparency (SD). Lake management agencies and organizations use these variables for measurements, along with various transformations such as the trophic state indices (TSI). The most consistently collected trophic state indicator, SD, is strongly correlated with the responses in the blue and red bands of Landsat TM/ETM+ data (Kloiber *et al.* 2002a, 2002b); therefore, most of our research to date has involved calibrating Landsat TM data with ground-based SD measurements and estimating SD for all lakes in an image from the regression equation developed in the calibration step. The results then can be mapped directly as distributions of SD in the lakes, or the estimated SD can be converted to Carlson's TSI based on transparency: TSI(SD) = 60 – 14.41 ln(SD).

Factors other than algal turbidity (as indicated by chlorophyll levels) may affect SD in lakes. Most important of these (nontrophic-state) factors are humic color and nonalgal turbidity (including soil-derived clays and suspended sediment). For this reason, we report our results based on SD calibrations as satellite-estimated SD or TSI(SD), which clearly identifies the value as an index based on transparency, rather than the generic term, TSI.

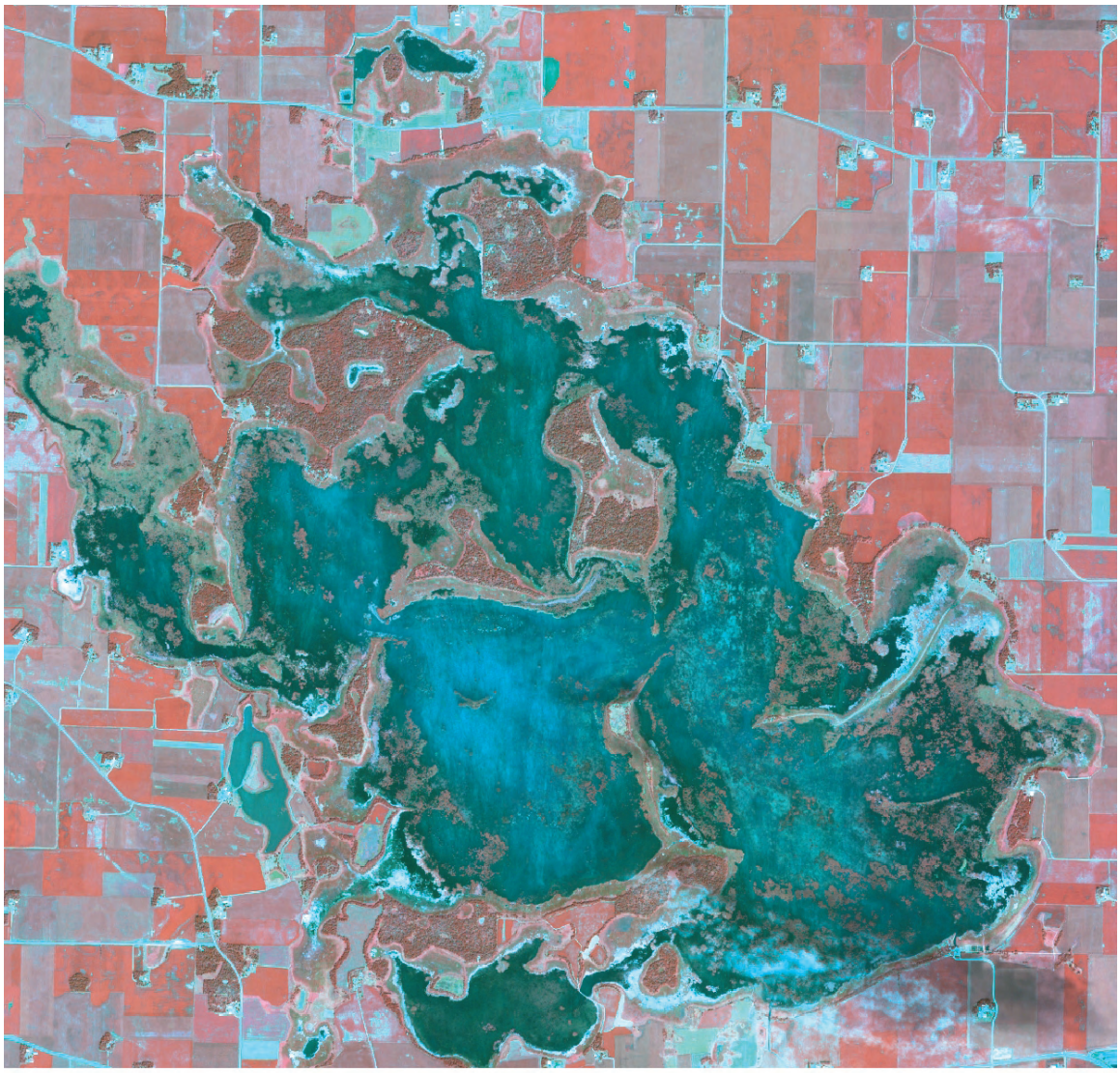

**Figure 5.6.** 1 September 2001 IKONOS image of Swan Lake in Nicollet County, MN. (IKONOS Imagery © GeoEye).

The specific objective for this study was to perform an assessment of TSI(SD) for the City of Eagan, Minnesota. This area was particularly well suited for this study because it has 375 small lakes, ponds and wetlands and a well-established lake monitoring program.

## Methods

We used methods developed by Olmanson (1997) and continued in subsequent studies (*e.g.*, Olmanson *et al.* 2001, 2002, Kloiber *et al.* 2002a, 2002b,) to apply Landsat imagery to regional scale assessments of lake water clarity. We made minor modifications including the addition of a lake polygon layer to minimize spectral confusion between open water, shadows and asphalt features to make these methods compatible with high-resolution satellite imagery.

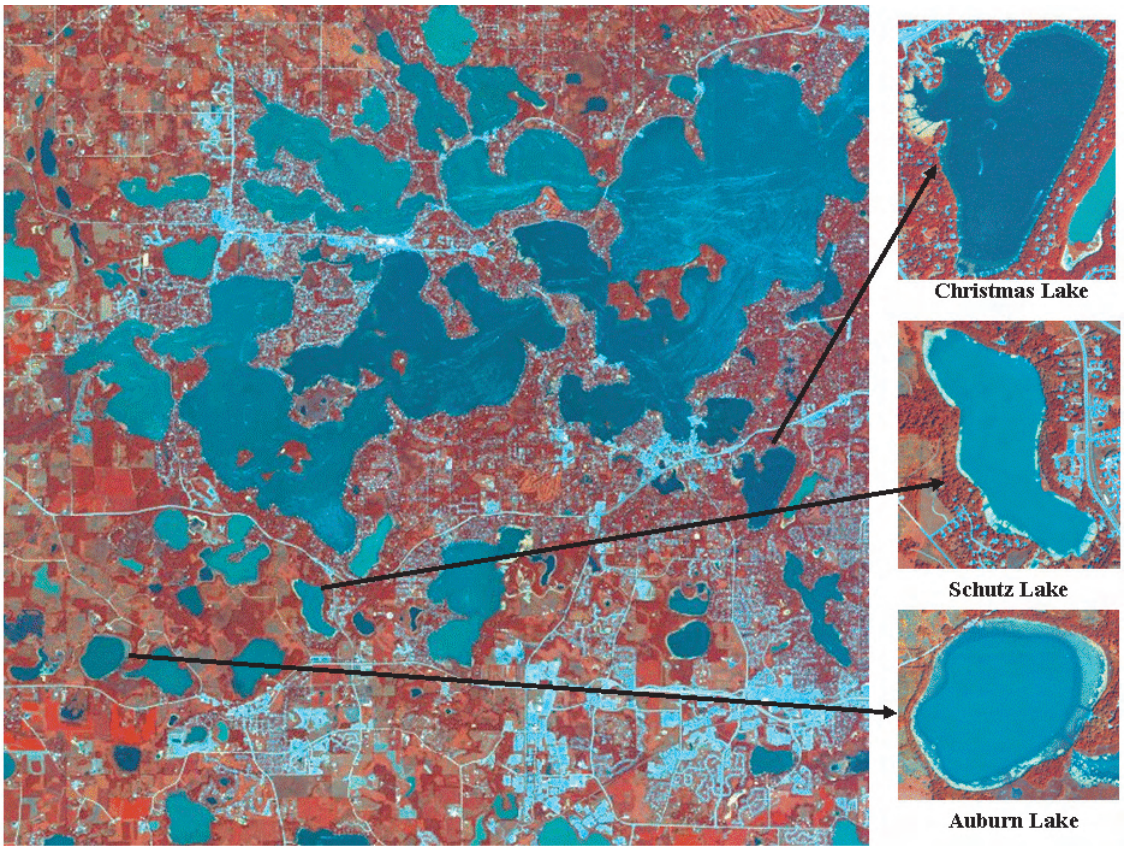


**Figure 5.7.** 28 July 2002 QuickBird image of the Lake Minnetonka Area and three lakes used for aquatic vegetation surveys near Minneapolis, MN (QuickBird imagery © Digital Globe).

### *Satellite imagery and lake reference data*

Images for water clarity assessment were selected from a late summer index period (15 Jul–15 Sep, with a preference for Aug), This period was found to be the best index period for remote sensing of water clarity in Minnesota (Kloiber *et al.* 2002a). Images from this period have at least two major advantages: (1) short-term variability in lake water clarity is at a seasonal minimum, and (2) most lakes have their minimum water clarity during this period. In addition, images from near anniversary dates are preferred for detecting change.

We acquired two satellite images, 30 August 2001 Landsat TM (path 27, rows 29 and 30) and 4 September 2001 IKONOS of Eagan, Minnesota, for this assessment. Both images were high quality and free of haze, clouds and sun glint. It is critical to avoid IKONOS images displaying specular reflection, or "sun glint" effects from lakes for this application. Certain combinations of IKONOS view azimuths and zenith angles can result in bidirectional reflectance that saturates the sensor, making the data unusable for this and other water-related applications. Although the imagery used in this analysis was suitable, specular reflectance effects have created problems for some images we acquired for lake water clarity assessments between 1999 and 2001. We did not perform atmospheric correction or normalization of the imagery for the regression method used.

The availability of lake reference data was excellent due to the City of Eagan's Water Resources program and volunteer participation in the Citizen Lake Monitoring Program. The programs provided 94 SD lake reference points for the Landsat image taken within three days of the image acquisition and 13 SD lake reference points for the IKONOS image taken within seven days of the image acquisition. The SD data were distributed over a wide range of water quality.

*Classification procedures*

This section summarizes our image classification procedures; more detail is provided by Olmanson *et al.* (2001), and the rationale for the procedures is described by Kloiber *et al.* (2002a). We used ERDAS Imagine, image processing software, and ArcView, geographic information system (GIS) software, for the image processing steps. Acquiring a representative image sample from each lake used for calibration or accuracy assessment was our primary objective. Ideally, the sample should represent the center portion of the lake in at least 5 m of water (or twice the SD measurement), where reflectance from vegetation, the shoreline or the lake bottom do not affect the spectral response. It was also critical to avoid shadowed portions of lakes, which would lead to unnaturally clear lake estimations.

We produced a "water-only" image by performing an unsupervised classification in ERDAS Imagine. Because water features tend to have very different spectral characteristics from terrestrial features, water was put into one or more distinct classes that we could easily identify. We then masked out terrestrial features creating a water-only image. This method worked well for the Landsat imagery; however, with IKONOS imagery this clustering also included pixels from shadows, asphalt and other dark features. Therefore, we created a lake polygon layer to mask the nonwater dark features on the IKONOS image. We then performed a second unsupervised classification on the water-only image and generated spectral signatures of each class. We used these signatures, along with the location where the pixels occur, to differentiate classes containing clear water, turbid water and shallow water (where sediment and/or macrophytes affect spectral response). Based on this analysis, we recoded classes to avoid shadow, vegetation, bottom and terrestrial effects when selecting lake sample locations. Digital number values from the imagery were obtained to develop relationships with measured SD. For this assessment, we used a polygon layer, described in Olmanson *et al.* (2001), to help automate the process. We used the signature editor in ERDAS Imagine to extract the spectral data from the image for each sample location.

We calibrated the Landsat image using the 94 SD measurements collected within three days of the image acquisition date. Using log-transformed SD data as the dependent variable and Landsat Thematic Mapper band 1 (TM1) and the TM1:TM3 ratio as independent variables, we performed a multiple regression. The regression model, with $r^2 = 0.76$ and SEE = 0.39, for prediction of SD from the Landsat TM data was:

$$\text{Ln(SD)} = 1.493*(\text{TM1:TM3}) - 0.035(\text{TM1}) - 1.956 \qquad \text{[Eq. 5.1]}$$

Once we developed the model for the Landsat image, we used another polygon layer with all of Eagan's lakes, ponds and wetlands ≥0.08 ha to extract data from all possible water-bodies with enough unaffected pixels to predict water clarity. Forty-eight of Eagan's lakes and ponds had a sample of at least eight unaffected pixels that we used to predict water clarity; we used the model above, developed from the entire Landsat image, to predict their water clarity. For this assessment, 1.5 ha was the smallest pond we were able to predict water clarity using the Landsat TM image.

We then calibrated the IKONOS image using two different datasets: 13 SD measurements collected within seven days of the image acquisition date and 48 water clarity measurements extracted from the Landsat image. We used the latter dataset to compare the compatibility of the IKONOS imagery with Landsat TM imagery and to explore an optional calibration method if sufficient ground observations were not available for a given scene. We performed a multiple regression using log-transformed SD data as the dependent variable and IKONOS band 1 (IK1) and the IK1:IK3 ratio as independent variables.

Lake water clarity maps can then be created from the regression model by two methods. The first applies the model to each individual water pixel, creating a pixel-level lake map to classify all water pixels and evaluate intra-lake variability. The second method uses the digital numbers collected from the sample of each lake to calculate an average water clarity estimate that can then be linked to a lake polygon layer to create a lake-level water clarity map. This latter method has the advantage of generating a single water clarity number for each lake that can be used in other analyses or included in a water clarity database.

## Results and discussion

This assessment showed strong relationships between both water clarity datasets (TM-derived and SD-derived) and the spectral-radiometric response of the IKONOS data. The regression model (n = 48, $r^2$ = 0.94, SEE = 0.15) for prediction of SD from the IKONOS data using the water clarity data derived from the Landsat TM image was:

$$Ln(SD) = 1.958*(IK1:IK3) - 0.004(IK1) - 2.957 \quad \text{[Eq. 5.2]}$$

The regression model (n = 13, $r^2$ = 0.89, SEE = 0.22) for prediction of SD from the IKONOS data using the available SD data (Fig. 5.8) was:

$$Ln(SD) = 1.832*(IK1:IK3) - 0.004(IK1) - 2.813 \quad \text{[Eq. 5.3]}$$

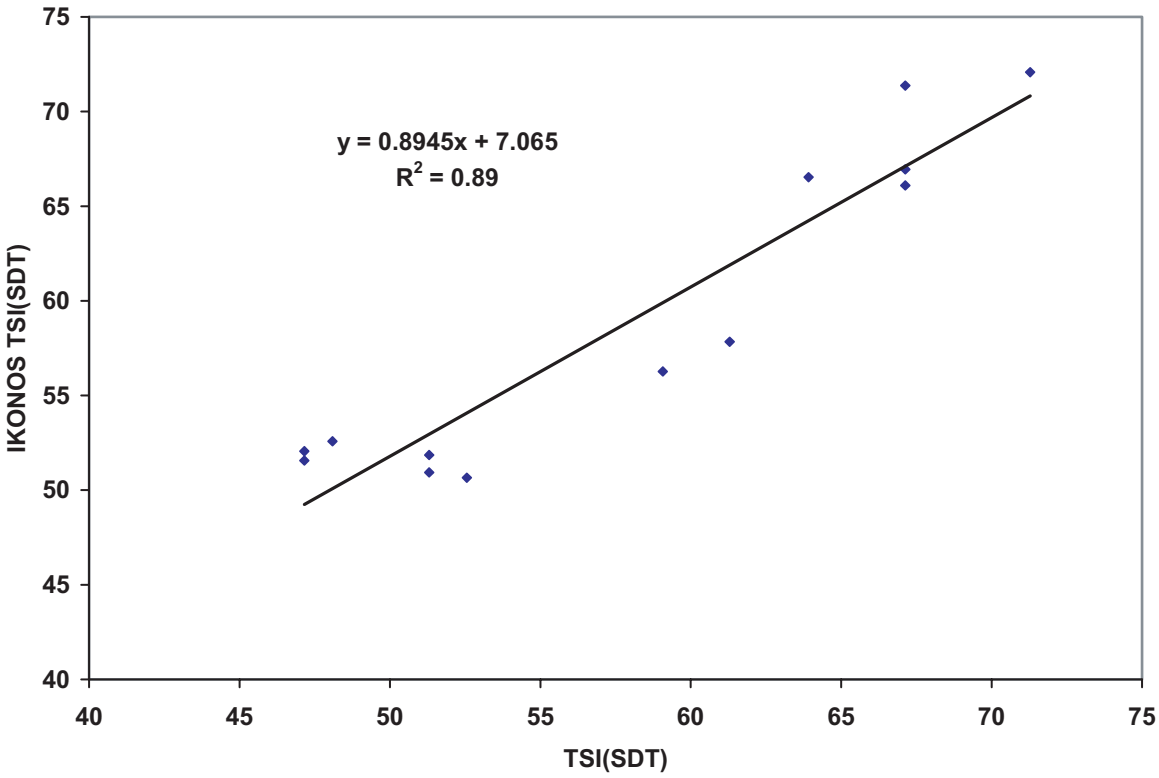


**Figure 5.8.** Comparison of IKONOS and field measurements of lake water clarity, TSI(SD).

The very strong relationship of $r^2$ = 0.94 using the Landsat-derived SD to calibrate the IKONOS image indicates that the two types of imagery are compatible and have similar spectral-radiometric responses. The strong relationship between SD and spectral-radiometric response of the IKONOS imagery, similar to results we have seen with Landsat imagery, indicates that IKONOS imagery can be used to assess the water clarity of smaller lakes and ponds. The similarity in the resulting models also indicates that Landsat imagery can be used to calibrate IKONOS images that do not have sufficient field reference data. A comparison of the resulting TSI(SD) values calculated from the Landsat image and from the IKONOS image using each model for 48 lakes and ponds both indicated a very strong agreement with an $r^2$ = 0.95 (Fig. 5.9).

The 4-m resolution of the IKONOS imagery allowed us to assess smaller water bodies than is possible with Landsat 30-m resolution imagery. We easily assessed water bodies with a minimum size of 0.08 ha included in the lake, pond and wetland polygon layer when open water conditions and unaffected pixels existed. We used 347 lake,

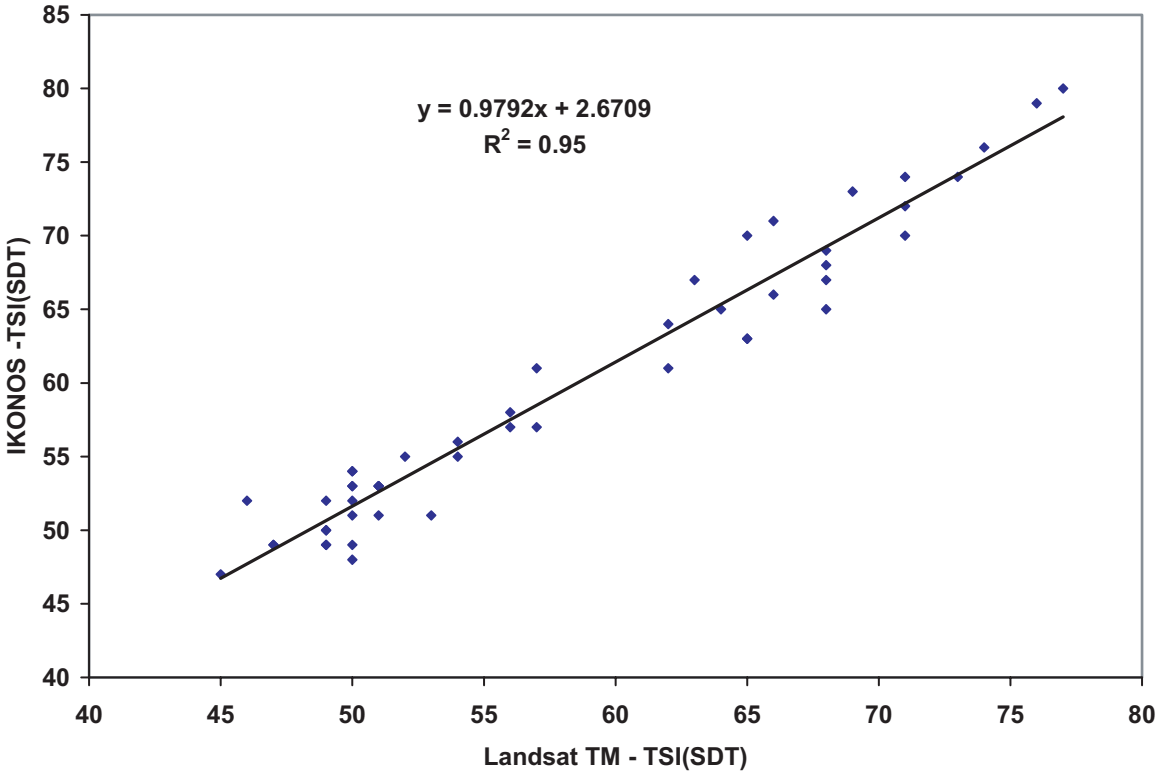


**Figure 5.9.** Comparison of Landsat and IKONOS estimates based on Landsat modeling of lake water clarity, TSI(SD).

pond and wetland polygons ≥0.2 ha on the Eagan lake polygon layer to extract the spectral-radiometric data from the imagery. Of those lakes and ponds, 236 had a sample of at least eight unaffected pixels used to predict water clarity. In contrast, we could only estimate and map the water clarity of 48 lakes and ponds in Eagan when using Landsat imagery because the minimum lake size assessed with Landsat 30-m resolution imagery was 1.5 ha.

High-resolution satellite data were also useful for general analysis of city land use and land cover features. Visual assessment of how land use and cover affects water clarity can be investigated by overlaying the classified lakes on the original IKONOS imagery. Different land use/cover features have corresponding effects on water clarity (Fig. 5.10; a more detailed pixel level water clarity map of a 23 August 2000 IKONOS image is available on Google Earth under the Gallery/NASA/ layer and at http://earthobservatory.nasa.gov/Newsroom/NewImages/images.php3?img_id=7784 ). For example, in the southeastern corner of Eagan, the Lebanon Hills Regional Park is an area with an abundance of forest and wetland areas and limited development in the form of parking lots and pavilions for park visitors. This area has relatively high lake water clarity with TSI(SD) of ~50 and SD of ~2 m. In many of the residential and commercially developed areas, stormwater is directed into lakes, using them as convenient reservoirs. The increase in impervious surface area and direct connection to the stormwater system has dramatically changed the hydrology of many water bodies in Eagan by increasing watershed size, increasing the amount of runoff and decreasing quality of runoff water. Water clarity of lakes and ponds in many of the developed areas is generally TSI(SD) 65–70 and SD of ~0.5 m due to eutrophication (Fig. 5.10).

This study showed the usefulness of high-resolution satellite imagery for water clarity assessments at a city scale, information that can be very useful in city planning and lake management to help monitor and protect water clarity at a local scale.

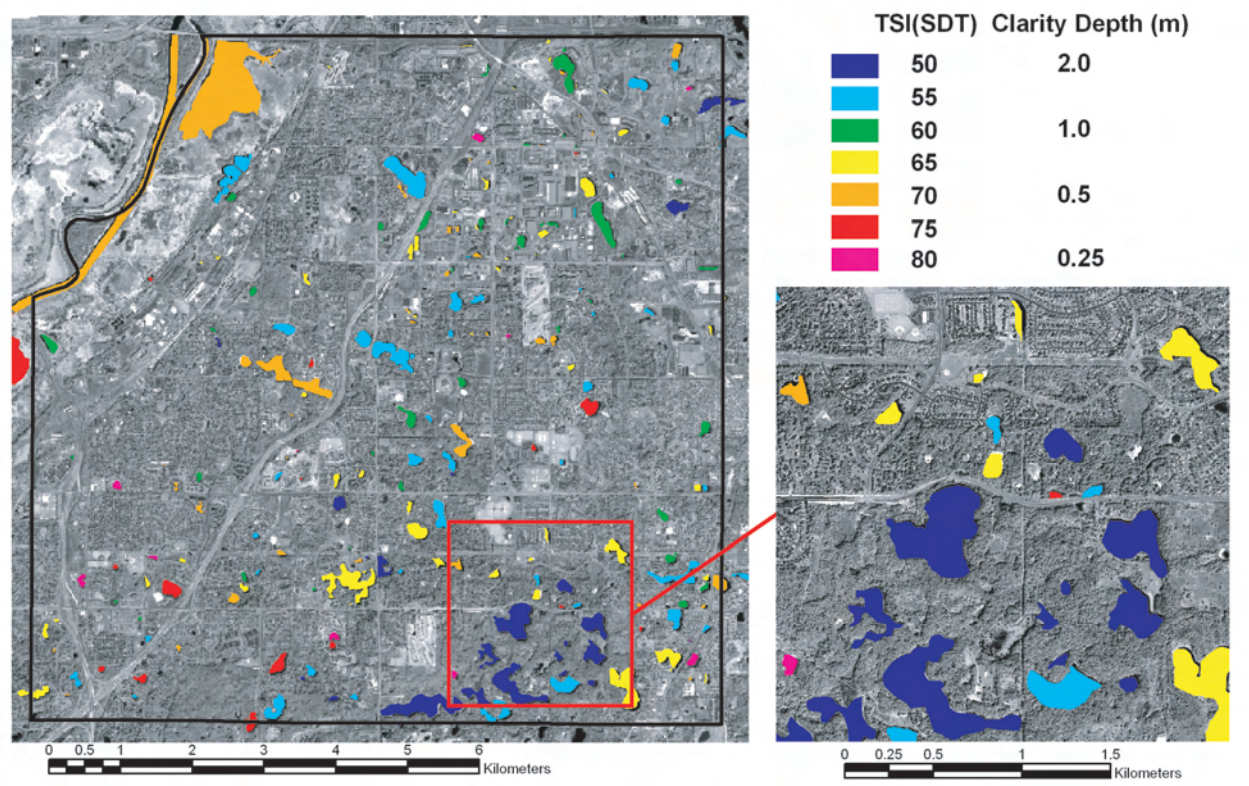


**Figure 5.10.** Lake level lake water clarity classification of IKONOS multispectral data overlaid on panchromatic image (IKONOS Imagery © GeoEye).

## 5.5. Case study 2 – Aquatic vegetation surveys (from Sawaya *et al.* 2003)

While lakes are well known for their recreational and aesthetic value, traditionally society has considered wetlands as nuisances and problems that need to be cleaned up. Statewide, Minnesota has drained more than half of the original wetlands (around 4.5 million ha) for agricultural and development purposes, and many of the remaining wetlands are degraded. A frequent cause of wetland degradation is increased storm water discharge resulting from changes such as increases in impervious surface area or installation of storm water systems in urban and suburban areas, as well as tiling and ditching systems in agricultural areas. Changes in hydrology affect the water quality and quantity and may severely impact the function of wetlands (Daily 1997). When too many wetland plants are removed or impacted, water quality, wildlife, and fish populations can suffer (Mitsch and Gosselink 1993). Wetland plants help protect water quality, provide habitat for fish and wildlife, and provide economic and aesthetic opportunities (Barbier *et al.* 1994).

Aquatic plants in lakes and wetlands are beginning to be recognized as important ecosystem features in need of protection. As a result, aquatic plant surveys and assessments are becoming part of routine monitoring efforts conducted by consultants, citizen groups, and state and local agencies. Aquatic plant diversity and abundance are important indicators of lake or wetland health, but accurate maps and data are difficult to acquire. Because ground-based mapping requires much time and human resources, only a small fraction of this large resource has been mapped by natural resource agencies.

The principal objective of this study was to evaluate the capability of high-resolution satellite imagery to map and classify aquatic plant groups for use by resource management agencies. To evaluate using IKONOS imagery, we conducted an aquatic plant survey on Swan Lake in Nicollet County, Minnesota, a large (>3600 ha), "type-4"

wetland, meaning it is classed as a deep freshwater marsh with standing water and abundant aquatic vegetation. To evaluate the use of QuickBird imagery for assessment of aquatic plants in open water lakes, we conducted aquatic plant surveys of three lakes south of Lake Minnetonka. The lakes include Christmas Lake (104 ha) mostly in Hennepin County, and West Auburn (55 ha) and Shutz (38 ha) Lakes in Scott County, Minnesota.

## Methods

We adapted methods typically used for land cover classification (Lillesand *et al.* 1998) and developed for water clarity assessments (Olmanson *et al.* 2001) for the evaluation. The aquatic plant classification methods consisted of two procedures: separation of image features into discrete units and classification of the pixels in each unit.

### *Satellite image data*

We used an IKONOS image of the Swan Lake area acquired 1 September 2001 and a QuickBird image of the Lake Minnetonka area acquired 28 July 2002. An acquisition window of 15 July through 15 September captures the presence of aquatic vegetation in Minnesota. The images were of high quality with only minor cloud cover over the southern portion of the IKONOS image. We applied a resolution enhancement of the multispectral bands using the panchromatic band. Atmospheric correction or normalization of the imagery was not necessary for the methods used in this study.

### *Aquatic vegetation reference data*

Due to the size of Swan Lake and the abundance of aquatic plants in the lake, the collection of reference data would be very difficult without the aid of modern technology. We used Global Positioning System (GPS) technology and the advanced GPS tracking software in ERDAS Imagine 8.5. We collected field reference data shortly after acquiring the imagery using a Fujitsu pen computer. While in the field, we identified different types of aquatic vegetation and located them directly on the IKONOS image using the field computer. Being able to accurately identify specific locations on the image while in the field was especially useful on this large wetland. Having the image available quickly after its acquisition for use in reference data collection was also a significant advantage in field sampling because we could identify unique areas with different spectral-radiometric responses on the image and target them for field identification. We targeted emergent vegetation for the evaluation but also noted the location of submerged vegetation appearing at the surface.

The Minnesota Department of Natural Resources collected the field data for the three lakes south of Lake Minnetonka, specifically targeting submerged plants using an echo sounder equipped with a GPS unit. The hydroacoustic survey collected data pertaining to lake depth and plant depth at thousands of points in the shallower portions of the lakes where aquatic plants were present but not at the surface. General point survey data were collected in areas where the submerged plants were topped at the surface or where there were floating or emergent plants.

### *Classification procedures*

The first step for the Swan Lake IKONOS image was to separate wetland features from terrestrial features by digitizing the aquatic terrestrial boundary around the entire wetland and all islands. We identified this boundary using spectral-radiometric differences and spatial patterns visible on the image. The image was then subset using the wetland polygon to mask out all terrestrial features and create a wetland-only image.

Swan Lake has a maximum depth of 2 m, clear water throughout and an abundance of aquatic vegetation; consequently, we assumed that aquatic vegetation was present throughout the wetland. An aquatic vegetation survey conducted by Tyler and Madsen (2001) recorded the presence or absence of 27 species of aquatic plants at 118 evenly distributed sample points on the lake verified this assumption. The next step was to stratify the wetland

into emergent and submergent vegetation by performing an unsupervised classification specifying 10 classes. Emergent vegetation types had very different spectral characteristics from most submerged vegetation and were put into distinct classes easily identified from the locations where they occurred. We masked out submerged vegetation features to create an emergent vegetation image and conducted a second unsupervised classification on the emergent image using 100 classes. Because of the difficulty in separating some emergent plant types, and because we found that some areas with very thick submergent plant mats floating on the surface were included in the image, we conducted "cluster busting" by stratifying the image further into two emergent images and a thick submergent image. We performed a third level of unsupervised classifications using 100 classes for the emergent vegetation images and 10 classes for the thick submergent vegetation image. Using the field reference data, we identified five different emergent classes on the emergent vegetation images and recoded the images to create an emergent vegetation map. We repeated this procedure for the thick submerged vegetation image and identified two submerged classes.

Next, we created a submerged vegetation image by masking the emergent vegetation features. We clustered the submergent vegetation image into 10 classes to identify different types of submergent aquatic vegetation. Using a graph of the spectral-radiometric signatures of the different classes and the reference data, we identified classes of different aquatic plant densities. Assuming that water clarity is similar throughout the wetland and that aquatic plants are located throughout the wetland, we attributed the differences in spectral response to differences in submerged aquatic plant depth and densities. We identified classes with higher radiometric response as areas where the submerged vegetation was highly dense and appeared at the surface, and areas with lower radiometric response as areas where submerged vegetation was deeper or thinner. We created the submerged vegetation map by combining the two submerged plant images and recoding the map into four different submerged plant density classes. Finally, we created an aquatic plant classification map by overlaying the submerged aquatic plant map and the emergent aquatic plant map over the panchromatic image (Fig. 5.11).

We followed similar procedures for the three lakes south of Lake Minnetonka with the exception of also stratifying the open water areas before classification of the submerged and emergent/floating aquatic plants.

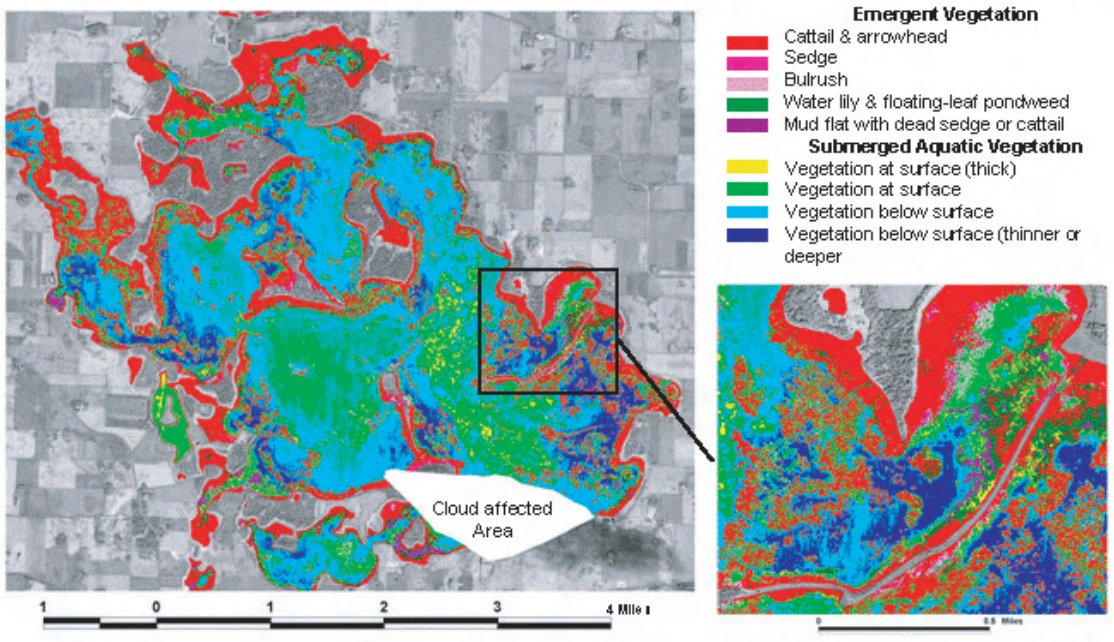


**Figure 5.11.** IKONOS image classification of aquatic vegetation of Swan Lake in Nicollet County, MN (IKONOS Imagery © GeoEye).

Stratification and unsupervised classification of the resolution-enhanced multispectral high-resolution imagery provided us with high-resolution maps that identify different aquatic vegetation groups throughout the Swan Lake and three lakes. Two datasets were available to evaluate the accuracy of the Swan Lake aquatic vegetation map. The first is the field data we collected and used to classify the imagery. Unfortunately, these locations were not random and are biased by our prior knowledge of the aquatic vegetation types.

The other dataset, collected by Tyler and Madsen (2001), has 118 evenly distributed data points identifying the presence or absence of 27 species of aquatic plants. A review of the locations of these data revealed that some points were not accurately positioned on the map. For example, the GPS coordinates of some aquatic plant points were in forested areas at least 50 m away from the nearest aquatic plants. Therefore, instead of using this survey for an accuracy assessment, we used it to compare the statistical distribution of plant species in Swan Lake.

## Results and discussion

The final classification map was created for Swan Lake with five classes of emergent and four classes of submerged aquatic vegetation (Fig. 5.11). Qualitative comparison to field observations that were initially acquired with the imagery indicates that the classes of vegetation were mapped quite accurately, with strong agreement between the field survey of plant distribution by Tyler and Madsen and the IKONOS classification (Table 5.2). We also have quantified the accuracy in an error matrix for the emergent classes and the submerged class as a whole (Table 5.3). The overall accuracy was 79.5%, with producers and users accuracies from 36 to 100% for the individual

**Table 5.2.** Comparison of IKONOS and field survey estimates of the distribution of aquatic vegetation diversity in Swan Lake, MN.

| | IKONOS (%) | Field Survey* (%) |
|---|---|---|
| **Submerged plants** | 63.6 | 58.5 |
| Cattail | 28.1 | 23.7 |
| Sedge & dead sedge | 2.5 | 5.1 |
| Bulrush | 1.6 | 6.8 |
| Water Lily & FLPW | 4.2 | 5.9 |

* Tyler and Madsen (2001)

**Table 5.3.** Accuracy of IKONOS image classification of aquatic vegetation for Swan Lake, MN (Bold indicates data where reference data and classified map agree).

| | Reference Data | | | | | | |
|---|---|---|---|---|---|---|---|
| **Classified Data** | **Cattail** | **Sedge** | **Sedge, dead** | **Bulrush** | **Lily** | **Sub-merged** | **User's Accuracy (% )** |
| Cattail | **24** | 3 | | | | | 88.9 |
| Sedge | | **4** | | 2 | | | 66.7 |
| Sedge, dead | | | **5** | | | | 100.0 |
| Bulrush | | | | **7** | | | 100.0 |
| Lily | | | | | **13** | 1 | 92.9 |
| Submerged | | 4 | 3 | 4 | | **13** | 54.2 |
| Producer's Accuracy (%) | 100.0 | 36.4 | 62.5 | 53.8 | 100.0 | 92.9 | **79.5** |

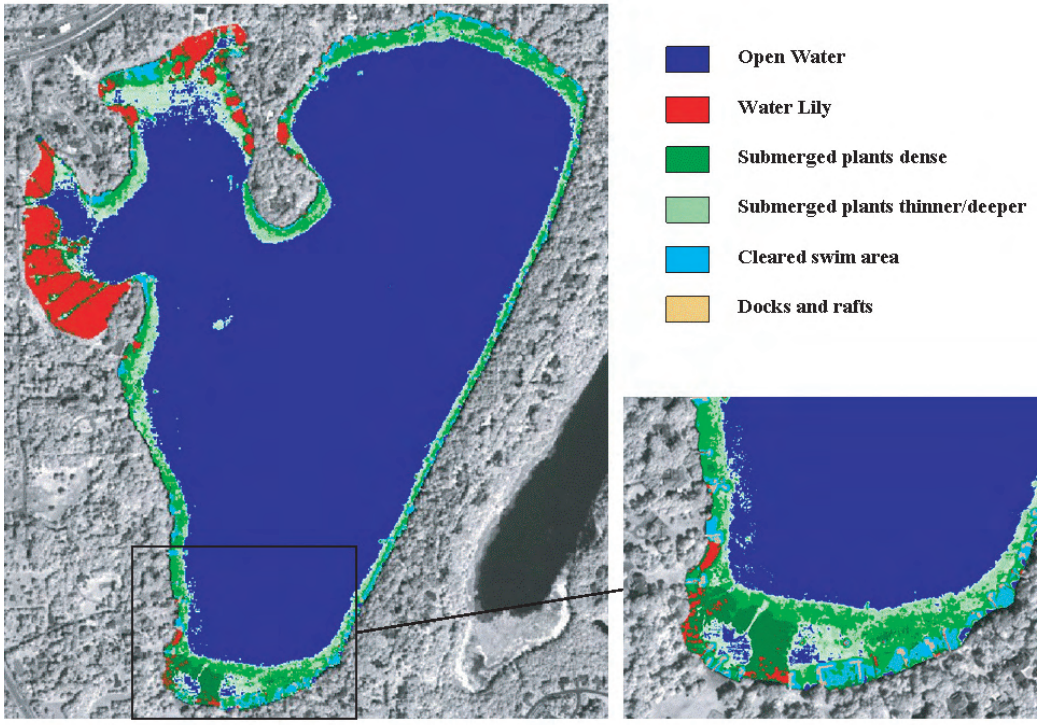


**Figure 5.12.** QuickBird image classification of aquatic vegetation of Christmas Lake near Minneapolis, MN (note Eurasian water milfoil associated with submerged plants dense class; QuickBird Imagery © Digital Globe.).

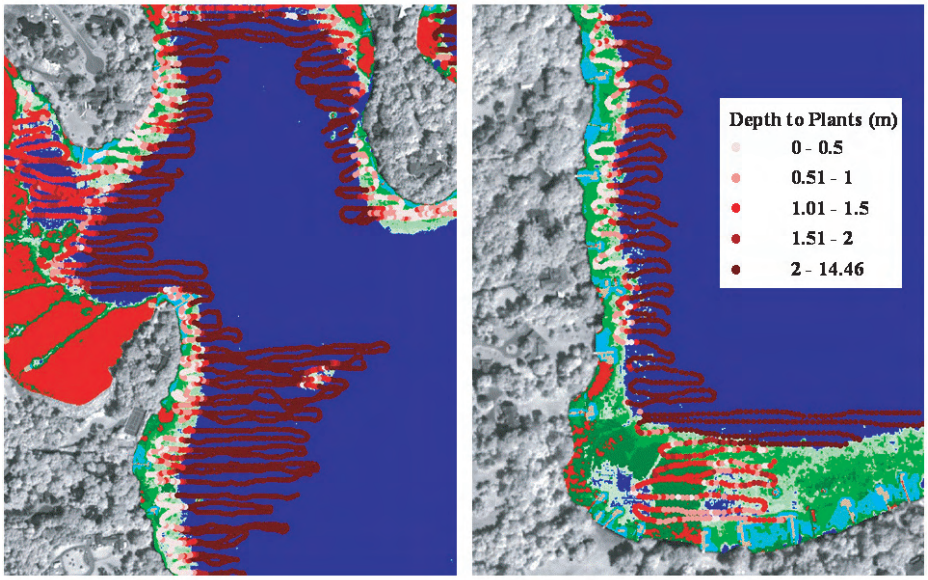


**Figure 5.13.** QuickBird image classification of aquatic vegetation of Christmas Lake near Minneapolis, MN, with hydroacoustic plant top depth points (note Eurasian water milfoil (dark green class) mechanically removed southwest portion of lake before hydroacoustic survey was conducted; QuickBird Imagery © Digital Globe).

classes. The highest accuracies occurred with plants that grow in homogeneous dense beds such as cattail and water lily/floating leaf pondweed. Plants that tend to have sparse growing characteristics and areas with more heterogeneous plant communities were more difficult to accurately classify. Ideally, the image would be taken back into the field after classification, shortly after image acquisition, to verify the classification using the GPS tracking software. Being able to accurately identify specific locations on the classified image while in the field would be especially useful for accuracy assessments and for improving the classification.

Review of the aquatic plant assessments of the three lakes south of Lake Minnetonka indicates that submerged plants can be separated from openwater areas and classified to a plant top depth of around 2 m or to the water clarity depth of 0.6 m in Schutz Lake. It also appears that submerged plants with more dense growing characteristics like Eurasian water milfoil (an exotic to Minnesota lakes) can be separated from other submerged plants that tend to have less dense growing characteristics. An aquatic vegetation map (Fig. 5.12) and a hydroacoustic survey plant top depth points (Fig. 5.13) are shown for Christmas Lake.

In a review of methods and results of satellite remote sensing of wetlands, primarily with Landsat and SPOT data, Özesmi and Bauer (2002) found that accurately mapping wetlands is a challenging task. However, this study indicates that the use of IKONOS and QuickBird imagery for aquatic plant surveys is promising. Stratification and unsupervised classification of pan-sharpened multispectral high-resolution imagery provided a map identifying different aquatic vegetation groups throughout a large type-4 wetland and three lakes. The high spatial resolution of the imagery enables the assessment of aquatic vegetation variation within lakes and wetlands that cannot be obtained from Landsat data, and the multispectral data enable classification beyond that commonly achieved with aerial photography. Future work will include object-based approaches to classification.

## 5.6. References

Barbier, E.B., J.C. Burgess and C. Folke. 1994. Paradise Lost? The Ecological Economics of Biodiversity. Earthscan Publications Ltd, London.

Carlson, R.E. 1977. A trophic state index for lakes. Limnol. Oceanogr. 22:361-369.

Daily, G.C. (ed.). 1997. Nature's Services: Societal Dependence on Natural Ecosystems. Island Press, Washington, DC.

Kloiber, S.M., P.L. Brezonik, L.G. Olmanson and M.E. Bauer. 2002a. A procedure for regional lake water clarity assessment using Landsat multispectral data. Remote Sens. Environ. 82(1):38-47.

Kloiber, S.M., P.L. Brezonik and M.E. Bauer. 2002b. Application of Landsat imagery to regional-scale assessments of lake clarity. Water Res. 36:4330-4340.

Lillesand, T., J. Chipman, D. Nagel, H. Reese, M. Bobo and R. Goldman. 1998. Upper Midwest gap analysis program image processing protocol. Report prepared for the U.S. Geological Survey, Environmental Management Technical Center, Onalaska, WI, EMTC 98-G001.

Mitsch, W.J. and J.G. Gosselink. 1993. Wetlands. 2nd ed. Van Nostrand Reinhold, New York.

Olmanson, L.G. 1997. Satellite remote sensing of the trophic state conditions of the lakes in the Twin Cities Metropolitan Area. MS thesis. Water Resources Science, University of Minnesota, St. Paul, MN.

Olmanson, L.G., S.M. Kloiber, M.E. Bauer and P.L. Brezonik. 2001. Image processing protocol for regional assessments of lake water quality. Water Resources Center and Remote Sensing Laboratory, University of Minnesota, St. Paul, MN. October 2001.

Olmanson, L.G., M.E. Bauer and P.L. Brezonik. 2002. Water quality monitoring of 10,000 Minnesota Lakes: statewide classification of lake water clarity using Landsat imagery. Proceedings, 15th William T. Pecora Memorial Remote Sensing Symposium. 8–15 November. Denver, CO. unpaginated CD ROM.

Ozesmi, S.L. and M.E. Bauer. 2002. Satellite remote sensing of wetlands. Wetlands Ecol. Manage. 10(5):381-402.

Sawaya, K., L. Olmanson. N. Heinert, P. Brezonik and M. Bauer. 2003. Extending satellite remote sensing to local scales: Land and water resource monitoring using high-resolution imagery. Remote Sens. Environ. 88:144-156.

Tyler M. and J.D. Madsen. 2001. Swan Lake aquatic vegetation survey field data. Biological Sciences Department, Minnesota State University, Mankato. Unpublished.

# Chapter 6. Satellite remote sensing III: Regional- to global-scale systems

## 6.1. Introduction

The final category of satellite remote sensing systems to be discussed in this guide are those designed to provide routine operational monitoring at regional to global scales. These systems generally share the following characteristics:

- Relatively coarse spatial resolution (nominally 250–1000+ m, but coarser off-nadir due to earth curvature and, in some cases, scanner geometry)
- Spectral resolution similar to, or slightly better than, the previously discussed satellite systems (typically 2–20 bands in the visible and near-infrared region)
- Wide field of view (±50° or more from nadir)
- Wide coverage area (1000 km or wider swath)
- Frequent coverage (may be daily, but constrained by cloud cover)
- Low (or no) cost for imagery

These types of systems are designed for monitoring broad-scale environmental conditions in the atmosphere, in the oceans and on the land surface. Their primary advantages for lake management applications are frequent coverage, wide spatial extent of coverage and availability of standard higher-level products. Their primary disadvantages are coarse spatial resolution (minimum lake size 200–1000 ha or larger depending on sensor design), and limited spectral resolution (compared to hyperspectral systems).

The most important global-scale satellite monitoring systems include:

- The Moderate Resolution Imaging Spectroradiometer (MODIS), carried on NASA's Terra and Aqua spacecraft. These two platforms provide daily to twice-daily coverage over virtually the entire globe. MODIS has two spectral bands at a resolution of 250 m (red and near-infrared), plus five more at 500-m resolution (blue, green, near-infrared and mid-infrared), and 29 additional specialized bands at 1000-m resolution (including nine designed for ocean color applications, plus thermal infrared bands for surface temperature measurement; Table 6.1). MODIS data can be obtained at no cost via NASA's EOS Data Gateway (see "Acquiring MODIS and MERIS imagery" later in this chapter). In some areas, MODIS data can also be obtained in near-real time via a network of Direct Broadcast Reception facilities (for the U.S. Midwest region, data can be obtained from the University of Wisconsin's X-band Direct Broadcast site at http://www.ssec.wisc.edu). The first MODIS data became available in February 2000.
- The Medium Resolution Imaging Spectrometer (MERIS), one of several instruments on the European Space Agency's Envisat-1, provides imagery at 300-m resolution (for land and coastal areas, or 1200 m in the open ocean). MERIS has 15 spectral bands in the visible and near-infrared. These bands are generally operated in a standard configuration, but their position and bandwidth can be reprogrammed from the ground for specialized applications. Unlike MODIS, the MERIS instrument is operated in an "on-demand" mode, meaning that data are collected in response to user requests (or, in the absence of such requests, in accordance with a long-term acquisition plan), rather than being operated continuously. MERIS allows global coverage every three days. Depending on the source and the end-user, MERIS data may be available at no cost (e.g.,

Table 6.1 Spectral bands on MODIS. Bands 1–5 and 8–16 are the most useful bands for lake water quality monitoring. Bands 17–36 are primarily used for atmospheric applications.

| Band | Resolution | Wavelength | Description |
|---|---|---|---|
| 1 | 250 m | 620–670 nm | Red |
| 2 | 250 m | 841–876 nm | Near-infrared |
| 3 | 500 m | 459–479 nm | Blue |
| 4 | 500 m | 545–565 nm | Green |
| 5 | 500 m | 1230–1250 nm | Near-infrared |
| 6 | 500 m | 1628–1652 nm | Mid-infrared |
| 7 | 500 m | 2105–2155 nm | Mid-infrared |
| 8 | 1000 m | 405–420 nm | Blue |
| 9 | 1000 m | 438–448 nm | Blue |
| 10 | 1000 m | 483–493 nm | Blue |
| 11 | 1000 m | 526–536 nm | Green |
| 12 | 1000 m | 546–556 nm | Green |
| 13 | 1000 m | 662–672 nm | Red |
| 14 | 1000 m | 673–683 nm | Red |
| 15 | 1000 m | 743–753 nm | Near-infrared |
| 16 | 1000 m | 862–877 nm | Near-infrared |
| 17–36 | 1000 m | Various | Various |

for approved research projects), or up to $500 per scene (fluctuating depending on the US$/Euro exchange rate). MERIS data have been available since mid-2002.

Other sensors may also be of interest:

- The Sea-viewing Wide-Field-of-View Sensor (SeaWiFS), designed for ocean color monitoring applications but may also be considered for studies of very large lakes. It includes eight narrow spectral channels in the visible and near-infrared, with a spatial resolution of 1100 m at nadir.
- The Advanced High-Resolution Imaging Spectroradiometer (AVHRR), carried on more than 10 satellites since 1979. Its spectral and spatial resolutions place severe constraints on its use for lake water quality monitoring (AVHRR includes only one visible and one near-infrared band, with a resolution of 1100 m at nadir); however, it has been used for studies of circulation patterns, surface areas, temperatures and other physical conditions in lakes, particularly in the pre-MODIS era.
- The Geostationary Operational Environmental Satellites (GOES), primarily meteorological in nature and widely used in weather forecasting. Unlike all other satellite systems discussed here, GOES systems are operated from geosynchronous, rather than near-polar, orbits and collect data from fixed locations on the earth. The two GOES satellites (GOES-East and GOES-West) acquire imagery of the entire eastern and western hemispheres of the earth, respectively, at frequencies up to once every 15 min. Thus, despite their very coarse resolution (>1000 m, and becoming progressively coarser with distance from the equatorial nadir-point), these systems can indicate meteorological and lake surface conditions at sub-hourly timescales. GOES includes one visible band and four thermal-infrared bands.

This chapter describes several studies that have used MODIS imagery to monitor environmental conditions in lakes. As mentioned previously, the MODIS instrument is carried on two satellites: Terra, which crosses the

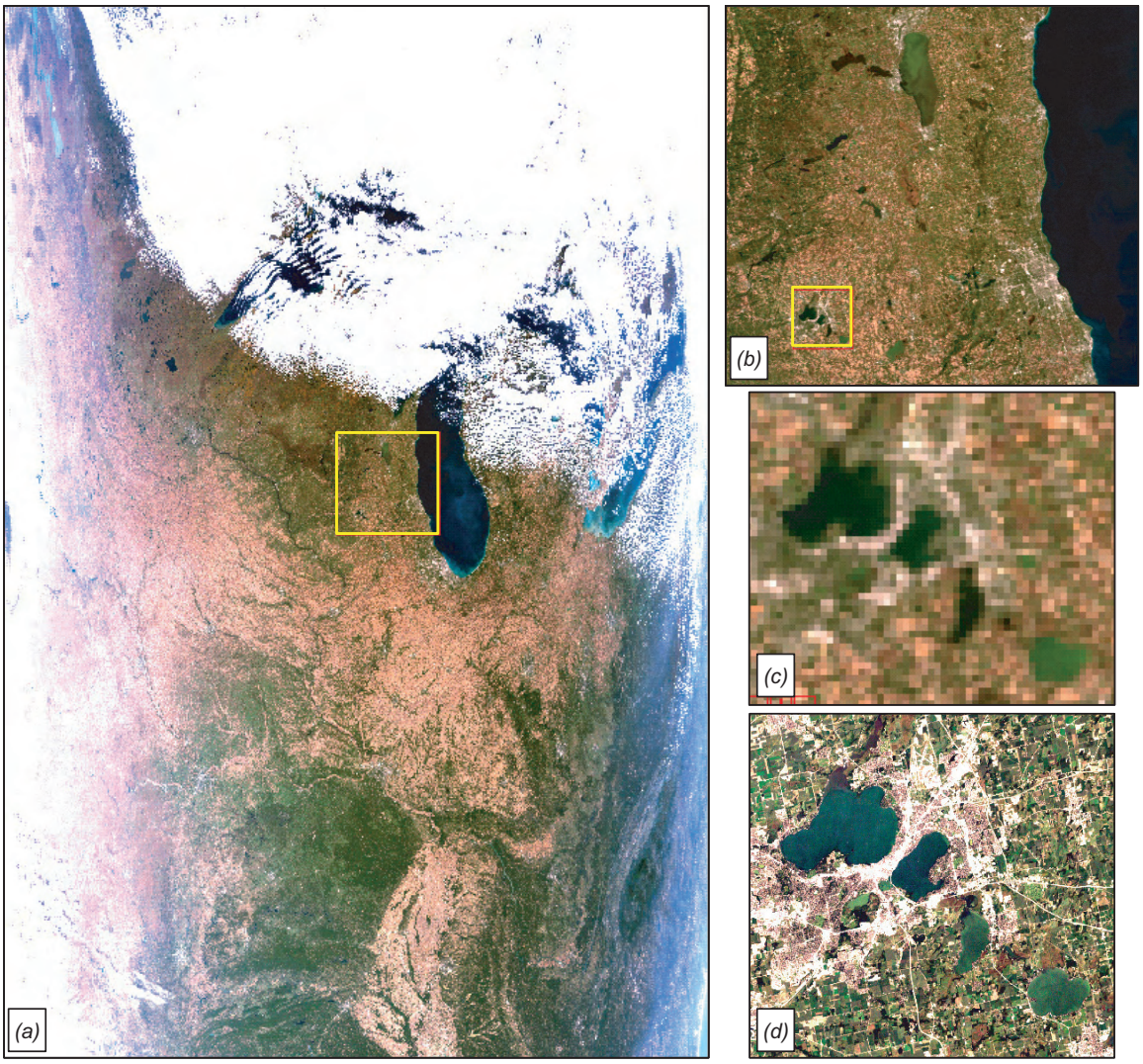


**Figure 6.1.** Terra MODIS true color image, 15 October 2005, bands 1, 4, 3 displayed as red, green, blue. (a) Raw HKM image of entire scene. (b) Enlargement of southeast Wisconsin area. (c) Further enlargement of Madison Lakes region, showing 500-m resolution pixels. (d) For comparison, Landsat-7 ETM+ image of area shown in (c), 2 September 2001.

equator in the morning, descending from north to south over the Midwest U.S.; and Aqua, with an orbital path that ascends from south to north, with an early afternoon equatorial crossing time.

An example of MODIS imagery over the U.S. Midwest region (Fig. 6.1) shows the relatively coarse spatial resolution (in this case, 500-m resolution at nadir). The atmosphere becomes much more "hazy" due to the increased path length at the extreme left and right sides of the image (Fig. 6.1a), and the geometry becomes highly distorted due to earth curvature and the cosine effect of off-nadir viewing inherent in this type of across-track scanner system. Lake surface temperatures can be calculated from the thermal-infrared bands on MODIS and mapped (Fig. 6.2).

Of the 36 spectral bands on MODIS, the most useful for lake water quality monitoring are bands 1–5 and 8–16; however, the 1000-m spatial resolution of bands 8–16 limits their use for all but the largest lakes. With the 500-m

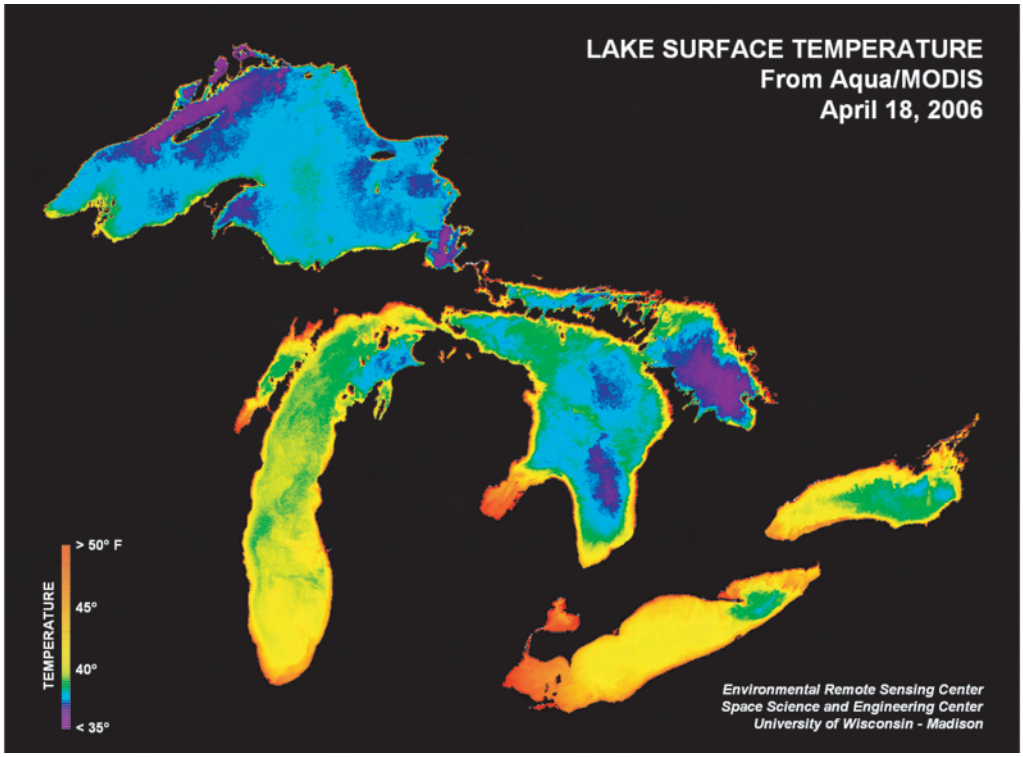


**Figure 6.2.** Lake surface temperature map of the entire Great Lakes region, derived from the Aqua MODIS thermal-infrared bands, April 18, 2006.

resolution bands, the set of lakes that can be routinely monitored should include roughly 500 lakes in the upper Midwest region of Michigan, Wisconsin and Minnesota (discussed in more detail later in this chapter).

When analyzing a single date of satellite imagery (such as the individual moderate- and high-resolution satellite images discussed in the previous chapters), employing atmospheric correction is often not strictly necessary; regression models can be developed that are specific to the image in question. For multi-temporal remote sensing applications, however, field data are not typically available on every image date and image-specific regression models cannot be developed. Thus, images must be radiometrically "normalized" or undergo an "atmospheric correction" process to convert the at-sensor radiance data to absolute surface reflectances.

Two standard atmospherically corrected products can be used with MODIS data: the surface reflectance product (MOD-09*, produced by the NASA Land Processes DAAC at Sioux Falls, SD) and the Level-2 or Level-3 water-leaving radiance products (provided by the MODIS Ocean Biology team). The surface reflectance product is available for the 500-m resolution bands and is among the products used in the two case studies described later in this chapter. The water-leaving radiance product is only available for the 1000-m resolution bands.

One frequent question is whether the standard MODIS ocean chlorophyll product can be used to estimate chlorophyll in inland lakes. If that were routinely possible, this chapter could be much shorter. Unfortunately, the oceanic chlorophyll algorithms are not well suited for optically complex inland waters. In essence, the structure of the chlorophyll model, and the spectral bands used to produce it, are not appropriate in more turbid environments.

* The file naming convention for MODIS images specifies that MODIS products from the Terra satellite begin with the prefix "MOD" while those from Aqua begin with "MYD." For simplicity's sake, in this chapter we will refer to generic MODIS products using the Terra naming convention.

An illustration of this problem (Fig. 6.3) shows the standard MODIS chlorophyll product for Lake Michigan's Green Bay (Fig. 6.3a). For comparison, chlorophyll concentration derived from the same date of imagery is also shown (Fig. 6.3b) but derived from an algorithm "tuned" to these more turbid inland waters. An assessment of the latter image (Fig. 6.3c) uses seven field sampling locations with chlorophyll values ranging from <20 to >80 µg/L. It can be seen that the model results using lake-specific algorithms (Fig. 6.3b) are quite close to the "ground truth." In contrast, the chlorophyll estimates using the standard MODIS Level-2 chlorophyll product (Fig. 6.3a) are not particularly accurate under these circumstances. In addition to the accuracy concerns, the standard chlorophyll product is produced at 1000-m resolution, while the lake-specific algorithm image (Fig. 6.3b) was produced using a version of the 500-m resolution imagery that had been resampled to 250 m using an "image-sharpening" algorithm. Thus, while the standard MODIS chlorophyll product is quite useful for oceanographic applications (its intended purpose), it cannot generally be used for inland lakes.

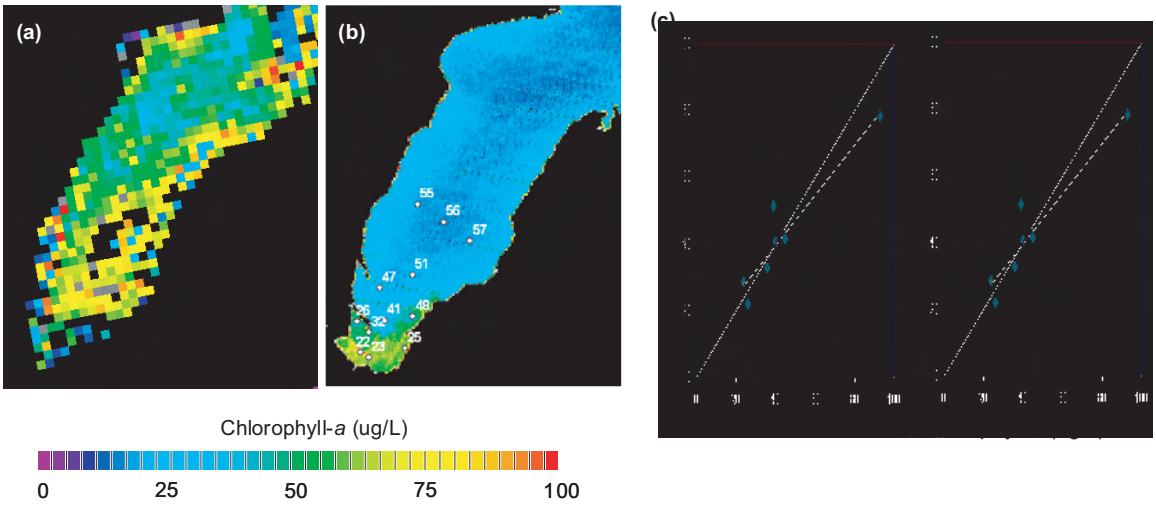


**Figure 6.3.** Estimated chlorophyll *a* concentration in Green Bay from Aqua MODIS imagery, 5 October 2004. (a) From standard MODIS Level-2 chlorophyll product, based on oceanographic chlorophyll algorithm using 1000-m MODIS bands. (b) From lake-specific algorithm using 500-m MODIS bands, resampled to 250 m. (c) Comparison of MODIS estimates from (b) with field-measured chlorophyll *a* concentrations.

While the ocean chlorophyll algorithm may not be suited for inland lakes, a number of previous studies have employed MODIS imagery for lake monitoring applications. Montesano (2006) examined the use of the 500-m resolution MODIS bands for estimating chlorophyll in lakes in Minnesota and Wisconsin, and parts of the work described in this chapter are based on (or related to) that study. Dall'Olmo *et al.* (2005) used simulated MODIS and SeaWIFS imagery (derived from airborne hyperspectral data) to assess the potential of those sensors for measuring chlorophyll *a* in lakes.

Several studies have used MODIS data to examine individual lakes or lakes at a sub-regional scale. Working in a 14,500 km$^2$ local area in Finland, Koponen *et al.* (2004) used MODIS 250 m data to classify lakes in terms of their generalized water quality. Pozdnyakov *et al.* (2003) developed a method to estimate chlorophyll *a* and other parameters from MODIS data for Lake Michigan in the U.S. Midwest region. In eastern China, Zhu *et al.* (2005) used a variety of MODIS spectral bands to develop chlorophyll *a* retrieval models for a single lake in each of the four seasons. They found that the band combinations that provided the best estimates of chlorophyll varied according to season, and that MODIS band combinations correlated poorly with chlorophyll in the winter. Hu *et al.* (2004) used MODIS imagery to examine water quality in Tampa Bay, Florida.

## 6.2. Acquiring MODIS and MERIS imagery

MODIS imagery is available for download from multiple sources. It comes in a variety of formats that describe terrestrial, oceanic and atmospheric features and can be used for studies of processes and trends on regional and global scales. The case studies discussed in this chapter are derived from two versions of MODIS data. The Level-1B imagery consists of calibrated "at-sensor" spectral radiance measurements, meaning that the returning signals from terrestrial and water features were measured after passing through the atmosphere. The surface reflectance (MOD-09) version of the imagery consists of measurements of radiance as a percentage of all irradiance incident upon the earth surface at a specific location. The surface reflectance data are distributed in a geocoded format, while the Level-1B imagery can be projected into a map coordinate system using free software (MRT-Swath).

Both the Level-1B and surface reflectance imagery are free and available through the NASA Earth Observing System Data Gateway (EDG). Level-1B data and other products can also be obtained from any of the EOS Direct Broadcast reception facilities located around North America (and elsewhere in the world). For the Midwest U.S., the EOS Direct Broadcast site at the University of Wisconsin is a useful source.

Online Resources:

Earth Observing System Data Gateway (EDG):
http://eos.nasa.gov/imswelcome

Guide to NASA Data Centers (DAACs) and their web sites:
http://nasadaacs.eos.nasa.gov/search.html

Information on MODIS data products:
http://modis.gsfc.nasa.gov/

MODIS Land Products:
http://edcdaac.usgs.gov/dataproducts.asp

MODIS Ocean Products:
http://oceancolor.gsfc.nasa.gov/

MRT-Swath software information and download:
http://edcdaac.usgs.gov/landdaac/tools/mrtswath/about.asp

Real-time data from the UW-Madison Space Science and Engineering Center:
http://www.ssec.wisc.edu/data/

As discussed previously, the MERIS instrument is operated by the European Space Agency and was launched in 2002. This spectrometer allows for global coverage every three days. For several reasons, MERIS data may not be as easily accessible as MODIS data, and the sensor is operated in an "on-demand" mode rather than a "continuous-operation" mode like MODIS. The BEAM software package can be used to work with MERIS data. This software enables the user to specify the data's projection and export the product to a GIS-ready format (.IMG, GeoTiff, and others), from which point it can then be used in the standard image processing software systems.

Online Resources:

ESA site discussing MERIS details:
http://earth.esa.int/object/index.cfm?fobjectid=1665

Browse MERIS data:
http://www.enviport.org:8080/meris/

BEAM software:
http://www.brockmann-consult.de/beam/

## 6.3. Case study 1: Estimating chlorophyll *a* concentration in Minnesota lakes

In late July and early August 2005, a group of scientists and citizen volunteers made 115 field surveys of lakes across Minnesota and western Ontario, collecting data on chlorophyll concentrations, water clarity and other measurements (Fig. 6.4). The data from this field sampling campaign are an ideal source for calibrating satellite-based water quality models because they include a wide range of lake types with very different levels of chlorophyll, colored dissolved organic carbon, suspended solids and water clarity.

Terra MODIS imagery of the study region was acquired from the NASA DAAC online distribution system in two formats: calibrated at-sensor spectral radiance measurements (Level 1-B) and atmospherically corrected surface reflectance measurements (MOD-09). Both types of imagery were used to estimate chlorophyll *a* concentrations in lakes. For each image, the process consisted of the following steps:

1. Acquire imagery from the NASA DAAC in HDF format.
2. Project the imagery into the UTM zone 15 map coordinate system, using nearest-neighbor resampling.
3. Use an unsupervised image classification, gray-level thresholding to mask out clouds, land and wetlands.
4. Extend this mask further using a 1-pixel–wide buffer to ensure that no mixed pixels along the edges of non-water areas were included. The resulting dataset is called a "water-only" image.
5. Extract the spectral signatures for each field-sampled point in the water-only image.
6. Use regression modeling to correlate various MODIS bands and band ratios with the natural logarithm of chlorophyll concentration.
7. Apply the models to predict chlorophyll concentration for all pixels in the water-only image.

The variability among the lakes in the Minnesota/Ontario study region can be seen when all non-water areas are rendered in grayscale, and the natural differences in color among the lakes are enhanced using a linear stretch (Fig. 6.5).

The best fit between the field data and the MODIS imagery was found using spectral band ratios from the Level-1B images, in particular the blue/red ratio (MODIS band 3 divided by MODIS band 1). In this case, an $R^2$ value of 0.79 was obtained using this ratio alone (Fig. 6.6), rising slightly to 0.84 with the inclusion of two additional band ratios (band 3/band 2 and band 3/band 4). The surface reflectance imagery (MOD-09) yielded slightly worse model fits, with $R^2$ values ranging from 0.60 (for band 1 alone) up to 0.74 (for various combinations of bands 1–4).

Chlorophyll *a* concentrations in lakes in northern Minnesota and western Ontario were predicted, based on the analysis of Level-1B Terra MODIS imagery acquired on 1 August 2005 and field data from the 2005 survey (Fig. 6.7).

The regression models used in this study use a log-transformed version of chlorophyll concentration as the dependent variable. The root mean square error (RMSE) value for the regression model with the Level-1B data (*i.e.*, the model used to produce Fig. 6.6) was 0.30 log-transformed units. When the log-transformed estimates are converted back to linear units, the error "envelope" is not constant. For example, a known concentration of 4.0 µg/L would have an expected 1-RMSE range of 3.0–5.4 µg/L, while a known concentration of 20 µg/L would yield a 1-RMSE range of 15–27 µg/L (Fig. 6.8).

Note that this RMSE estimate includes multiple sources of error. One is the obvious inherent limit in the ability of the algorithm to accurately predict chlorophyll concentrations. Others, however, are artifacts of the analytical process and do not necessarily imply actual error in the predictive ability of MODIS. These include (1) field measurements were not all acquired on the same date as the MODIS image; (2) (unknown) error in the field

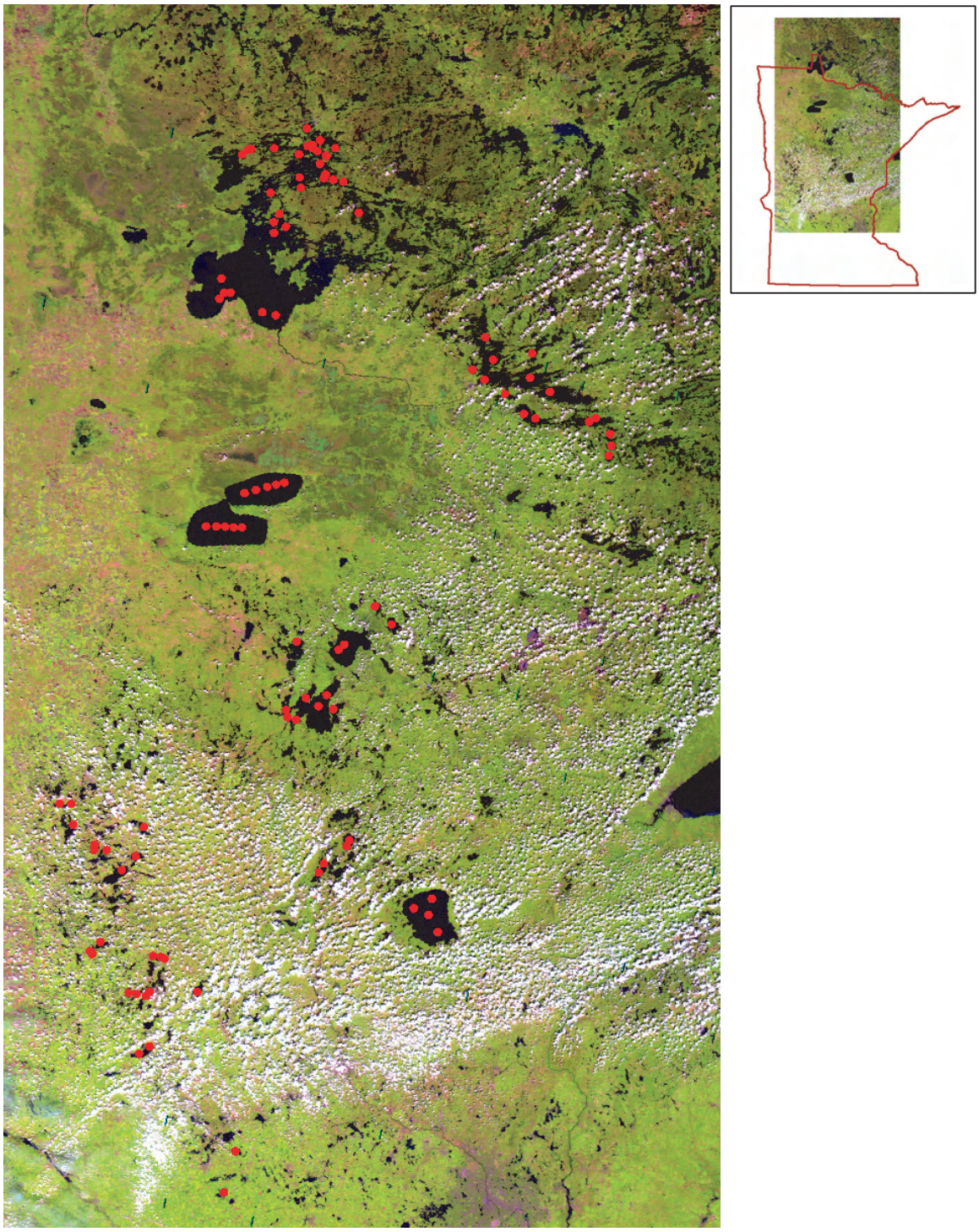

**Figure 6.4.** Portion of a reprojected true color MODIS image of Minnesota and western Ontario, 1 August 2005. Bands 1, 4, 3 displayed as red, green, blue. Red dots indicate sampling locations from the summer 2005 field survey.

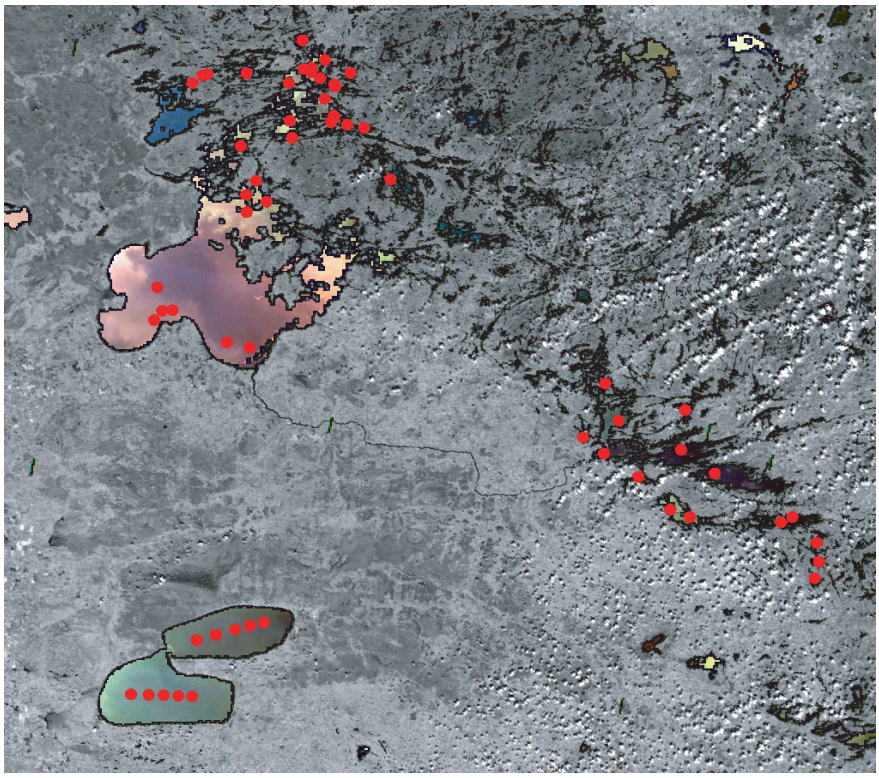

**Figure 6.5.** Enlargement of the 1 August 2005 MODIS image of the Minnesota/Ontario border region. Bands 1, 4, 3 displayed as red, green, blue.

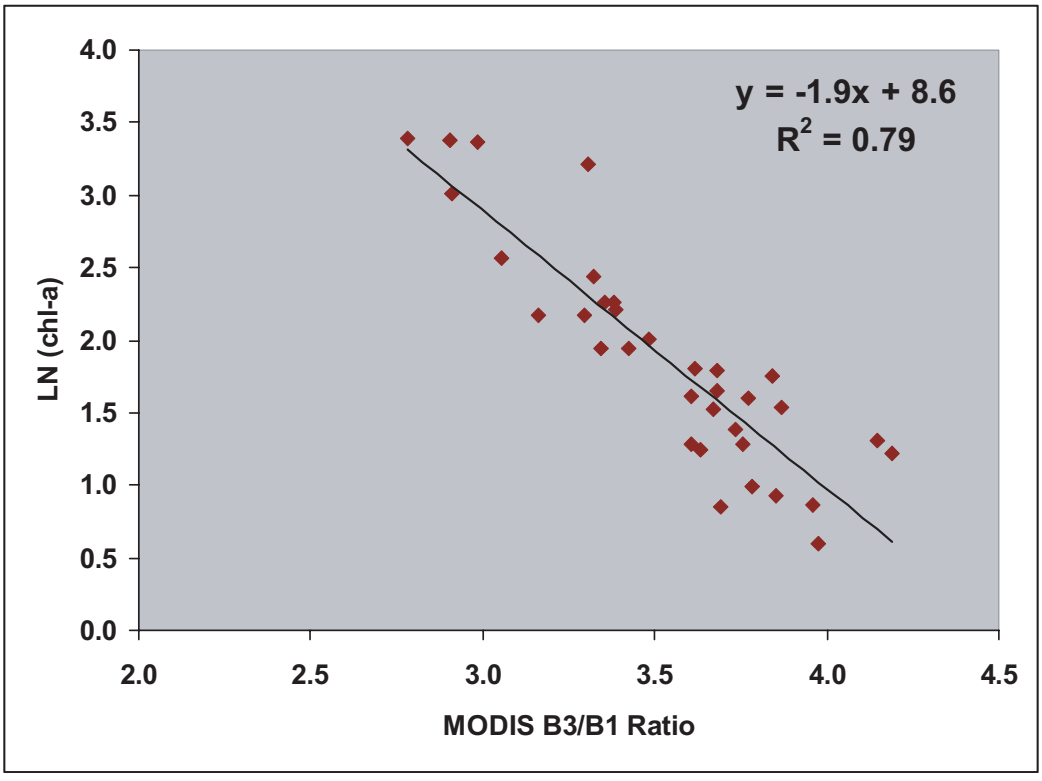


**Figure 6.6.** Relationship between the MODIS blue/red spectral radiance ratio (band 3/band 1) and the natural logarithm of chlorophyll *a* concentration for field-sampled lakes.

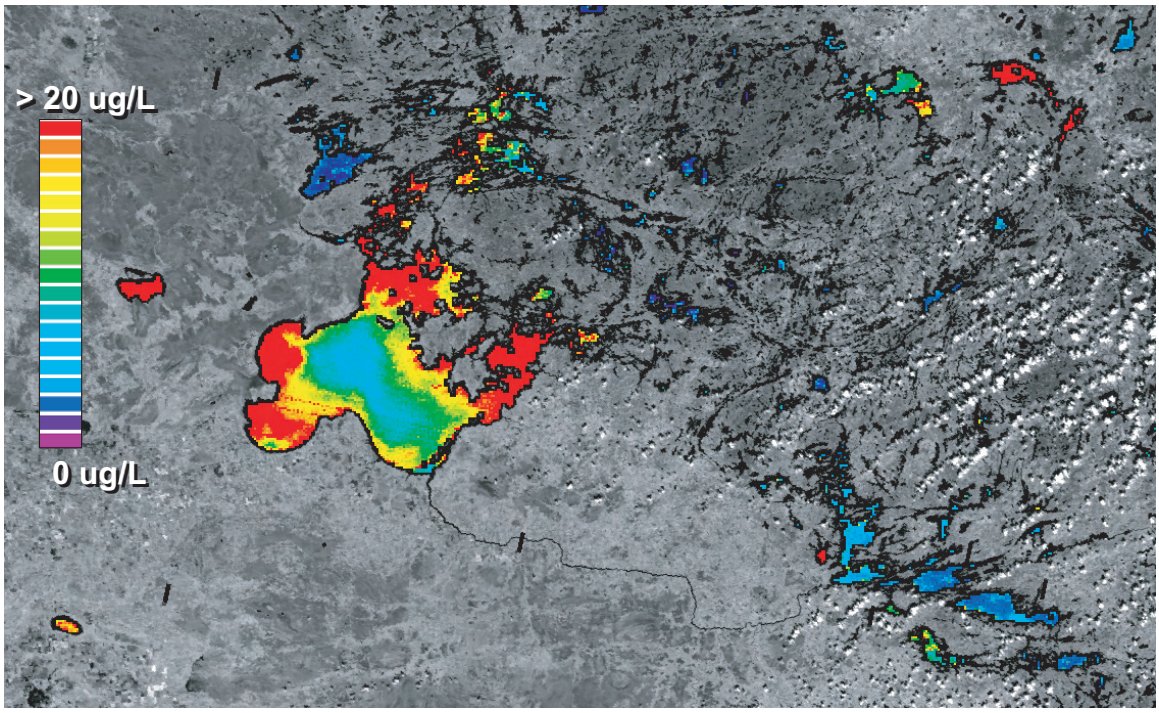


**Figure 6.7.** Estimated chlorophyll *a* concentration for lakes along the Minnesota/Ontario border region, based on MODIS imagery, 1 August 2005.

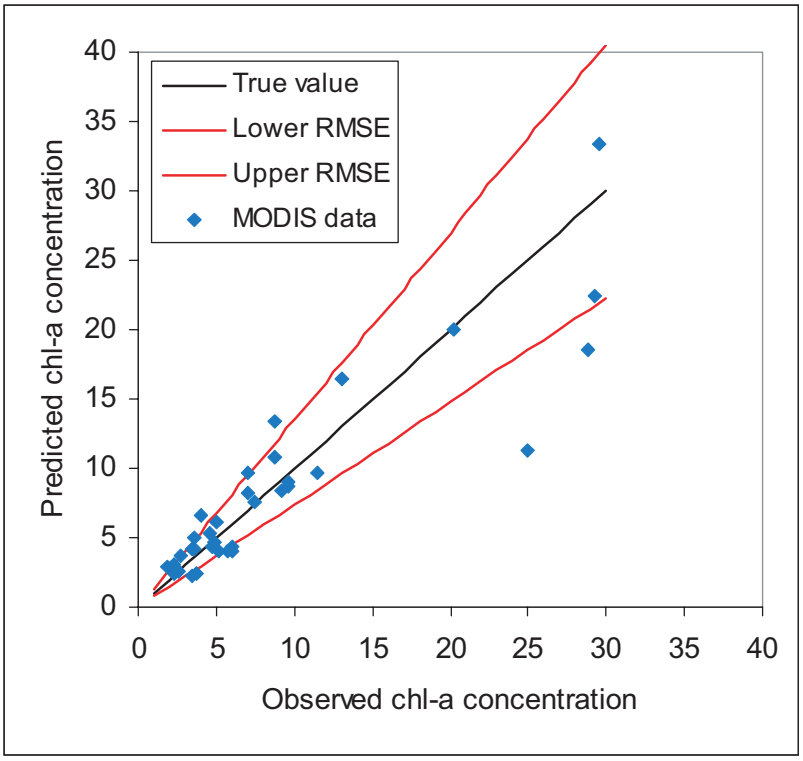


**Figure 6.8.** Error analysis of MODIS chlorophyll *a* predictions. Units are µg/L.

measurements; and (3) difference in spatial scale between the field measurements (collected at individual points) and the MODIS pixels (integrating radiance from a nominal 500 × 500 m area).

## 6.4. Case study 2: Estimating Secchi depth, chlorophyll *a* concentration, suspended solids and turbidity in Green Bay and Lake Michigan

One of the primary advantages of MODIS is the availability of no-cost data over large areas at frequent intervals (daily to weekly, depending on cloud cover) so that water quality in a lake, or a group of lakes, can be monitored on many dates across a single season. To demonstrate this, we conducted a case study focused on Lake Michigan's Green Bay, the largest estuarine system in the Great Lakes. It is severely impaired by multiple stressors, including phosphorus, suspended solids and toxins (Harris 1993). These water quality impacts are in turn translated to Lake Michigan through substantial export of nutrients and suspended solids from Green Bay into the main basin of the lake. Consequently, remediation of the water quality in Green Bay commands national attention; 11.2 km of the Lower Fox River and 55 km$^2$ of southern Green Bay are designated an Area of Concern (AOC) by the International Joint Commission (IJC) as the result of multiple impaired uses identified in this aquatic resource.

Water quality in southern Green Bay is monitored on a weekly to biweekly frequency during the May–October period by the Green Bay Metropolitan Sewerage District (GBMSD). Sampling is conducted from boats at 12 stations on the Bay itself (Fig. 6.9), with additional stations on the Fox River.

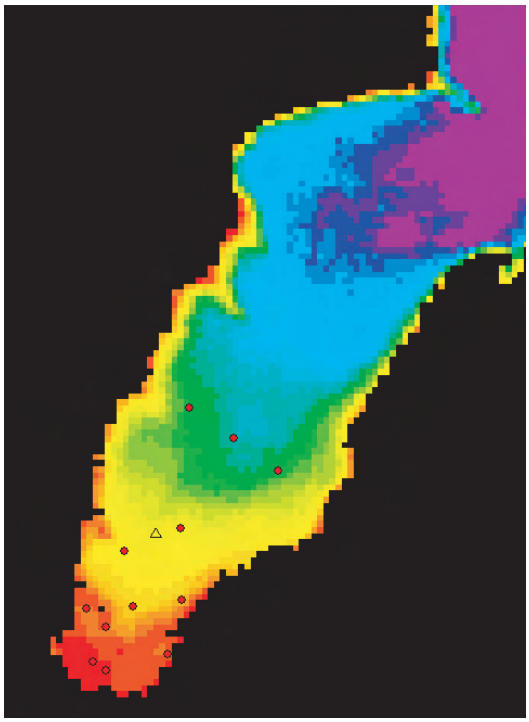

**Figure 6.9.** Locations of GBMSD sampling stations (red dots) in southern Green Bay, Lake Michigan, superimposed on a map of the seasonal average Secchi depth in the bay, derived from MODIS imagery. See Figure 6.11 for Secchi color codes.

For the Green Bay study, atmospherically corrected surface reflectance imagery from both Terra and Aqua (MOD-09 and MYD-09) was used to improve the applicability of models across multiple images. Twenty-two dates of imagery were acquired during June through October 2004. The general process used to analyze these images (Fig. 6.10) follows a series of steps, as with the previous case study, including projecting the image, subsetting out the study area, and masking out clouds and land areas. In this case, an automated algorithm was developed to identify and mask out clouds based on their spectral properties. The water-only image is then used to estimate the following water quality parameters, presented as a series of images (Fig. 6.11):

- Secchi depth, m
- Chlorophyll concentration, µg/L
- Total suspended solids concentration, mg/L
- Turbidity, NTU

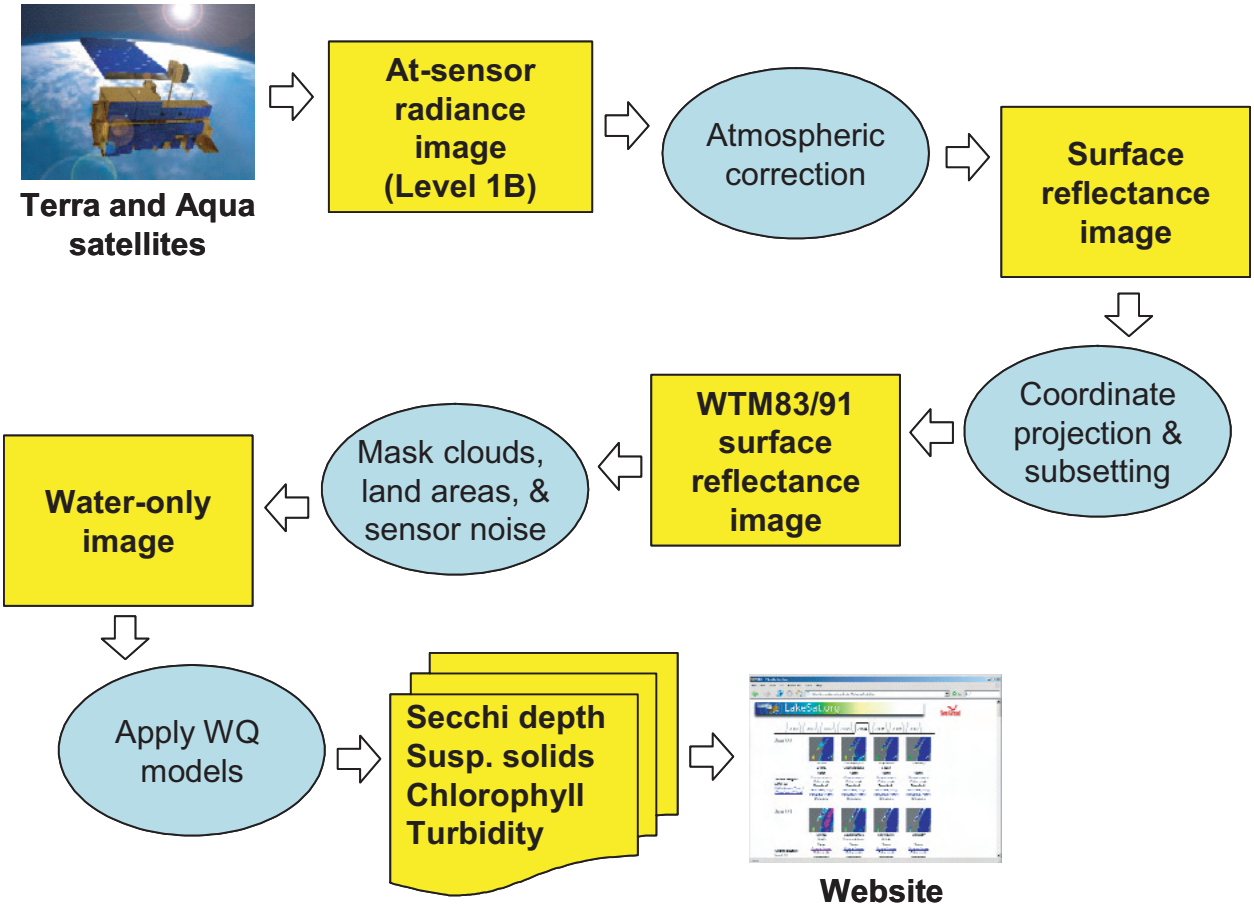


**Figure 6.10.** Analytical process for MODIS water quality mapping in Green Bay, Lake Michigan.

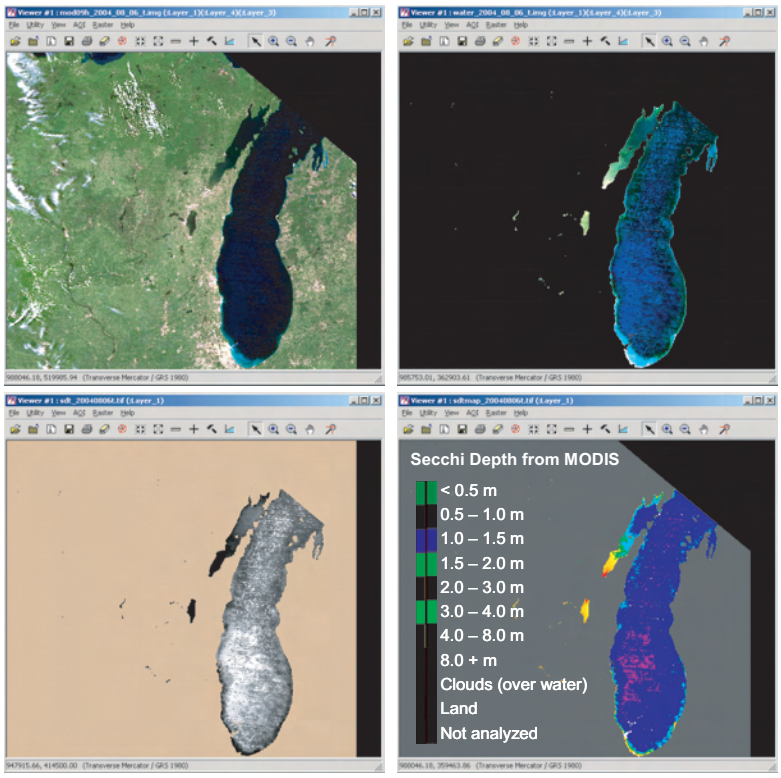


**Figure 6.11.** Example of MODIS water quality mapping in Green Bay, for Terra MODIS image acquired on 6 August 2004. Upper left: atmospherically corrected image. Upper right: water-only image. Lower left: modeled Secchi depth (lighter tones represent greater Secchi depths). Lower right: color-coded version of Secchi map.

The models for Secchi depth, chlorophyll concentration, suspended solids and turbidity were developed by combining all the GBMSD image/field data pairs that occurred within ±2 days of each other during the 2004 season, plus some of the data from the Minnesota/Ontario field sampling in 2005. For each parameter, a multiple regression model was developed to relate the parameter to various combinations of the MODIS bands 1–4. Some examples of the results mapped turbidity on four dates in June, July, August and September 2004 (Fig. 6.12).

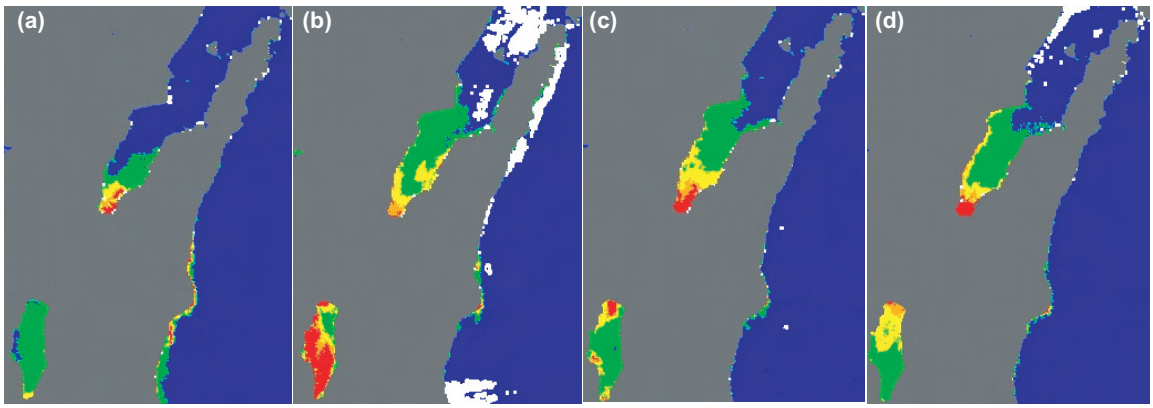


**Figure 6.12.** Examples of MODIS-based turbidity maps for Green Bay for dates in 2004. (a) June 4, (b) July 26, (c) August 6, and (d) September 10. White areas represent cloud cover on each date.

## 6.5. Determining the number of lakes suitable for monitoring with MODIS at 500 m

There are two primary considerations in determining the set of lakes that can be routinely monitored with MODIS:

1. Given the coarse resolution, only a limited number of lakes can be monitored even under the most favorable viewing geometry. The data extraction and analysis protocol should be designed to capture each of these lakes.
2. To avoid problems with mixed land/water pixels, only pixels falling completely within a lake's boundary should be included.

To identify the set of lakes in the upper Midwest region that are potentially suitable for monitoring with the 500-m resolution bands on MODIS, statewide hydrographic GIS layers (typically based on 1:24,000-scale source data) were acquired for Minnesota, Wisconsin and Michigan. To reduce the computational effort, and because small lakes are known to be undetectable in MODIS imagery, all lake polygons <100 ha were deleted. A 100-m buffer was then applied inside all the remaining lake polygons. This buffer compensates for the uncertainty in MODIS geolocations and also has the side effect of avoiding most of the littoral zone in many lakes. Two additional buffers were then applied within the remaining lake area, resulting in the following two sets of lakes:

- Maximum possible lakes. This set includes all theoretically useable lakes, on at least an occasional basis. A 250-m buffer (inside the first 100-m buffer) was used, to select all lakes that include at least one 500 × 500 m water-only area. There are 2744 lakes in the tri-state upper Midwest region that meet this requirement, but many of these lakes would only very rarely be useable.
- Routine MODIS lakes. This set includes those lakes that should provide some water-only pixel(s) on most or all days with reasonably favorable viewing geometry (*i.e.*, at least 8–9 days out of 16). A 500-m buffer (inside the first 100-m buffer) was used to select all lakes that will always include one or more water-only pixels regardless of where the pixel grid falls in any given image (Figure 6.13).

The numbers of routine MODIS lakes in each state were summarized (Table 6.2). Note that this method predicts 90 lakes in Wisconsin should be routinely suitable for monitoring. In fact, demonstration studies show that all 90 of these lakes can in fact be covered over the course of several image acquisitions (with partial cloud cover on each date. As lake surface area decreases, the likelihood that a lake will be usable in MODIS imagery decreases (Table 6.3).

**Table 6.2.** Number of lakes that should be routinely suitable for MODIS monitoring.

| State | Lakes |
|---|---|
| Michigan | 108 |
| Wisconsin | 90 |
| Minnesota | 388 |

**Table 6.3.** Routine MODIS lakes in Wisconsin, as a function of lake size.

| Lake size | Total lakes | MODIS lakes | Percent |
|---|---|---|---|
| >600 ha | 71 | 54 | 76% |
| 400–600 ha | 52 | 22 | 42% |
| 200–400 ha | 134 | 14 | 10% |
| 100–200 ha | 271 | 0 | 0% |

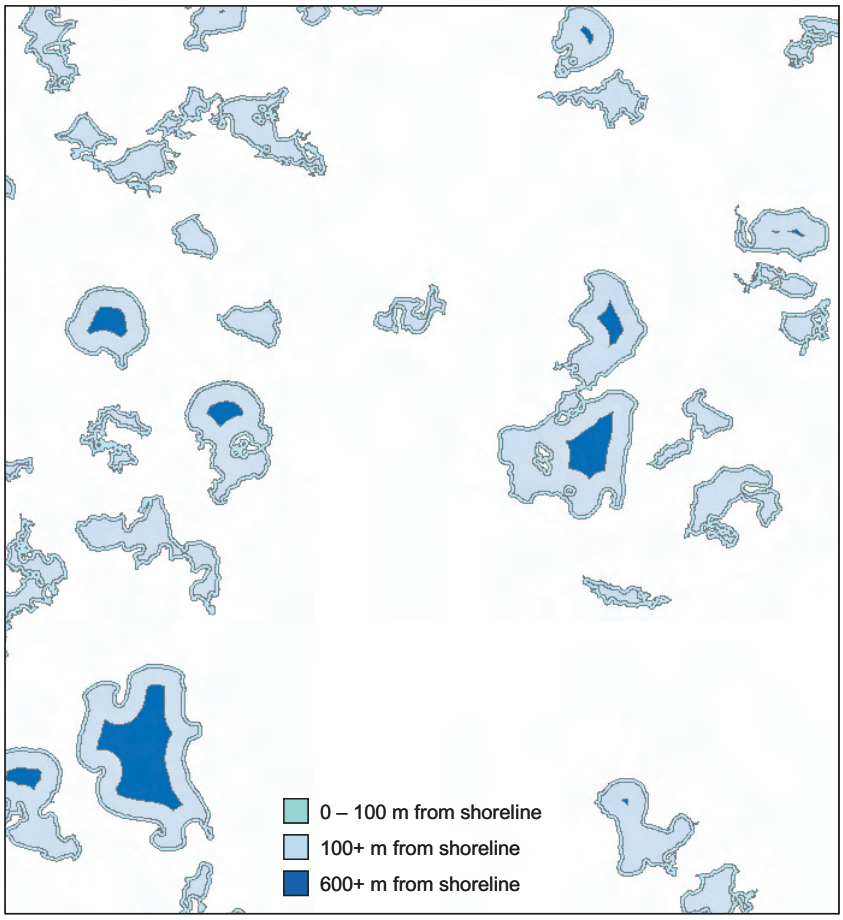


**Figure 6.13.** Examples of lakes with buffers. Lakes that include any dark blue polygons are suitable for MODIS monitoring when viewing geometry is adequate.

## 6.6. Costs and resource requirements

As discussed in the introduction to this chapter, one of the advantages of regional-to-global-scale sensors is that large quantities of data can generally be acquired for free (*e.g.*, MODIS, or in some cases MERIS) or at a relatively low cost. However, costs still apply to any organization adopting these methods for lake monitoring:

*Software licenses:* The work described in these case studies primarily involved the use of the Leica Geosystems Imagine image-processing software, but other similar software systems (*e.g.*, RSI ENVI) could possibly be used. If this software is not already available in-house, the costs of licenses will need to be considered, which vary widely depending on the vendor's pricing policies, the type of organization (*e.g.*, educational vs. commercial), the number of licenses and other factors. Typically, costs may run from US$500–5000/yr.

*Personnel time:* Work conducted by an analyst new to this field (or new to the software involved) may require a lengthy training period. Several individual images per day can be analyzed once the analyst is familiar with the procedures involved and all data (imagery and field data) have been acquired. If a semi-automated process is employed, completely analyzing an entire season's worth of imagery in a single day is possible once all images are compiled.

*Field data collection:* Some field data from lakes in the specific region being studied must be available to develop and validate models. For many U.S. states, existing lake monitoring programs can be used to acquire

at least some of these data; however, supplementing these with additional, new sampling campaigns might be necessary.

In summary, the cost of the imagery is negligible in this case, but other costs associated with the infrastructure needed to use the imagery must be considered. These costs will be relatively low for agencies that already have remote sensing software, trained remote sensing analysts and access to existing field data (or personnel to acquire them). Costs will be much steeper for organizations using this technology for the first time, and they should consider working with a local university or other center of expertise on a pilot project before proceeding to develop a fully operational system.

## 6.7. References

Dall'Olmo, G., A.A. Gitelson, D.C. Rundquist, B Leavitt, T. Barrow and J.C. Holz. 2005. Assessing the potential of SeaWiFS and MODIS for estimating chlorophyll concentration in turbid productive waters using red and near-infrared bands. Remote Sens. Environ. 96:176–187.

Harris H.J. 1993. The state of the bay: a watershed perspective. The condition of the Bay of Green Bay/Lake Michigan 1993. Institute of Land and Water Studies, University of Wisconsin-Green Bay.

Hu, C., Z. Chen, T.D. Clayton, P. Swarzenski, J.C. Brock and F.E. Muller-Karger. 2004. Assessment of estuarine water-quality indicators using MODIS medium-resolution bands: Initial results from Tampa Bay, FL. Remote Sens. Environ. 93:423-441.

Koponen, S., K. Kallio, J. Pulliainen, J. Vepsalainen, T. Pyhalahti, and M. Hallikainen. 2004. Water quality classification of lakes using 250-m MODIS data. Geosci. Remote Sens. Lett. IEEE 1(4):287.

Montesano, P.M. 2006. Estimating chlorophyll *a* in lakes with MODIS: A regional assessment. MS thesis in Environmental Monitoring, University of Wisconsin, Madison.

Pozdnyakov, D., A. Korosov, R. Schuman and R. Edson. 2003. Development of a tool for the assessment of water quality from visible satellite imagery taken over turbid inland waters (with Lake Michigan as an example). Geoscience and Remote Sensing Symposium, 2003. IGARSS '03. Proceedings. 2003 IEEE International. 2:746-748.

Zhu, L., S. Wang, Y. Zhou, F. Yan and L. Wang. 2005. Determination of chlorophyll *a* concentration changes in Taihu Lake, China using multi-temporal MODIS image data. Geoscience and Remote Sensing Symposium, 2005. IGARSS 2005. Proceedings. 2005 IEEE International. 7:4535-4538.

## 6.8. Acknowledgments

Many individuals and organizations contributed to the work described in this chapter. At the University of Wisconsin Environmental Remote Sensing Center, we would like to acknowledge the work of Tom Lillesand, Sam Batzli, Jeff Schmaltz, Paul Montesano, Scott Peckham, Peter Wolter, Ben Spaier, and Jamon Vandenhoek. The University of Wisconsin Space Science and Engineering Center, and Liam Gumley in particular, provided real-time access to MODIS data. For the Minnesota/Ontario lakes study, we thank all the participants and organizers, including: Ontario Ministry of Natural Resources and their coordination of Lake of the Woods citizen volunteers; Leif Olmanson for coordination of the University of Minnesota efforts; and Steve Heiskary for coordination in Minnesota, which included Minnesota Pollution Control Agency staff and volunteer monitors, Rainy Lake Conservancy volunteers, and staff from the Red Lake Band. For the Green Bay study, we gratefully acknowledge the contributions of the Green Bay Metropolitan Sewerage District, the Wisconsin Self-Help Citizens Lake Monitoring Program, and the Wisconsin Department of Natural Resources. Portions of the work described in this chapter were supported by the Wisconsin Sea Grant program, the NASA Terrestrial Hydrology Program and the NASA/UW Affiliated Research Center (ARC), while NALMS and the US EPA supported the writing of the chapter itself.

# Chapter 7. Future developments in remote sensing for lake management

Predicting the future of any high-technology field is notoriously difficult. When satellite imagery was distributed by national space agencies (and a handful of private corporations) on 9-mm tape cartridges 15 or 20 years ago, the idea that terabytes of satellite data would be posted daily on the Internet in near-real time would seem far-fetched. Just 10 years ago it was widely expected that at least three satellite hyperspectral instruments would be launched "shortly," although none of the originally proposed systems were ever launched, and the experimental EO-1 Hyperion instrument remains the sole spaceborne hyperspectral system to date.

With that cautionary history in mind, there are several directions in which this field is expected to grow during the next decade.

## 7.1. Access to new sensors

One obvious area for advances in sensor technology is the category of "high spatial resolution" systems, discussed in Chapter 5. Over the past decade, the number of high-resolution satellite platforms has expanded dramatically, while the spatial resolution and other characteristics of these systems have simultaneously improved. This trend is virtually certain to continue, with many future systems planned or scheduled for launch during the next ten years.

While options for moderate-resolution multispectral remote sensing platforms have also expanded, as discussed in Chapter 4, many of the recent satellites in this category are less than optimal for remote sensing of lakes in some respects, such as lacking a spectral channel in the 0.4–0.5 μm (blue) region and lacking a narrower band around the chlorophyll absorption peak at 0.67 μm and scattering peak at the red edge near 0.7 μm that could be used for accurate chlorophyll assessment as discussed in Chapters 2 and 3. Given this situation, the deterioration of Landsat-5 and -7 is a subject of particular concern. While the launch of a follow-on mission to Landsat-7 has been repeatedly delayed, the eventual result of the Landsat Data Continuity Mission should be well suited for lake monitoring of water clarity. In the meantime, other systems, such as the new RapidEye satellite constellation, may provide excellent sources for lake remote sensing applications that can justify the higher cost of commercial imagery and that will benefit from the high-frequency image acquisition opportunities offered by a five-satellite constellation.

Following the success of the MODIS instrument on NASA's Terra and Aqua satellites, anticipation is high for the next generation global monitoring sensor intended to replace MODIS. The Visible Infrared Imaging spectro-Radiometer Suite (VIIRS) is intended to be carried on the forthcoming spacecraft from the National Polar-Orbiting Operational Environmental Satellite System (NPOESS) and NPOESS Preparatory Project (NPP), joint missions. Unfortunately, both systems have experienced a series of delays, and as of this writing, the launch dates for these spacecraft are still unknown. Launch for NPP is scheduled for 2010, and the first of four planned NPOESS spacecraft for 2013. When it becomes available, VIIRS should be a high-quality instrument for monitoring large lakes across continental and global scales. The system will have 22 spectral bands grouped into three major bandsets: nine bands in the visible and near-infrared plus a day/night panchromatic band, eight short- to mid-infrared bands, and four thermal infrared bands. The swath width will be approximately 3000 km with spatial resolutions of 370 m and 740 m at nadir. There will be 24 applied products generated (environmental data records or EDRs). The VIIRS instruments will be flown on three platforms: NPP and two NPOESS spacecraft, one of which will be in an afternoon sun-synchronous polar orbit and the other in an early morning orbit, providing multiple coverage on a daily basis.

Technological improvements in airborne hyperspectral sensors and field spectroradiometers attract less attention than the development and launch of new satellite systems, but the manufacturers of these instruments have benefited from the same advances in optical engineering and information technology that facilitate the development of new satellite remote sensing systems. Thus, over the next 10 years the spatial, spectral and radiometric properties of these high spectral resolution systems should continue to improve. While increases in fuel prices are raising the cost of airborne remote sensing deployments, the significant advantages of these systems for applications requiring fine spectral resolution should ensure continued high demand for their data.

## 7.2. Improvements in cyberinfrastructure

All steps of the remote sensing process—from mission planning to data analysis to dissemination of results—are increasingly dependent upon the information technology environment, or cyberinfrastructure. Geospatial data may be analyzed within a geographic information system (GIS) for site selection and characterization, aerial mission planning, and as an aid to the analysis of the remote sensing data themselves. Multiple sources of imagery and ancillary data may be obtained from servers and geodatabases operated by different agencies or data providers and distributed via the Internet. Finally, end-users increasingly access the data via interactive web-based mapping applications or other online visualization and analysis tools. Likewise, end-users are more likely to directly use the outputs from a remote sensing analysis in digital format as inputs to their own GIS or other modeling system rather than simply being handed a static paper map or report. All these developments are facilitated by the expansion of the Internet and particularly by the exponential growth in software tools for distributing, analyzing, visualizing and managing imagery and GIS data.

## 7.3. Improvements in data analysis algorithms

As discussed in this report, many of the methods used for analyzing remote sensing data in lake management applications could be characterized as relatively "mature." Nonetheless, advances are likely to continue in the algorithms used, particularly in the areas of hyperspectral image analysis, atmospheric correction, multi-image fusion and the analysis of multi-image time series. In addition, efforts are under way to both improve the accuracy of current products (*e.g.*, remotely sensed Secchi depth, chlorophyll *a* concentration) and develop new algorithms for products that are not widely implemented (*e.g.*, other pigments, dissolved organic carbon).

# Chapter 8. Conclusion

The nation's lakes provide many economic and ecological benefits, providing support for recreation, fisheries and wildlife, and water for agriculture, industry and domestic consumption. The EPA and many state and local agencies have the responsibility of monitoring the health of the nation's lakes to ensure the continued availability of these resources for future generations. Traditionally, such monitoring activities have relied on *in situ* measurement of water quality and collection of samples for laboratory analysis. While this approach can provide the most accurate information about water quality in individual lakes, it is time-consuming and expensive. As a result, only a small fraction of the nation's lakes are included in direct water quality monitoring programs.

As discussed in this guide, remote sensing—using spaceborne, airborne or proximal sensors—can complement and extend traditional lake sampling methods. Using these remote sensing systems, it is possible to look at much larger numbers of lakes, or to monitor lakes more frequently, or to study spatial variability in water quality within individual lakes. While no single remote sensing system provides the ideal resource for lake management applications, the different types of systems discussed in this manual can collectively provide a wealth of information about lakes and their bio-optical properties.

Each chapter of this report has addressed one particular type of remote sensing system, providing an overview of its strengths and weaknesses for lake monitoring applications. These include discussion of each type of sensor's principles and operation, characteristics of the data provided by the sensing system, and costs and resources required to acquire these data. The chapters also include case studies demonstrating the use of each type of remote sensing system in real-world projects. Taken as a whole, these case studies show how water quality parameters such as water clarity, chlorophyll concentration, suspended solids and turbidity can be estimated remotely, at scales ranging from individual lakes to multi-state regions.

As with any new endeavor, an agency or organization interested in adopting remote sensing methods for lake management will need to acquire certain tools and expertise. In this field that may include hardware (if field spectroradiometry will be used), software, data/imagery and personnel (or training existing personnel). For analysis of airborne and spaceborne imagery, the software needed will typically consist of both digital image processing and geographic information system (GIS) software. In many cases, these costs may be mitigated or reduced if the resources can be shared among different remote sensing projects: for example, sharing the software license costs, the imagery, and potentially even the same analysts among multiple projects.

We hope that resource managers considering adopting remote sensing methods for monitoring water quality in lakes will benefit from the discussions and case studies provided in this guide. With new remote sensing systems becoming available, and constant improvements to both the hardware and software used in collecting and analyzing remotely sensed data, the potential benefits of this approach and its accessibility to agencies and organizations has never been higher. Although we emphasize that in most cases the adoption of these techniques should not be considered as a replacement for existing *in situ* lake sampling programs, they can be viable ways to extend or supplement traditional sampling programs at relatively low cost. This is particularly true when an organization can benefit from synergy in using the same resources (hardware, software, data and analyst expertise) for multiple natural resource management objectives.

Finally, we encourage lake managers and remote sensing specialists to collaborate, discuss ideas and learn from each other's fields. In the past few years, the authors of this guidance manual have led workshops on remote sensing at lake management symposia and have presented talks on lake management applications at remote sensing conferences. In the coming years, we hope and expect to see many more examples of innovative applications of remote sensing in monitoring and managing the nation's lakes.

# Remote Sensing Glossary

This glossary of remote sensing terms was compiled by Jeff Hemphill of the University of California Santa Barbara (UCSB) Geography Department and published online at the UCSB Map and Imagery Laboratory (http://www.sdc.ucsb.edu/services/rsgloss_v2.htm). Used with permission. Some revisions and alterations have been made for this version. Original sources noted at end of glossary.

## A

**absorption band** – Wavelength interval within which electromagnetic radiation is absorbed by the atmosphere or by other substances.

**advanced very high resolution radiometer (AVHRR)** – Crosstrack multispectral scanner on a NOAA polar-orbiting satellite that acquires five spectral bands of data (0.55–12.50 μm) with a ground resolution cell of 1.1 × 1.1 km.

**aerial photograph** – a photograph of the earth's surface taken (either directly downward or obliquely) from an airplane.

**airborne visible and infrared imaging spectrometer (AVIRIS)** – Experimental airborne along-track multispectral scanner under development at JPL to acquire 224 images in the spectral region from 0.4 to 2.4 μm.

**albedo (A)** – Ratio of the amount of electromagnetic energy reflected by a surface to the amount of energy incident upon it.

**altimeter** – An instrument that indicates the vertical distance above a specified datum plane.

**ancillary data** – In remote sensing, secondary data pertaining to the area or classes of interest, such as topographic, demographic or climatological data.

**angular field of view** – Angle subtended by lines from a remote sensing system to the outer margins of the strip of terrain that is viewed by the system.

**aperture** – Opening in a remote sensing system that admits electromagnetic radiation to the film in radar systems.

**apogee** – The farthest point in an elliptical orbit of a satellite from the body (*e.g.*, the earth, which it is orbiting).

**artifact** – A feature on an image produced by the optics of the system or by digital image processing, sometimes masquerading as a real feature.

**atmospheric correction** – Image-processing procedure that compensates for effects of selectively scattered light in multispectral images.

**attitude** – Angular orientation of remote sensing system with respect to a geographic reference system.

**AVHRR** – Advanced Very High Resolution Radiometer, a multispectral imaging system carried by the TIROS-NOAA series of meteorological satellites.

**AVIRIS** – Airborne visible and infrared imaging spectrometer.

## B

**background** – Area on an image or the terrain that surrounds an area of interest or a target.

**background noise** – Ambient response of the recorder or receiver, either independent of the signal or added to that signal.

**backscatter** – In radar, the portion of the microwave energy scattered by the terrain surface directly back toward the antenna.

**backscatter coefficient** – A quantitative measure of the intensity of energy returned to a radar antenna from the terrain.

**band** – A wavelength interval in the electromagnetic spectrum. For example, in Landsat images the bands designate specific wavelength intervals at which images are acquired.

**bandwidth** – The number of cycles per second between the limits of a frequency band; also the range of frequencies recorded by an antenna.

**base-height ratio** – Air base divided by aircraft height. This ratio determines vertical exaggeration on stereo models.

**beam** – A focused pulse of energy.

**beam width** – A measure of the concentration of power of a directional antenna.

## C

**calibration** – the process of quantitatively defining the system response to known, controlled signal inputs.

**C band** – Radar wavelength region from 3.75 to 7.5 cm.

**centerpoint** – The optical center of a photograph.

**charge-coupled device (CCD)** – A device in which electron are stored at the surface of a semiconductor.

**classification** – Process of assigning individual pixels of an image to categories, generally based on spectral reflectance characteristics.

**clustering** – The analysis of a set of measurements to detect their inherent tendency to form clusters in multispectral space.

**contrast enhancement** – Image-processing procedure that improves the contrast ratio of images. The original narrow range of digital values is expanded to utilize the full range of available digital values.

**contrast filter** – A color filter chosen to make a colored subject stand out sharply from surrounding objects.

**contrast ratio** – On an image, the ratio of reflectances between the brightest and darkest parts of an image.

**contrast stretching** – Expanding a measured range of digital numbers in an image to a larger range to improve the contrast of the image and its component parts.

**control point** – Any station in a horizontal and/or vertical control system that can be identified on a photograph and used for correlating the data shown on that photo.

## D

**digital image** – An image where the property being measured has been converted from a continuous range of analogue values to a range expressed by a finite number of integers, usually recorded as binary codes from 0 to 255, or as one byte.

**digital image processing** – Computer manipulation of the digital-number values of an image.

**digital number (DN)** – Value assigned to a pixel in a digital image.

**digitization** – Process of converting an analog display into a digital display.

**distortion** – On an image, changes in shape and position of objects with respect to their true shape and position.

**Doppler principle** – Describes the change in observed frequency that electromagnetic or other waves undergo as a result of the movement of the source of waves relative to the observer.

## E

**Earth Science Enterprise (ESE)** – An ongoing NASA program that will use space platforms with several multipurpose sensors to gather information about the Earth System.

**edge enhancement** – Image-processing technique that emphasizes the appearance of edges and lines.

**electromagnetic radiation (EMR)** – Energy propagated in the form of and advancing interaction between electric and magnetic fields. All electromagnetic radiation moves at the speed of light.

**electromagnetic spectrum** – Continuous sequence of electromagnetic energy arranged according to wavelength or frequency.

**element** – The smallest definable object of interest in the survey; a single item in a collection, population, or sample.

**enhancement** – Process of altering the appearance of an image so that the interpreter can extract more information.

**EROS Data Center (EDC)** – Facility of the U.S. Geological Survey at Sioux Falls, South Dakota, that archives, processes and distributes images.

## F

**false color image** – A color image where parts of the nonvisible EM spectrum are expressed as one or more of the red, green and blue components, so that the colors produced by the earth's surface do not correspond to normal visual experience. Also called a false-color composite (FCC). The most commonly seen false-color images display the very-near infrared as red, red as green, and green as blue.

**false color photograph** – Another term for IR color photograph.

**far infrared** – Extends through the thermal or emissive infrared region (5.6–1000 μm).

**feature** – Has several meanings, depending on context: (1) overall appearance; (2) a set of measurable properties diagnostic of a class or material; (3) referring to geometric or geomorphic entities, such as a hill, stream, on anything found on a natural or manmade surface.

**field of view** – The solid angle through which an instrument is sensitive to radiation.

**film** – Light-sensitive photographic emulsion and its base.

**filtering** – In analysis, the removal of certain spectral or spatial frequencies to highlight features in the remaining image.

**flight path** – Line on the ground directly beneath a remote sensing aircraft or space craft. Also called flight line.

**focal length** – In cameras, the distance from the optical center of the lens to the plane at which the image of a very distant object is brought into focus.

**Fourier Analysis** – A mathematical procedure that breaks complex sinusoidal curves into the sets of different harmonics that cause the observed variations.

## G

**gain** – Denotes an increase in signal power or amplification.

**Gaussian** – A statistical term that refers to the normal distribution of values.

**GCP** – Ground-control point: a geographic feature of known location that is recognizable on an image and can be used to determine geometrical corrections.

**geocoding** – Geographic referencing or coding of the location of data items.

**geoid** – The figure or shape of the earth as generalized by extending mean sea level continuously through the continents.

**geometric correction** – Image-processing procedure that corrects spatial distortions in an image.

**Geostationary Operational Environmental Satellite** – a NOAA satellite that acquires visible and thermal IR images for meteorologic purposes.

**geostationary orbit** – An orbit at 41,000 km in the direction of the earth's rotation, which matches speed so that a satellite remains over a fixed point on the earth's surface.

**Goddard Space Flight Center (GSFC)** – The NASA facility at Greenbelt, Maryland, that is also a Landsat ground receiving station.

**GMT** – Greenwich Mean Time. This international 24-h system is used to designate the time at which Landsat images are acquired.

**GOES** – Geostationary Operational Environmental Satellite.

**gray scale** – A sequence of gray tones ranging from black to white.

**ground-control point** – A geographic feature of known location that is recognizable on images and can be used to determine geometric corrections.

**ground receiving station** – Facility that records data transmitted by a satellite, such as Landsat.

**ground resolution cell** – Area on the terrain covered by the IFOV of a sensor.

**ground truth** – Jargon coined for data, information and observations obtained on the surface or subsurface about features or classes used to aid in interpretation of remotely sensed data; ground data is a preferred term.

**GSFC** – Goddard Space Flight Center

## H

**high-pass filter** – A spatial filter that selectively enhances contrast variations with high spatial frequencies in an image. It improves sharpness and enhances edges.

**histogram** – A means of expressing the frequency of occurrence of values in a data set within a series of equal ranges or bins; the height of each bin represents the frequency at which values in the data set fall within the chosen range. A cumulative histogram expresses the frequency of all values falling within a bin and lower in the range. A smooth curve derived mathematically from a histogram is termed the probability density function (PDF).

**hue** – In the IHS system, represents the dominant wavelength of a color.

**hyperspectral** – Refers to sensors that measure radiation in very narrow bandwidths (typically, around 0.02 μm), from which a quasi-continuous spectral curve can be produced.

## I

**IFOV** – Instantaneous field of view; solid angle through which a detector is sensitive to radiation. In a scanning system, the solid angle subtended by the detector when the scanning motion is stopped.

**IHS** – Intensity, hue and saturation system of colors.

**image** – pictorial representation of a scene recorded by a remote sensing system. Although image is a general term, it is commonly restricted to representations acquired by nonphotographic methods.

**image enhancement** – Any of a group of operations (*e.g.*, contrast stretch, spatial filtering) that improve the detectability and presentation of targets or categories in an image.

**image processing** – Encompasses all the various operations that can be applied to producing the final photographic or computer-based image rendition.

**image swath** – See ground swath.

**incidence angle** – In radar, the angle formed between an imaginary line normal to the surface and another connecting the antenna and the target.

**index of refraction (n)** – Ratio of the wavelength or velocity of electromagnetic radiation in a vacuum to that in a substance.

**infrared** – Pertaining to EMR in the 0.7–100 μm region of the spectrum.

**instantaneous field of view** – see IFOV.

**intensity** – In the IHS system, brightness ranging from black to white.

**interpretation** – The process in which a person extracts information from an image.

**interpretation key** – Characteristic or combination of characteristics that enable an interpreter to identify an object on an image.

**IR** – Infrared region of the electromagnetic spectrum that includes wavelengths from 0.7 μm to 1 mm.

## J

**Johnson Space Flight Center (JSC)** – A NASA facility in Houston, Texas, home of the manned spacecraft program.

**JPL** – Jet Propulsion Laboratory, a NASA facility at Pasadena, California, operated under contract by the California Institute of Technology.

## K

**kernel** – Two-dimensional array of digital numbers used in digital filtering.

**kinetic energy** – The ability of a moving body to do work by virtue of its motion. The molecular motion of matter is a form of kinetic energy.

**kinetic temperature** – Internal temperature of an object determined by random molecular motion. Kinetic temperature is measured with a contact thermometer.

**Kirchhoff's Law** – The radiation law which states that at a given temperature the ratio of the emissivity to the absorptivity for a given wavelength is the same for all bodies and is equal to the emissivity of an ideal blackbody at that temperature and wavelength.

**KSC** – Kennedy Space Center, NASA's main launch facility at Cape Canaveral, Florida.

## L

**Lambertian surface** – An ideal, perfectly diffusing surface, which reflects energy equally in all directions.

**large scale** – Aerial photography with a representative fraction of 1:500 to 1:10000; maps with a RF (scale) greater than 1:100000.

**L band** – Radar wavelength region from 15 to 30 cm.

**lens** – One or more pieces of glass or other transparent material shaped to form an image by refraction of light.

**lidar** – Light intensity detection and ranging, which uses lasers to stimulate fluorescence in various compounds and to measure distances to reflecting surfaces.

**light** – Electromagnetic radiation ranging from 0.4 to 0.7μm in wavelength that is detectable by the human eye.

**look angle** – The angle between the vertical plane containing a radar antenna and the direction of radar propagation. Complementary to the depression angle.

**look direction** – Direction in which pulses of microwave energy are transmitted by a radar system. The look direction is normal to the azimuth direction. Also called range direction.

**look-up table** (**LUT**) – A mathematical formula used to convert one distribution of data to another, most conveniently remembered as a conversion graph.

**low-sun-angle photograph** – Aerial photograph acquired in the morning, evening or winter when the sun is at a low elevation above the horizon.

## M

**map projection** – A systematic drawing of lines on a plane surface to represent the parallels or latitude and the meridians or longitude of the earth.

**median filter** – A spatial filter that substitutes the median value of DN from surrounding pixels for that recorded at an individual pixel; useful for removing random noise.

**medium scale** – Ranging from 1:100,000 to 1:1,000,000.

**microwave** – Region of the electromagnetic spectrum with wavelengths from 0.1 to 100 cm.

**mid-infrared** (**MIR**) – The range of EM wavelengths from 1.3 to 3.0 μm.

**Mie scattering** – The scattering of EM energy by particles in the atmosphere with comparable dimensions to the wavelength involved.

**mixed pixel** – A pixel whose DN represents the average energy reflected or emitted by several types of surface present within the area that it represents on the ground.

**mosaic** – Composite image or photograph made by piecing together individual images or photographs covering adjacent areas.

**MSS** – Multispectral scanner system of Landsat that acquires images of four wavelength bands in the visible and reflected IR regions.

**multispectral** – Refers to use of two or more bands in remote sensing.

**multispectral classification** – Identification of terrain categories by digital processing of data acquired by multispectral scanners.

**multispectral scanner** – Scanner system that simultaneously acquires images of the same scene at different wavelengths.

**multivariate analysis** – A data-analysis approach that makes use of multidimensional interrelations and correlation within the data for effective discrimination.

## N

**nadir** – Point on the ground directly in line with the remote sensing system and the center of the earth.

**NASA** – National Aeronautical and Space Administration.

**near infrared (NIR)** – The shorter wavelength range of the infrared region of the EM spectrum from 0.7 to 1.3 μm.

**near range** – Refers to the portion of a radar image closest to the aircraft or satellite flight path.

**negative photograph** – Photograph on film or paper in which the relationship between bright and dark tones is the reverse of that of the features on the terrain.

**NHAP** – National High Altitude Photography program of the U.S. Geological Survey.

**NOAA** – National Oceanic and Atmospheric Administration.

**noise** – Random or repetitive events that obscure or interfere with the desired information.

**nondirectional filter** – Mathematical filter that treats all orientations of linear features equally.

**non-selective scattering** – The scattering of EM energy by particles in the atmosphere that are much larger than the wavelengths of the energy, causing all wavelengths to be scattered equally.

**non-spectral hue** – A hue not present in the spectrum of colors produced by the analysis of white light by a prism of diffraction grating. Examples are brown, magenta and pastel shades.

**nonsystematic distortion** – Geometric irregularities on images that are not constant and cannot be predicted from the characteristics of the imaging system.

## O

**oblique photograph** – Photograph acquired with the camera intentionally directed at some angle between horizontal and vertical orientations.

**orbit** – Path of a satellite around a body, such as the earth, under the influence of gravity.

**orthophotograph** – A vertical aerial photograph with distortions due to varying elevation, tilt and surface topography removed so that it represents every object as if viewed directly from above.

**overlay** – A transparent sheet that supplements information shown on maps; a tracing of selected details on a photograph.

**overlap** – Extent to which adjacent images or photographs cover the same terrain, expressed as a percentage.

## P

**panchromatic film** – Black and white film sensitive to all visible wavelengths.

**panorama** – A photograph of a wide expanse of terrain, taken on or near the surface; a series of overlapping photographs.

**parallax** – Displacement of the position of a target in an image caused by a shift in the observation system.

**parallax difference** – The difference in the distance on overlapping vertical photographs between two points, which represent two locations on the ground with different elevations.

**parameter** – Any quantity in a problem or equation that is not an independent variable; can be assigned arbitrary values in problem solutions.

**pass** – In digital filters, refers to the spatial frequency of data transmitted by the filter. High-pass filters transmit high-frequency data; low-pass filters transmit low-frequency data.

**passive microwaves** – Radiation in the 1 mm to 1 m range emitted naturally by all materials above absolute zero.

**passive remote sensing** – Remote sensing of energy naturally reflected or radiated from the terrain.

**path-and-row index** – System for locating Landsat MSS and TM images.

**pattern** – Regular repetition of tonal variations on an image or photograph.

**P band** – A wavelength band used in radar extending from 30 cm to 1 m.

**perigee** – The orbital point nearest the body a satellite is orbiting.

**periodic line dropout** – Defect on Landsat MSS or TM images in which no data are recorded for every sixth or sixteenth scan line, causing a black line on the image.

**periodic line striping** – Defect on Landsat MSS or TM images in which every sixth or sixteenth scan line is brighter or darker than the others. Caused by the sensitivity of one detector being higher or lower than the others.

**perspective** – Representation on a plane or curved surface of objects as they appear to the eye.

**photograph** – Representation of targets on film that results from the action of light on silver halide grains in the film's emulsion.

**photographic IR** – Short-wavelength portion (0.7–0.9 μm) of the IR band detectable by IR color film or IR black-and-white film.

**photographic UV** – Long-wavelength portion of the UV band (0.3–0.4 μm) transmitted through the atmosphere and detectable by film.

**photomosaic** – Mosaic composed of photographs.

**picture element** – In a digitized image, the area on the ground represented by each digital number. Commonly contracted to pixel.

**pitch** – Rotation of an aircraft about the horizontal axis normal to its longitudinal axis that causes a nose-up or nose-down attitude.

**pixel** – Contraction of picture element; the spatial variable defines the apparent size of the resolution cell and the spectral variable defines the intensity of the spectral response (at specified wavelength[s]) for that cell.

**point spread function (PSF)** – The image of a point source of radiation, such as a star, collected by an imaging device. A measure of the spatial fidelity of the device.

**polarization** – The direction of orientation in which the electrical field vector of electromagnetic radiation vibrates.

**polar orbit** – An orbit that passes close to the poles, thereby enabling a satellite to pass over most of the surface, except the immediate vicinity of the poles themselves.

**polarized radiation** – Electromagnetic radiation in which the electrical field vector is contained in a single plane instead of having random orientation relative to the propagation vector. Most commonly refers to radar images.

**precision** – A (statistical) measure of the dispersion of the values observed when measuring a characteristic of elements in a population; a clustering of values around their average.

**primary colors** – A set of three colors that in various combinations produce the full range of colors in the visible spectrum. There are two sets of primary colors, additive and subtractive.

**principal component analysis** – The analysis of covariance in a multiple data set so that the data can be projected as additive combinations on to new axes, which express different kinds of correlation among the data.

**principal point** – Optical center of an aerial photograph.

**probability density function (PDF)** – A function indicating the relative frequency with which any measurement may be expected to occur. In remote sensing it is represented by the histogram of DN in one band for a scene.

**pushbroom system** – An imaging device consisting of a fixed linear array of many sensors that is swept across an area by the motion of the platform, thereby building up an image. It relies on sensors with nearly instantaneous response and reading so that the image swathe can be segmented into pixels representing small dimensions on the ground.

## Q

**quantization** – The process of converting from continuous values of information to a finite number of discrete values.

## R

**radar** – Acronym for radio detection and ranging. Radar is an active form of remote sensing that operates in the microwave and radio wavelength regions.

**radial relief displacement** – The tendency of vertical objects to appear to lean radially away from the center of a vertical aerial photograph. Caused by the conical field of view of the camera lens.

**radian** – Angle subtended by an arc of a circle equal in length to the radius of the circle 1 rad = 57.3º.

**radiance** – Radiant flux in power units (*e.g.*, Watts) leaving an extended source in some direction.

**radiant temperature** – Concentration of the radiant flux from a material. Radiant temperature is the kinetic temperature multiplied by the emissivity to the one-fourth power.

**raster** – The scanned and illuminated area of a video display, produced by a modulated beam of electrons sweeping the phosphorescent screen line by line from top to bottom at a regular rate of repetition.

**raster format** – A means of representing spatial data in the from of a grid of DN, each line of which can be used to modulate the lines of a video raster.

**Rayleigh scattering** – Selective scattering of light in the atmosphere by particles that are small compared with the wavelength of light.

**real time** – Refers to images or data made available for inspection simultaneously with their acquisition.

**rectification** – The process of projecting or transforming a tilted or oblique photograph onto a horizontal reference plane, the angular relation between the photograph and the plane being determined by ground reconnaissance.

**reflectance** – Ratio of the radiant energy reflected by a body to the energy incident on it. Spectral reflectance is the reflectance measured within a specific wavelength interval.

**registration** – Process of superposing two or more images or photographs so that equivalent geographic points coincide.

**relief** – Vertical irregularities of a surface; local difference in elevations.

**relief displacement** – Geometric distortion on vertical aerial photographs. The tops of objects appear in the photograph to be radially displaced from their bases outward from the photograph's centerpoint.

**remote sensing** – collection and interpretation of information about an object without being in physical contact with the object.

**resampling** – The calculation of new DN for pixels created during geometric correction of a digital scene, based on the values in the local area around the uncorrected pixels.

**resolution** – Ability to separate closely spaced objects on an image or photograph. Resolution is commonly expressed as the most closely spaced line-pairs per unit distance that can be distinguished. Also called spatial resolution.

**roughness** – In radar, the average vertical relief of a small-scale irregularities of the terrain surface. Also called surface roughness.

## S

**sample** – A subset of a population selected to obtain information concerning the characteristics of the entire population.

**saturation** – In the IHS system, represents the purity of color. Saturation is also the condition where energy flux exceeds the sensitivity range of a detector.

**scale** – Ratio of distance on an image to the equivalent distance on the ground.

**scan line** – Narrow strip on the ground that is swept by IFOV of a detector in a scanning system.

**scanner** – An imaging system in which the IFOV of one or more detectors is swept across the terrain.

**scanner distortion** – Geometric distortion characteristic of cross-track scanner images.

**scattering** – Multiple reflections of electromagnetic waves by particles in the atmosphere or from surfaces.

**sensor** – Device that receives electromagnetic radiation and converts it into a signal that can be recorded and displayed as either numerical data or an image.

**sidelap** – Extent of lateral overlap between images acquired on adjacent flight lines.

**side-looking airborne radar (SLAR)** – An airborne side scanning system for acquiring radar images.

**signal** – Information recorded by a remote sensing system; the effect of a pulse of EMR conveyed over a communication path onto a sensor.

**signal to noise radio (S/N)** – The ratio of the level of the signal carrying real information to that carrying spurious information as a result of defects in the system.

**signature** – Any characteristic or series of characteristics by which a material or object may be recognized in an image, photo or data set.

**SLAR** – Side-looking airborne radar.

**small-scale** – For aerial photos, those with a representative fraction smaller than 1:40,000; for maps, RF less than 1:1,000,000.

**smoothing** – The averaging of densities in adjacent areas to produce more gradual transitions.

**spectral band** – An interval in the electromagnetic spectrum defined by two end wavelengths.

**spectral hue** – A hue present in the spectral range of white light analyzed by a prism or diffraction grating.

**spectral interval** – The width, generally expressed as wavelength or frequency, of a particular portion of the EM spectrum.

**spectral reflectance** – Reflectance of electromagnetic energy at specified wavelength intervals.

**spectral sensitivity** – Response, or sensitivity, of a film or detector to radiation in different spectral regions (designated ranges of wavelengths).

**spectral signature** – Quantitative measurement of the properties of an object or material over one to several wavelength intervals; the diagnostic spectral response for that entity.

**spectral vegetation index** – An index of relative amount and vigor of vegetation. The index is calculated from two spectral bands of AVHRR imagery.

**spectrometer** – Device for measuring intensity of radiation absorbed or reflected by a materiel as a function of wavelength.

**spectrum** – Continuous sequence of electromagnetic energy arranged according to wavelength or frequency.

**SPOT** – Systeme Probatoire d'Observation del la Terre. Unmanned French remote sensing satellite orbiting in the late 1980s.

**Stefan-Boltzmann constant** – $5.68 \times 10^{-12}$ W cm$^{-2}$ K$^{-4}$; appropriate to Law of Stefan-Boltzmann stating that the amount of energy radiated per unit time from a unit surface of an ideal black body is proportional to the fourth power of the absolute temperature (in units of K) of that body.

**stereo base** – Distance between a pair of correlative points on a stereo pair that are oriented for stereo viewing.

**stereo pair** – Two overlapping images or photographs that may be viewed stereoscopically.

**subscene** – A portion of an image used for detailed analysis.

**subtractive primary colors** – Yellow, magenta, and cyan. When used as filters for white light, these colors remove blue, green and red light, respectively.

**sun-synchronous** – Earth satellite orbit in which the orbit plane is nearly polar and the altitude is such that the satellite passes over all places on earth having the same latitude twice daily at the same local sun time.

**supervised classification** – Digital-information extraction technique in which the operator provides training-site information that the computer uses to assign pixels to categories.

**swath width** – The overall plane angle or linear ground distance covered by a scanner in the across-track dimension.

**synchronous satellite** – An equatorial west to east satellite orbiting the earth at 34,900 km, an altitude resulting in one revolution in 24 h, synchronous with the earth's rotation.

**synoptic view** – The ability to see or otherwise measure widely dispersed areas at the same time and under the same conditions.

**systematic distortion** – Geometric irregularities on images that are caused by known and predictable characteristics.

## T

**terrain** – Surface of the earth.

**texture** – Frequency of change and arrangement of tones on an image.

**thematic map** – A map designed to demonstrate particular features or concepts.

**Thematic Mapper (TM)** – A cross-track scanner deployed on Landsat that records seven bands of data from the visible through the thermal IR regions.

**thermal band** – Generally refers to thermal IR intervals associated with atmospheric windows, at 3–5 and 8–14 μm wavelengths.

**thermal IR** – Generally, the IR region from 3 to 1000 μm; specifically connotes the two intervals employed in remote sensing (3–5 and 8–14 μm) This spectral region spans the radiant power peak of the earth.

**tie-point** – A point on the ground that is common to two images. Several are used in the co-registration of images.

**tilt** – The angle between the optic axis of the camera or sensor and the plumb line to a given photo or image.

**tone** – Each distinguishable shade of gray from white to black on an image.

**topographic inversion** – An optical illusion that may occur on images with extensive shades. Ridges appear to be valleys, and valleys appear to be ridges. The illusion is corrected by orienting the image so that the shadows trend from the top margin of the image to the bottom.

**topographic reversal** – A geomorphic phenomenon in which topographic lows coincide with structural highs and vice versa. Valleys are eroded on crests of anticlines to cause topographic lows, and synclines form ridge, or topographic highs.

**tracking** – The process of following the movement of a satellite or rocket by radar, radio or photographic observations.

**training site** – Area of terrain with known properties or characteristics; used in supervised classification.

**transmissivity** – Property of a material that determines the amount of energy that can pass through the material.

**transmittance** – The ratio of the radiant energy transmitted through a body to that incident upon it.

**transparency** – Image on a transparent photographic material, normally a positive image.

## U

**uncontrolled mosaic** – A mosaic made without correction for any type of distortion.

**unsupervised classification** – Digital information extraction technique in which the computer assigns pixels to categories with no instructions from the operator.

**UV** – Ultraviolet region of the electromagnetic spectrum ranging in wavelengths from 0.01 to 0.4 m.

## V

**Validation** – The process of assessing by independent means the quality of the data products derived from the system outputs.

**Vandenberg AFB** – Military and civilian rocket launch facilities, including the Landsats.

**variance** – A measure of the dispersion of the actual values of a variable about its mean. It is the mean of the squares of all the deviations from the mean value of a range of data.

**vector format** – The expression of points, lines and areas on a map by digitized Cartesian coordinates, directions and values.

**Verification** – The process of proving that the system performance is within specification.

**vertical exaggeration** – In a stereo model, the extent to which the vertical scale appears larger than the horizontal scale.

**volume scattering** – In radar, interaction between electromagnetic radiation and the interior of a material.

## W

**wavelength** – Distance between successive wave crests or other equivalent points in a harmonic wave.

**window** – A band of EMR that offers maximum obtainable transmission and minimal attenuation through a particular medium with use of a specific sensor; wavelengths of optimum sensing.

## X

**X band** – Radar wavelength region from 2.4 to 3.75 cm.

## Y

**yaw** – Rotation of an aircraft about its vertical axis so that the longitudinal axis deviates left or right from the flight line.

## Sources

Jeff Hemphill, Remote Sensing Research Unit, UCSB, web site for the class, Aerial Photogrammetry.

ERS-1 Calibration and Validation, ESA bulletin no 65, February 1991, by E. Attema and R. Francis.

Manual of Remote Sensing, Leonard Bowden, American Society Photogrammetry and Remote Sensing, Falls Church VA, copyright 1975.

# Appendix A. Remotely sensed spectra and bio-optical properties of lakes

## A.1. Chlorophyll concentration retrieval

A central concept in remote sensing is "spectral signature". This term has been defined in different ways by various authors, but it essentially involves recording and identifying a set of repeatable spectral characteristics for individual targets and materials. Spectra generated for particular water quality conditions, therefore, could be construed as depicting the spectral signature for a mix of components that interact with light; the so-called optically active constituents, including phytoplankton pigments (chlorophylls, carotenoids, phycocyanin and others); colored dissolved organic matter (CDOM); inorganic and non-living organic suspended matter; and pure water itself. While remote sensing scientists often apply the concept of spectral signature to data collected by multispectral sensors with limited numbers of spectral bands, we focus on sensors that measure reflectance in hundreds or even thousands of individual narrow wavelengths of light. As an example, the Ocean Optics spectroradiometer system, described in Chapter 2, generates more than 2,000 discrete channels of information.

Of particular interest are the specific wavelengths where pigments and other suspended materials absorb. It is useful to employ the reciprocal of reflectance, which is related directly to the total absorption coefficient of all constituents in a water column:

$$R^{-1} \propto \frac{(a + b_b)}{b_b} \qquad \text{[Eq. A.1]}$$

where $a$ and $b_b$ are total absorption and backscattering coefficients of all constituents and pure water, respectively. Several distinct features of reciprocal reflectance (Fig. A.1, upper panel) and reflectance (Fig. A.1, lower panel) show: (1) high reciprocal reflectance in the blue range due to the blue chl-*a* absorption maximum, absorption by colored dissolved organic matter (CDOM), and tripton (Chl, CDOM, tripton in Fig. A.1); (2) a trough in the green range near 550–570 nm (B in Fig. A.1) due to the minimal absorption of all algal pigments; scattering by inorganic suspended matter and phytoplankton cells control the magnitude of reflectance in this range; (3) a peak near 625 nm due to phycocyanin absorption (PC in Fig. A.1) that typically covaries with cyanobacterial abundance and seasonality; (4) a peak at 670–680 nm corresponding to the *in situ* red chl-*a* absorption maximum (chl-*a* in Fig. A.1); and (5) a minimum in the range near 700 nm (A in Fig. A.1).

In the blue spectral range between 400 and 500 nm, chlorophyll *a* (chl-*a*) and carotenoids strongly absorb light (Fig. A.1). Thus, in the reflectance spectra (Fig. A.2), the minimum near 440 nm corresponds to chl-*a* absorption and is almost indistinct, while the reflectance in the 400–500 nm range is low with no pronounced spectral features over a broad range of turbidity and phytoplankton densities. Absorption by dissolved organic matter, tripton, and scattering by particulate matter all contribute to reflectance in the 400–500 nm range, and a common characteristic of reflectance spectra in this range is a general low sensitivity of reflectance to chl-*a*. As a result, the blue to green ratio R440/R550 (Gordon and Morel 1983) widely employed for chl-*a* retrieval in oceanic waters is not suitable for estimating chl-*a* in inland waters.

Although chl-*a* absorbs red light, the magnitude of reflectance at 670 nm, corresponding to the red chl-*a* absorption peak, is poorly correlated with chl-*a* concentration (*e.g.*, Gitelson *et al.* 2007). Previous studies have shown that, in addition to chl-*a* concentration, reflectance in productive turbid waters was strongly affected by nonorganic suspended matter concentration (Gitelson and Kondratyev 1991, Dekker 1993, Yacobi *et al.* 1995, Gitelson *et*

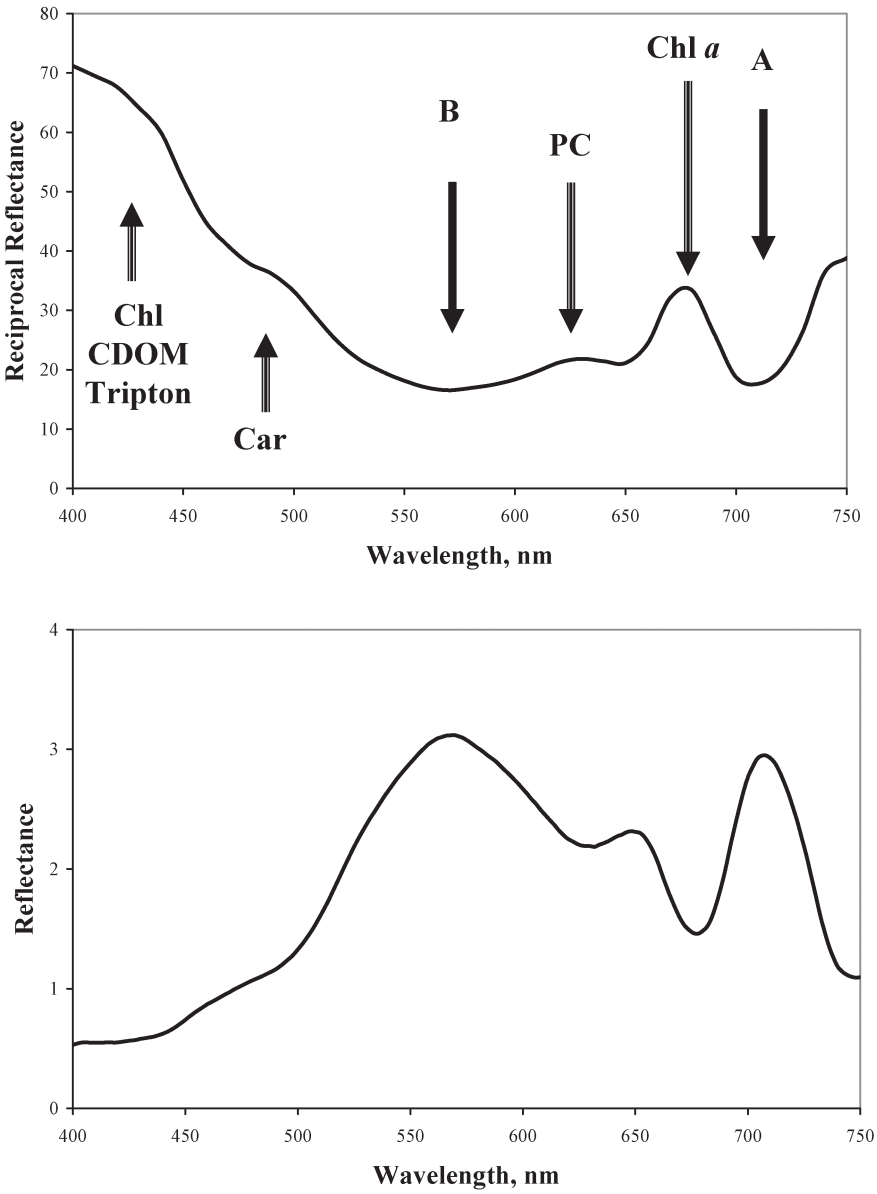


**Figure A.1.** Typical reciprocal reflectance (upper panel) and reflectance (lower panel) spectra of inland waters. Chl, CDOM, Tripton = maximal absorption by all chlorophyll (isoforms) present as well as absorption by colored dissolved organic matter and tripton; Car = maximal absorption by carotenoids; PC = maximal absorption by phycocyanin; A = the position of minimum absorption by chlorophyll *a*, inorganic suspended matter and water; B = minimal absorption by phytoplankton pigments; chl-*a* = maximal absorption by chlorophyll *a*.

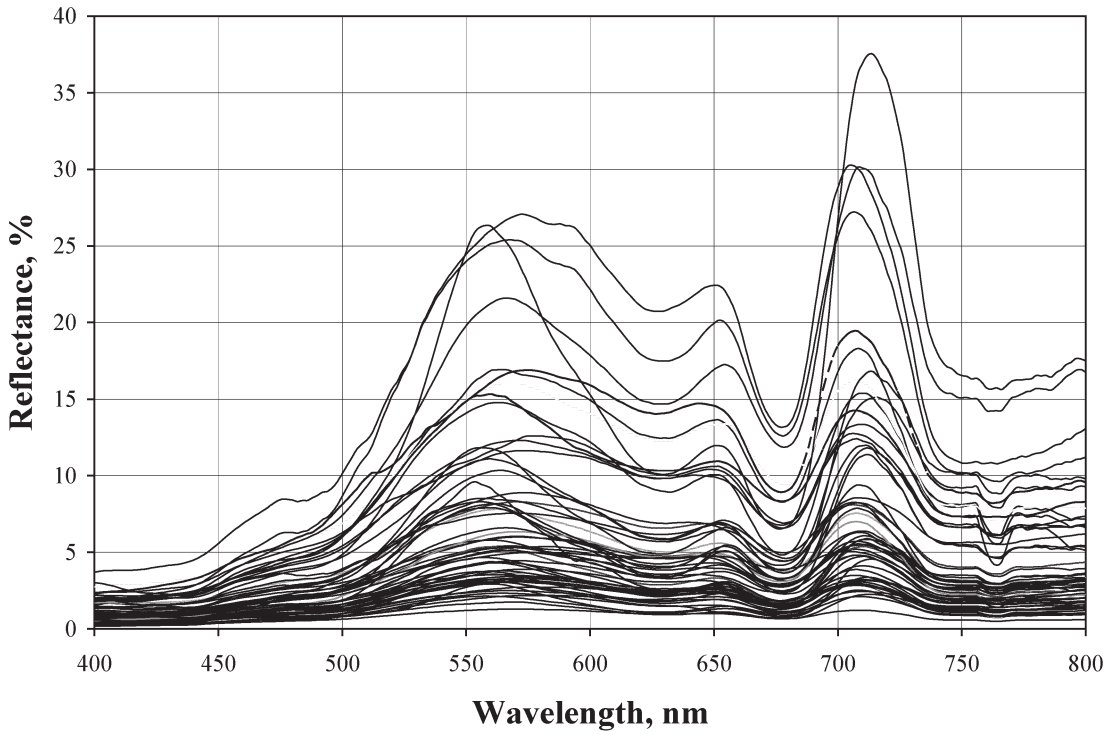


**Figure A.2.** Reflectance spectra of inland waters.

*al*. 2007). The effect of chl-*a* absorption on reflectance is reduced by light-scattering from phytoplankton cell walls and inorganic suspended matter; the concentrations of these constituents are poorly co-related.

Thus, to accurately retrieve chl-*a* from reflectance data, it is critical to subtract the effects of other factors on reflectance around 670 nm. To remove these factors, we recommend an approach based on a conceptual model developed and used to estimate pigment concentration in aquatic and terrestrial vegetation (Gitelson *et al*. 2003; Dall'Olmo *et al*. 2003):

$$\textit{Pigment concentration} \propto [R^{-1}(\lambda_1) - R^{-1}(\lambda_2)] \times R(\lambda_3) \qquad \text{[Eq. A.2]}$$

where $R^{-1}(\lambda_1)$ and $R^{-1}(\lambda 2)$ are reciprocal reflectances at wavelengths $\lambda_1$ and $\lambda_2$, and $R(\lambda_3)$ is reflectance at wavelength $\lambda_3$. Note that $\lambda_1$ is a spectral region such that $R^{-1}(\lambda_1)$ is maximally sensitive to the absorption by the pigment of interest, although it is still affected by the absorption of other pigments and scattering by all particulate matter, while $\lambda_2$ is a spectral region such that $R^{-1}(\lambda_2)$ is minimally sensitive to the absorption by the pigment of interest, and maximally sensitive to the absorption by other constituents. Absorption by other constituents at $\lambda_2$ is assumed to be close to that at $\lambda_1$. Thus, the difference $[R^{-1}(\lambda_1) - R^{-1}(\lambda_2)]$ is related to the concentration of a pigment of interest. However, it is still affected by the variability in scattering by the medium (Gitelson *et al*. 2003; Dall'Olmo *et al*. 2003; Dall'Olmo and Gitelson 2005). Wavelength range $\lambda_3$ is a spectral region where reflectance is minimally affected by the absorption of pigments and is therefore used to account for the variability in scattering between samples. Optimal spectral bands are (Dall'Olmo and Gitelson 2005, Gitelson *et al*. 2007; 2008):

Band 1 ($\lambda_1$) = 665–675 nm
Band 2 ($\lambda_2$) = 705–725 nm
Band 3 ($\lambda_3$) = 730–755 nm

## A.2. Suspended matter concentration retrieval

Numerous techniques for retrieval of the total suspended matter concentration in a column of water have been developed (*e.g.*, Curran and Novo 1988, Ritchie and Cooper, 1991). Using Landsat MSS imagery, Ritchie and Cooper (1991) showed that the ratio of reflectances in the range 500–600 nm to that in the band 600–700 nm is a proxy for suspended sediments in turbid waters. Gitelson and Kondratyev (1991) suggested using spectral channels in the ratios $R_{(600–700)}/R_{(700–800)}$ and/or $R_{(520-600)}/R_{(760–900)}$ for retrieval of suspended matter concentrations in rivers and reservoirs. Doxaran *et al*. (2002, 2005) established empirical relationships between reflectance ratios in the near infrared (850 nm) and visible wavelengths (550 or 650 nm) and total suspended matter concentration.

## A.3. References

Curran, P.J. and E.M.M. Novo. 1988. The relationship between suspended sediment concentration and remotely sensed spectral radiance: A review. J. Coast.al Res. 4:351-368.

Dall'Olmo, G. and A.A. Gitelson. 2005. Effect of bio-optical parameter variability on the remote estimation of chlorophyll *a* concentration in turbid productive waters: experimental results. Appl. Opt. 44:412-422 (see also Erratum Appl. Opt. 44(16):3342).

Dekker, A. 1993. Detection of the optical water quality parameters for eutrophic waters by high resolution remote sensing. Ph.D. dissertation. Free University, Amsterdam, The Netherlands.

Doxaran, D., J.M. Froidefond and P. Castaing. 2002. A reflectance band ratio used to estimate suspended matter concentrations in coastal sediment-dominated waters. Int. J. Remote Sens. 23:5079-5085.

Doxaran, D.R., C.N. Cherukuru and S.J. Lavender. 2005. Use of reflectance band ratios to estimate suspended and dissolved matter concentrations in estuarine waters. Int. J. Remote Sens. 26:763-1769.

Gitelson, A.A. and K.Y. Kondratyev. 1991. Optical models of mesotrophic and eutrophic water bodies. Int. J. Remote Sens. 12:373-385.

Gitelson, A.A., U. Gritz and M.N. Merzlyak. 2003. Relationships between leaf chlorophyll content and spectral reflectance and algorithms for non-destructive chlorophyll assessment in higher plant leaves. J Plant Physiol. 160:271-282.

Gitelson, A.A., J.F. Schalles and C.M. Hladik. 2007. Remote chlorophyll *a* retrieval in turbid, productive estuaries: Chesapeake Bay case study. Remote Sens. Environ. 109:464-472.

Gitelson, A.A., G. Dall'Olmo, W. Moses, D.C. Rundquist, T. Barrow, T.R. Fisher, D. Gurlin and J. Holz. 2008. A simple semi-analytical model for remote estimation of chlorophyll *a* in turbid waters: Validation. Remote Sens. Environ. 112:3582–3593, doi:10.1016/j.rse.2008.04.015.

Gordon, H. and A. Morel. 1983. Remote assessment of ocean color for interpretation of satellite visible imagery. A review. Lecture notes on Coastal and Estuarine Studies 4. Springer-Verlag.

Ritchie, J.C. and C.M. Cooper. 1991. An algorithm for using Landsat MSS for estimating surface suspended sediments. Water Resour. Bull. 27:373 379.

Yacobi, Y.Z., A.A. Gitelson and M. Mayo. 1995. Remote sensing of chlorophyll in Lake Kinneret using high spectral resolution radiometer and Landsat TM: Spectral features of reflectance and algorithm development. J. Plankton Res. 17:2155-2173.

# Appendix B. The CDAP software package for field spectroradiometry

The CDAP (CALMIT Data Acquisition Program) system (Fig. B.1) was developed at the University of Nebraska-Lincoln's Center for Advanced Land Management Information Technologies (CALMIT), for analysis of high-spectral resolution data from field spectroradiometers.

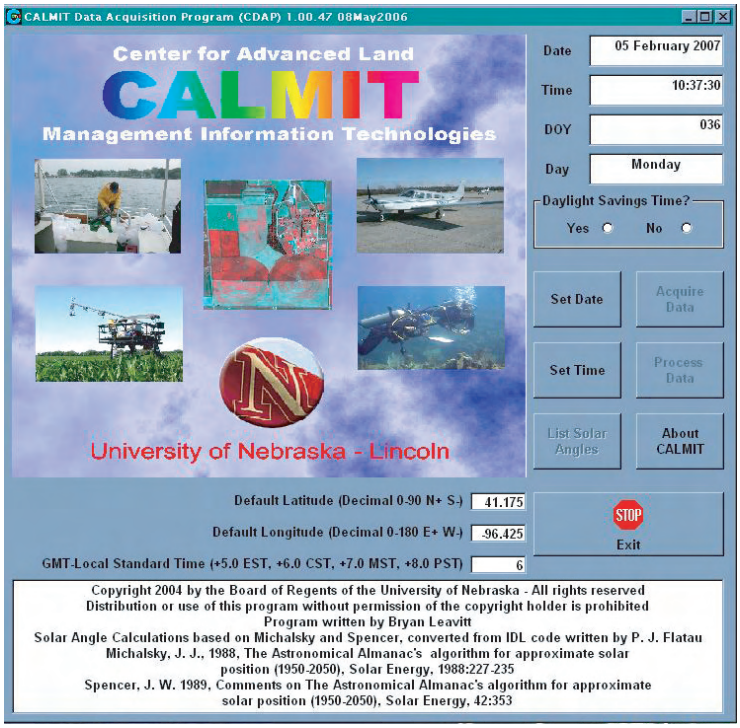


**Figure B.1.** CDAP start-up screen.

CDAP was developed by and for scientists performing remote sensing observations. It is designed to configure, calibrate and operate single or dual-head Ocean Optics hyperspectral radiometers and to simultaneously collect data from dataloggers, digital still cameras and GPS systems. A post-processing mode uses calibration information to calculate reflectance. Radiance and irradiance measurements can also be corrected given user-supplied calibration data. Raw and derived data are written to tab-delimited text files which can, in turn, be easily imported into a spreadsheet or statistical analysis program.

A dual-headed sensor configuration with simultaneous upwelling radiance and downwelling irradiance measurement permits the determination of reflectance under highly variable, nonoptimal lighting and atmospheric conditions. The CDAP software is specifically capable of handling data acquisition and processing for this mode of operation.

## B.1. CDAP Features

- Integrated hyperspectral and ancillary instrument control, data collection and post-processing
- Sets appropriate operating parameters for and collects data from hyperspectral sensors

  - Currently operates with Ocean Optics USB 2000, SD 2000 and USB 4000 instruments; the system can also operate the Spectron SE 590 hyperspectral sensor
  - Integration time is optimized based on actual presample measurements
  - Equipped to process "dual-headed" instruments measuring upwelling radiance and downwelling irradiance simultaneously
  - RS-232 interface allows 100+ ft separation from computer
- Collects datalogger output such as IR temperature
- Position and time-tags using external GPS data
- Automatic data correction for instrument calibration
- Handles single and dual headed spectral observations
  - Automatically produces calibrated reflectance data
- Collects images synchronized to data scans from compatible Olympus USB digital cameras
- Post-processes collected data to create text files containing upwelling and downwelling measurements and derived reflectance.
  - Produces tab-delimited text files easily imported into other software
  - Entire directory of raw data processed automatically
  - No limit on number of files processed
- Extensive logging to facilitate trouble-shooting or instrument configuration confirmation
- Specialized software modifications and incorporation of other sensors or equipment at customer expense can be considered

## B.2. Examples of CDAP screens

Figures B.2-B.10 are examples of CDAP screens showing the capabilities of the program to verify and analyze the data as it is being collected.

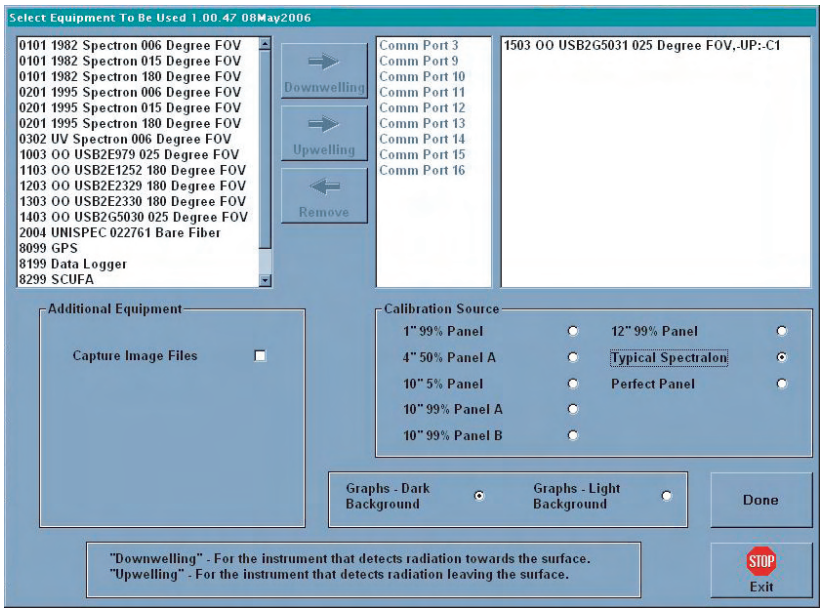


**Figure B.2.** Equipment configuration screen. Establishes which instruments are available and how they are connected to the computer.

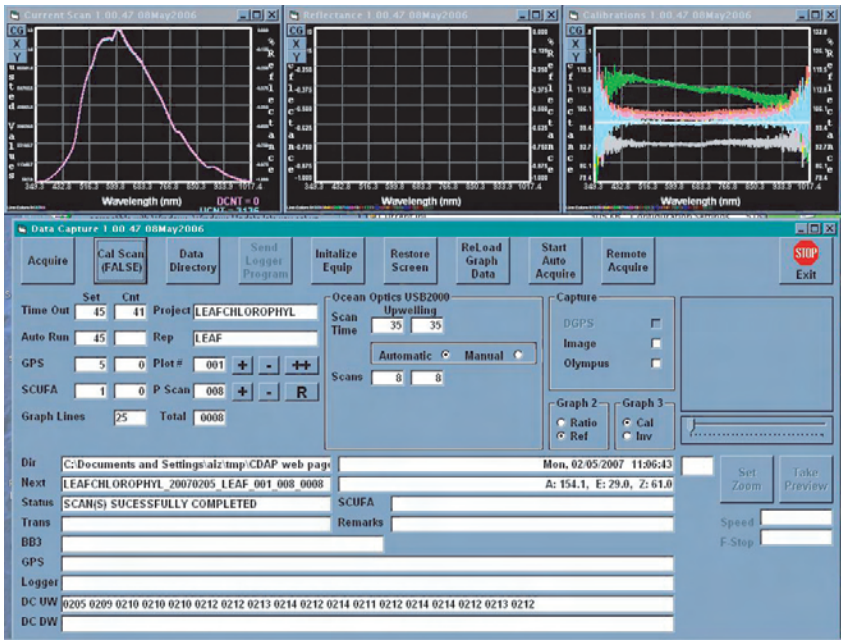


**Figure B.3.** Calibration screen. Provides data showing instrument response to measurement of white reference panel during instrument calibration (left panel) and its reflectance (right panel).

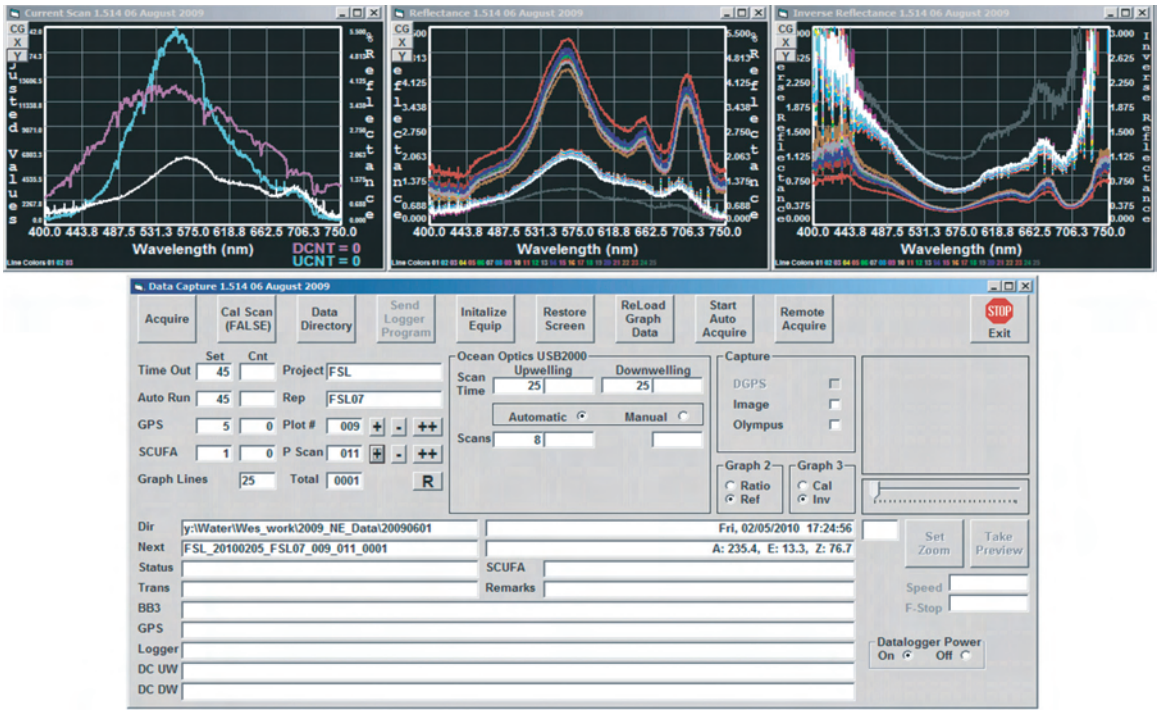


**Figure B.4.** Data collection screen. Fields provided show Ocean Optics operating conditions, data from a GPS, datalogger, and other information. Graphs provide real-time measured upwelling radiance of reflectance panel, raw reflectance and calibrated reflectance (left panel); calibrated reflectances (central panel); and reciprocal of reflectance (right panel).

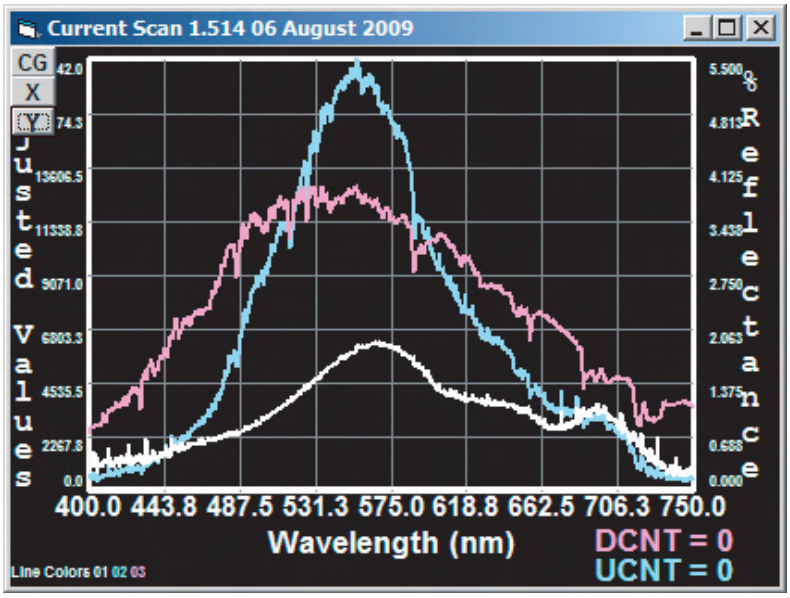


**Figure B.5.** Current scan graph. Shows response from white reference panel (magenta), raw reflectance (green) and calibrated reflectance (white). Note: all graphs can be magnified to full screen.

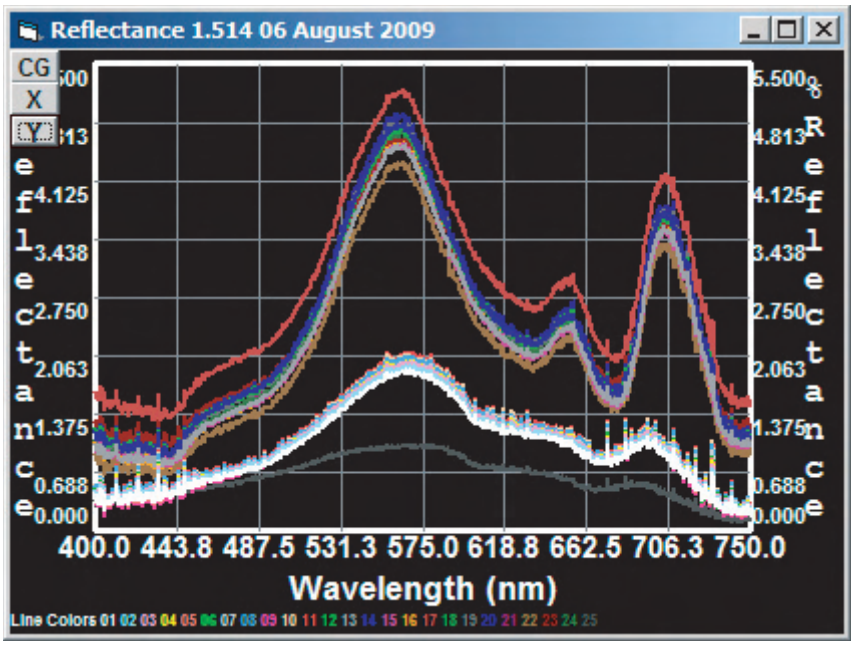


**Figure B.6.** Calculated reflectance graph. Traces are color-coded by age of scan; most recent scan is white.

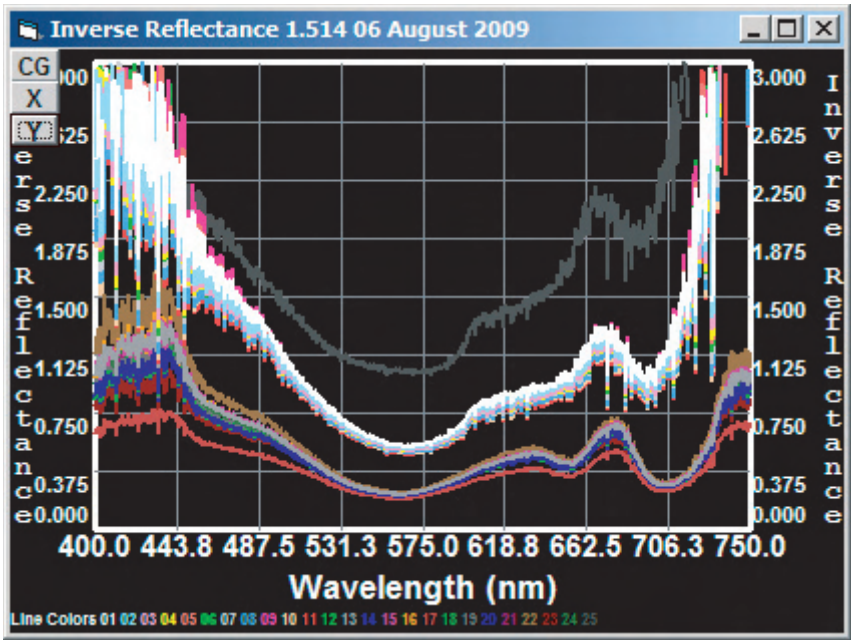


**Figure B.7.** Calculated inverse reflectance graph. Trace colors correspond to those in Fig. B.6.

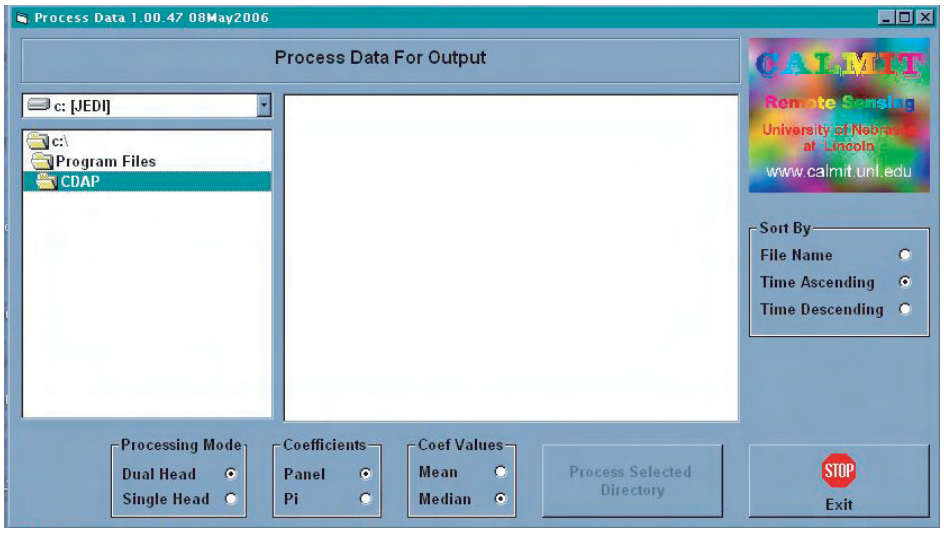


**Figure B.8.** Post-processing set-up screen. Indicates the source directory for data and required parameters. CDAP will automatically process all raw data in the directory. During processing reflectance, upwelling radiance and downwelling irradiance are retrieved and are written to tab-delimited text files that can be imported into an Excel spreadsheet.

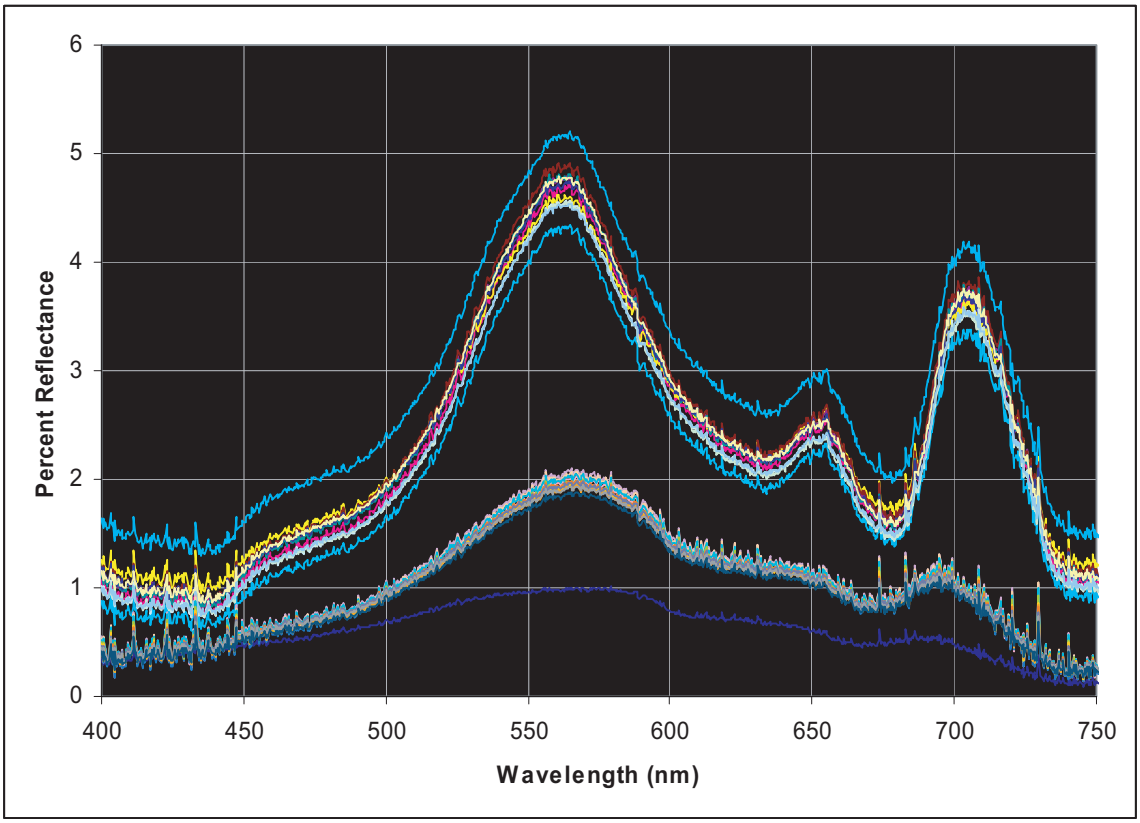


**Figure B.9.** Post-processed reflectance for waters studied. Data were exported from CDAP as text files and imported into an Excel spreadsheet for analysis.

# Appendix C. Processing AISA Eagle airborne hyperspectral imagery

## C.1. Level 1 data processing

Raw AISA Eagle data consist of raw digital numbers from the AISA sensor, aircraft location and attitude information collected synchronously for each pixel in the image. The raw image data are a combination of two separate datasets: an irradiance value (downwelling solar radiation) and radiance (upwelling reflected radiation from the surface).

In the raw image (Fig. C.1) the irradiance data can be identified as the dark band at the top of the image.

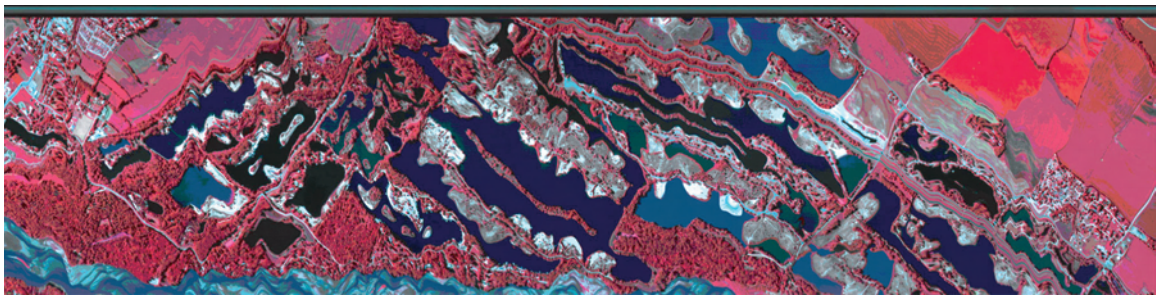

**Figure C.1.** Raw AISA image.

The ratio of radiance to irradiance is commonly referred to as reflectance. This ratio is an indication of how the individual targets interacted with the incoming light, by absorbing or reflecting particular wavelengths. When working with the standard reflectance product generated in Level 1 processing, users need to bear in mind that the reflectance was calculated "at-platform" and does not include corrections for atmospheric conditions between the aircraft and the surface.

Much of the remotely sensed imagery from satellites is radiance data rather than reflectance; exceptions are MODIS and MERIS surface reflectance data. If a project involves direct comparisons between radiance satellite imagery and airborne AISA imagery, a radiance product should be requested.

Aircraft position and attitude information are collected synchronously with the raw AISA image by a C-Migits III™ (CM-III) unit, manufactured by Systron-Donner (Fig. C.2). The CM-III is a combination Global Positioning System and an Inertial Navigation System (GPS/INS) sensor connected to the AISA sensor. The GPS part of the system provides latitude, longitude, altitude and time. The INS part system provides information related to the aircraft's attitude (roll, pitch and yaw). The raw CM-III data are stored in ASCI format.

A proprietary software package, CaliGeo, is used to pre-process AISA-Eagle data.

### Preprocessing

Preprocessing of the data involves adjustment of the raw radiance/irradiance values to account for (1) the known variability of the sensor, and (2) any stray radiation that may be present inside the instrument. This preprocessing is commonly referred to as radiometric correction.

Radiometric calibration data are provided by SPECIM, the Finland-based company that produces the sensor. The University of Nebraska-Lincoln's Center for Advanced Land Management Information Technologies (CALMIT)

**Figure C.2.** C-Midgets III Inertial Motion Unit.

supports a calibration facility with a National Institute of Standards and Technology NIST traceable power supply, light source and integrating sphere (URS-600) manufactured by LabSphere (Fig. C.3). Stability of the AISA sensor is recalibrated against the original calibration supplied by SPECIM at least twice per year to ensure the instrument stability. New calibration coefficients can be generated if necessary. To date, the instrument has demonstrated no variability from the original calibration provided by SPECIM.

**Figure C.3.** Labsphere URS-600, NIST traceable power supply, light source and integrating sphere.

During the preprocessing phase, these data are written to a text file used to assign spatial reference information to the individual pixels during the georectification phase of Level 1 processing.

### Step 1 processing

End products of the Level 1 image processing procedures are rectified radiance or rectified reflectance products, depending on the end-user's choice. Intermediate products produced in this step include map location, global look-up table (GLT), unrectified radiance or reflectance and irradiance data. The term unrectified means that the spatial component is not associated with the individual pixels. In this situation, the spatial component(s) are written to a GLT file that can be used to georeference the data at a later time. These intermediate data are saved and are available for use in the development of Level 2 and/or Level 3 data products.

### Step 2 rectification

The steps in the development of the basic Level 1 image products are presented in the diagram (Fig. C.4).

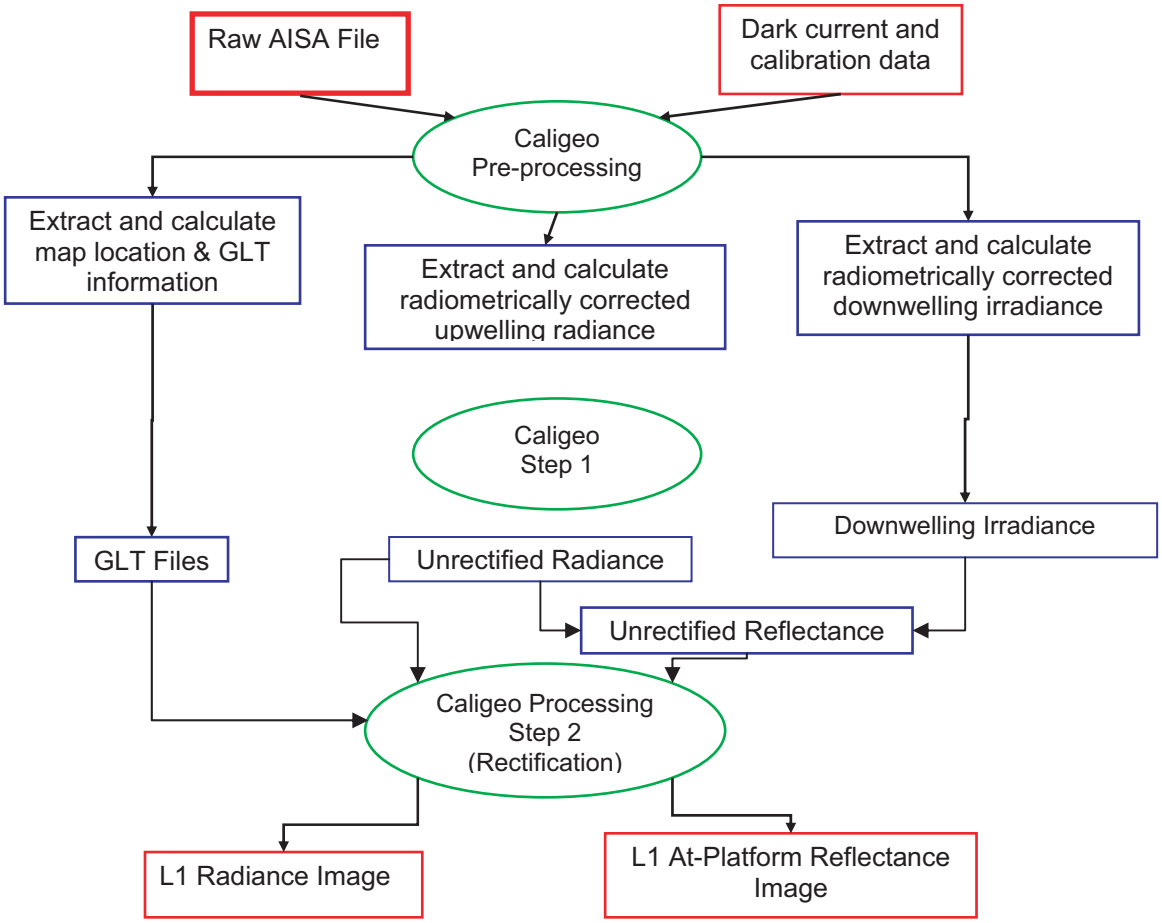


**Figure C.4.** Level 1 AISA Processing Stream.

During the rectification process, each pixel of either the unrectified radiance or the unrectified reflectance product is assigned spatial coordinates contained in the GLT.

An example of the output from Level 1 processing of AISA Eagle imagery (Fig. C.5 and C.6) identifies a water pixel (Fig. C.5, yellow arrow) from a spectral profile (Fig. C.6). The user of this product must bear in mind that the reflectance values of imagery produced by Level 1 processing are calculated as at-platform. Reflectance levels Chlorophyll absorption is evident by the "trough" at around 680 nm (Fig. C.6).

Example: Fig. C.5 is a Level 1 processed of AISA Eagle image. Fig.C.6 is a spectral profile collected from a water pixel in the image.(Fig. C.5, yellow arrow).

**Figure C.5.** Rectified reflectance image.

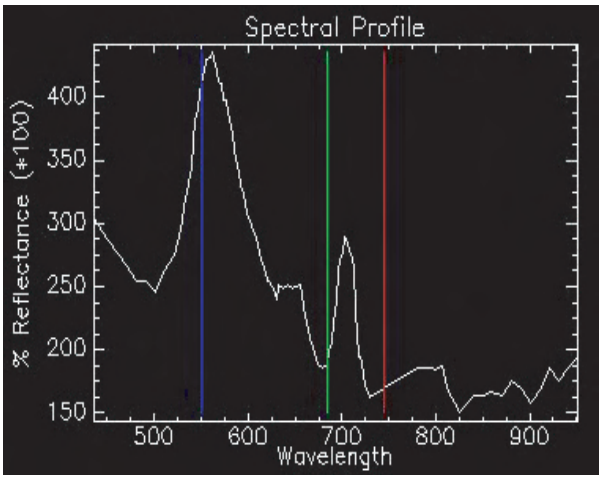


**Figure C.6.** Spectral reflectance graph.

## C.2. Level 2 processing

### Atmospheric correction

The ENVI FLAASH module is used to atmospherically correct (remove atmospheric effects) the Level 1 data when requested. The resulting reflectance image represents canopy/surface level reflectance.

A comparison of the spectral curves in Figures C.6 and C.7 demonstrates the effect of the atmospheric corrections applied to the imagery.

At this point, the data have been prepared for any additional processing that may be required to complete the objectives of the specific project.

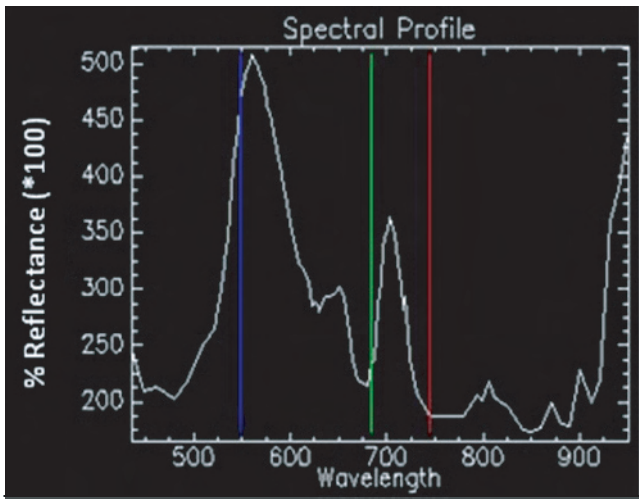


**Figure C.7.** Atmospherically corrected spectral reflectance profile.

# Appendix D. Recommended AISA Eagle band centers for aquatic targets (97 bands)

| Band # | Band center (nm) | Band width (nm) |
|---|---|---|
| 1 | 950.39 | 9.64 |
| 2 | 940.77 | 9.64 |
| 3 | 931.14 | 9.64 |
| 4 | 921.52 | 9.64 |
| 5 | 911.90 | 9.61 |
| 6 | 899.92 | 9.61 |
| 7 | 890.34 | 9.60 |
| 8 | 880.76 | 9.60 |
| 9 | 871.18 | 9.60 |
| 10 | 859.20 | 9.60 |
| 11 | 849.62 | 9.60 |
| 12 | 840.03 | 9.60 |
| 13 | 830.45 | 9.60 |
| 14 | 818.45 | 9.60 |
| 15 | 806.44 | 9.60 |
| 16 | 794.43 | 9.60 |
| 17 | 780.01 | 9.60 |
| 18 | 744.10 | 9.44 |
| 19 | 733.49 | 2.36 |
| 20 | 728.77 | 2.36 |
| 21 | 724.06 | 2.36 |
| 22 | 721.70 | 2.36 |
| 23 | 719.34 | 2.36 |
| 24 | 716.99 | 2.36 |
| 25 | 714.63 | 2.36 |
| 26 | 712.27 | 2.36 |
| 27 | 709.92 | 2.36 |
| 28 | 707.56 | 2.36 |
| 29 | 705.20 | 2.36 |
| 30 | 702.84 | 2.36 |
| 31 | 700.49 | 2.36 |
| 32 | 698.13 | 2.36 |
| 33 | 695.78 | 2.35 |
| 34 | 693.42 | 2.35 |
| 35 | 691.07 | 2.35 |
| 36 | 688.72 | 2.35 |
| 37 | 686.37 | 2.35 |
| 38 | 684.02 | 2.35 |
| 39 | 679.32 | 2.35 |
| 40 | 674.62 | 2.35 |
| 41 | 669.92 | 2.35 |
| 42 | 665.22 | 2.35 |
| 43 | 660.52 | 2.35 |
| 44 | 655.82 | 2.35 |
| 45 | 651.12 | 2.35 |
| 46 | 646.42 | 2.35 |
| 47 | 641.72 | 2.35 |
| 48 | 637.01 | 2.35 |
| 49 | 632.31 | 2.35 |
| 50 | 629.96 | 2.35 |
| 51 | 627.61 | 2.35 |
| 52 | 625.26 | 2.35 |
| 53 | 622.91 | 2.35 |
| 54 | 620.56 | 2.35 |
| 55 | 618.21 | 2.35 |
| 56 | 613.51 | 2.35 |
| 57 | 608.81 | 2.35 |
| 58 | 604.11 | 2.35 |
| 59 | 599.41 | 2.35 |
| 60 | 597.06 | 2.35 |
| 61 | 594.71 | 2.35 |
| 62 | 592.36 | 2.35 |
| 63 | 590.01 | 2.35 |
| 64 | 587.66 | 2.35 |
| 65 | 585.30 | 2.35 |
| 66 | 582.95 | 2.35 |
| 67 | 580.60 | 2.35 |
| 68 | 578.26 | 2.34 |
| 69 | 575.93 | 2.32 |
| 70 | 573.61 | 2.32 |
| 71 | 571.29 | 2.32 |
| 72 | 568.97 | 2.32 |
| 73 | 566.65 | 2.32 |
| 74 | 564.33 | 2.32 |
| 75 | 562.01 | 2.32 |
| 76 | 559.69 | 2.32 |
| 77 | 557.37 | 2.32 |
| 78 | 555.05 | 2.32 |
| 79 | 552.73 | 2.32 |
| 80 | 550.41 | 2.32 |
| 81 | 548.09 | 2.32 |
| 82 | 545.79 | 2.28 |
| 83 | 543.52 | 2.26 |
| 84 | 541.26 | 2.26 |
| 85 | 539.00 | 2.26 |
| 86 | 536.74 | 2.26 |
| 87 | 534.48 | 2.26 |
| 88 | 532.23 | 2.26 |
| 89 | 529.97 | 2.26 |
| 90 | 520.93 | 2.26 |
| 91 | 509.63 | 2.26 |
| 92 | 500.59 | 2.26 |
| 93 | 491.55 | 2.26 |
| 94 | 480.26 | 2.26 |
| 95 | 462.18 | 2.26 |
| 96 | 448.62 | 2.26 |
| 97 | 435.09 | 2.20 |

# Appendix E. Example of CALMIT AISA Eagle mission planning form

## Mission Planning Form

**Contact Information:**

Cooperator:_____ Phone_____
Address: _____ Fax_____
_____ Email:_____
_____Zip_____ Funding Source_____

**Project Information:**

Title: _____
Project Description/Research Questions (Use additional sheet if necessary):_____
_____
_____
_____

Acquisition Date(s) 1)_____ 2)_____ 3)_____
4)_____ 5)_____ 6)_____
(Mission critical dates/phenological states)

Daily Acquisition Time: am_____pm_____ Acceptable Sky Conditions:_____
Instrument to be used: AISA Imager _____ Thermal Infrared Camera _____
Spatial Resolution Required 1.0 meter_____ 1.5-meter_____ 2.0 meter_____ 2.5-meter____
Will ground truth data be collected? Yes____ No____ If so, what types and when will the data be collected._____
_____
_____

**Target Information:**

General Description: _____
Corner Coordinates of Site (please supply Arc Shapefile)
Projection: WGS 84 UTM Zone: ____ Avg Elevation (in meters): _____ Approximate Target Area: _____
Upper Left: Latitude (DD)_____ Longitude (DD)_____
Easting: _____ Northing:_____
Lower Right: Latitude (DD)_____ Longitude (DD)_____
Easting: _____ Northing:_____
Will ground reference points be established? _____ Calibration Tarps be used? _____

**Product Delivery:**

AISA Base Product: Reflectance _____ Radiance _____ Both _____ Atmospheric Correction_____
Format: ENVI (standard) Erdas Imagine_____ Tiff/GeoTiff_____ Other_____
Additional Research Products available:
NDVI (r)_____ NDVI(g)_____ VARI_____ Other Indice(s) _____Ratio: _____ / _____

### Contact Information

If you have need of additional information please feel free to contact:

Rick Perk
CALMIT Hyperspectral Imaging Project Coordianator
University of Nebraska-Lincoln
312 Hardin Hall
Lincoln, NE 68583-0973
Phone 402.472.0310
Email rperk1@unl.edu

*Copies are available from*
The North American Lake Management Society (NALMS)
PO Box 5443, Madison, WI 53705-0443
phone: (608) 233-2836
info@nalms.org
www.nalms.org